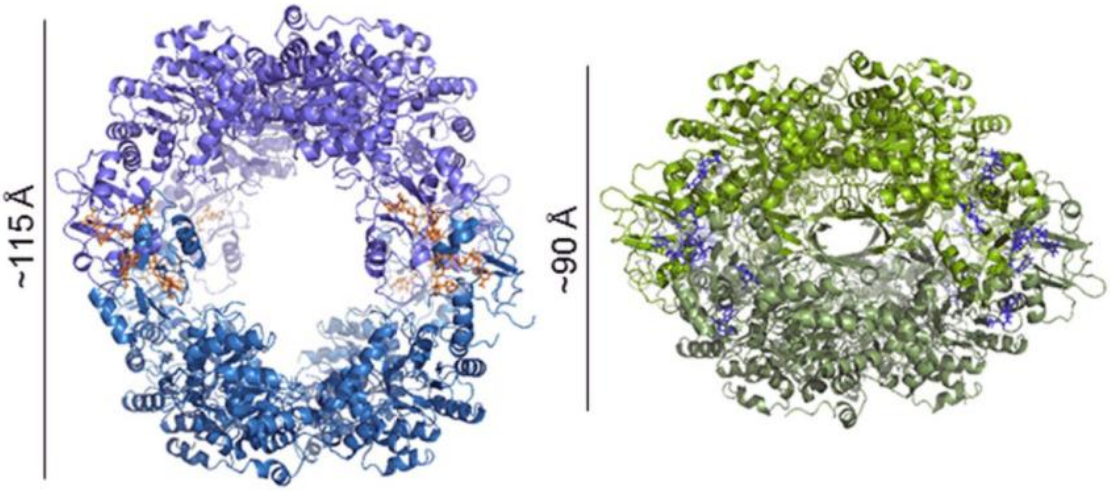
VNiVERSiDAD D SALAMANCA

CAMPUS DE EXCELENCIA INTERNACIONAL

Mecanismos moleculares de regulación alostérica de la enzima IMP deshidrogenasa



DEPARTAMENTO DE MICROBIOLOGÍA Y GENÉTICA
FACULTAD DE BIOLOGÍA

David Fernández Justel

Salamanca, Julio 2022

UNIVERSIDAD DE SALAMANCA

DEPARTAMENTO DE MICROBIOLOGÍA Y GENÉTICA
FACULTAD DE BIOLOGÍA

Mecanismos moleculares de regulación alostérica de la enzima IMP deshidrogenasa

David Fernández Justel
Graduado en Biotecnología

Director de tesis: Dr. Rubén Martínez Buey
Codirector de tesis: Dr. José Luis Revuelta Doval

Salamanca, Julio 2022

La Conserjería de Educación de la Junta de Castilla y León concedió a D. David Fernández Justel una beca durante el periodo julio 2018 – junio 2022 destinada a financiar su contratación predoctoral, cofinanciada por el Fondo Social Europeo (Orden EDU/574/2018, de 28 de mayo, apartado C3).

Tesis por compendio de artículos

Esta tesis doctoral corresponde a un compendio de artículos previamente publicados:

Artículo 1:

- Título: A Nucleotide-Dependent Conformational Switch Controls the Polymerization of Human IMP Dehydrogenases to Modulate their Catalytic Activity
- Autores: David Fernández-Justel[1], Rafael Núñez[2], Jaime Martín-Benito[3], David Jimeno[4], Adrián González-López[1], Eva María Soriano[1], José Luis Revuelta[1], Rubén M Buey[1]
- Revista: Journal of Molecular Biology. 1;431(5):956-969 (2019)
- DOI: 10.1016/j.jmb.2019.01.020

Artículo 2:

- Título: The Bateman domain of IMP dehydrogenase is a binding target for dinucleoside polyphosphates
- Autores: David Fernández-Justel[1], Rafael Peláez[5], José Luis Revuelta[1], Rubén M Buey[1]
- Revista: The Journal of Biological Chemistry. 4;294(40):14768-14775 (2019)
- DOI: 10.1074/jbc.AC119.010055

Artículo 3:

- Título: Diversity of mechanisms to control bacterial GTP homeostasis by the mutually exclusive binding of adenine and guanine nucleotides to IMP dehydrogenase
- Autores: David Fernández-Justel[1], Íñigo Marcos-Alcalde[6 7], Federico Abascal[8], Nerea Vidaña[1], Paulino Gómez-Puertas[6], Alberto Jiménez[1], José L Revuelta[1], Rubén M Buey[1]
- Revista: Protein Science: a publication of the Protein Society. 31(5):e4314 (2022)
- DOI: 10.1002/pro.4314

Afiliación de los autores:
1. Metabolic Engineering Group, Dpto. Microbiología y Genética, Universidad de Salamanca, Campus Miguel de Unamuno, 37007, Salamanca, Spain.
2. Centro de Investigaciones Biológicas (CIB), Spanish National Research Council (CSIC), Ramiro de Maeztu 9, 28040 Madrid, Spain.
3. Centro Nacional de Biotecnología (CNB), Spanish National Research Council (CSIC), Darwin 3, 28039 Madrid, Spain.
4. Instituto de Biología Molecular y Celular del Cáncer (CSIC-Universidad de Salamanca), Campus Miguel de Unamuno, 37007 Salamanca, Spain.
5. Laboratorio de Química Orgánica y Farmacéutica, Departamento de Ciencias Farmacéuticas, Universidad de Salamanca, Campus Miguel de Unamuno, 37007 Salamanca, Spain.
6. Molecular Modeling Group, Centro de Biología Molecular Severo Ochoa, CBMSO (CSIC-UAM), Madrid, Spain.
7. Biosciences Research Institute, School of Experimental Sciences, Universidad Francisco de Vitoria, Madrid, Spain.
8. Wellcome Sanger Institute, Hinxton, UK.

EJECUCIÓN DE ACUERDOS

La Comisión Académica del Programa de Doctorado en Microbiología y Genética Molecular, reunida el día 10 de junio de 2022 a través de ZOOM , ha acordado autorizar la presentación de la tesis doctoral de David Fernández Justel en formato compendio de artículos, de acuerdo a la normativa de la Universidad de Salamanca.

En Salamanca, 16 de junio de 2022
El Coordinador del Programa de Doctorado

Alberto Jiménez García

Autorización del director para la presentación de la Tesis Doctoral en la modalidad Compendio de Artículos

Director: Martínez Buey, Rubén D.N.I.: 12777404-F
Correo electrónico: ruben.martinez@usal.es Teléfono: 666 509 016
Centro: Microbiología y Genética, Universidad de Salamanca, Salamanca, España.

Autoriza que el doctorando David Fernández Justel, DNI: 71039673-X, presente su tesis doctoral: "Mecanismos moleculares de regulación alostérica de la enzima IMP deshidrogenasa" en modalidad compendio de artículos.

Rubén Martínez Buey
Salamanca, 4 de julio de 2022

ÍNDICE

Introducción ……..……..…….. 1

1. Antecedentes …….. 1
2. Hipótesis de trabajo, objetivos y principales conclusiones ……... 8
3. Resultados del proyecto de tesis adicionales a los publicados en los 3 artículos que componen la tesis doctoral ……..…… 10
4. Bibliografía ……. 13

Artículo 1 ……..... 15

Artículo 2 ……..…….. 47

Artículo 3 ……..….. 65

Introducción

1. Antecedentes.

Los nucleótidos de guanina son moléculas esenciales para la célula. Entre otras funciones, son necesarios para la síntesis de ácidos nucleicos, tienen papeles esenciales en el metabolismo y son la principal fuente de energía para la traducción en los ribosomas y la polimerización de microtúbulos.

Las células sintetizan nucleótidos de purina de dos maneras diferentes: en la ruta *de novo*, el sistema de anillos de purina se ensambla secuencialmente desde precursores biosintéticos del metabolismo de carbohidratos y aminoácidos. Por otro lado, en las rutas *de reciclaje* se reciclan nucleobases, nucleósidos y nucleótidos preformados. Ambas rutas biosínteticas están fuertemente reguladas para mantener un equilibrio apropiado entre los *pools* de nucleótidos de adenina y guanina, así como una carga energética óptima a lo largo del ciclo celular [1].

En la ruta *de novo* de biosíntesis de purinas, la inosina-5'-monofosfato (IMP) es la primera molécula de la ruta en tener un sistema de anillos de purina completamente formado y es el precursor común de los nucleótidos de guanina y de adenina, encontrándose justo en el punto de ramificación de ambas rutas. La enzima IMP deshidrogenasa (IMPDH), cataliza la reacción oxidativa de IMP a xantosina-5'-monofosfato (XMP), que es posteriormente convertida a guanosina-5'-monofosfato (GMP) en una reacción catalizada por la enzima GMP sintasa (figura 1) [2].

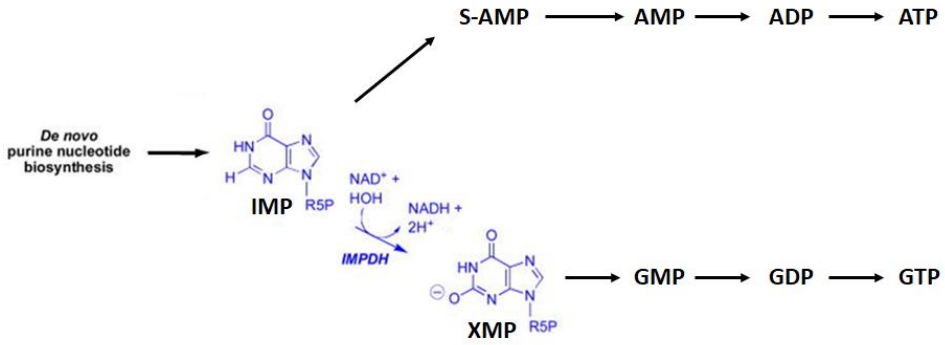


Figura 1. Rutas de biosíntesis *de novo* de nucleótidos de guanina y adenina. La reacción catalizada por la IMPDH está representada en azul [modificada de 2].

La reacción catalizada por la IMPDH representa el paso limitante en la biosíntesis *de novo* de nucleótidos de guanina, por tanto, la IMPDH es una enzima esencial que controla los niveles intracelulares de nucleótidos de purina. La inhibición farmacológica de la IMPDH provoca una fuerte reducción de éstos y tiene efectos antiproliferativos [3]. Por ello, la enzima IMPDH tiene un elevado potencial terapéutico, que ha sido ampliamente explorado durante las últimas décadas y ha generado un grupo diverso de fármacos con actividades antitumorales, antivirales, antiparasitarias, antibacterianas e inmunosupresoras. Entre estos fármacos se incluyen el ácido micofenólico (CellCept®), la mizoribina (Bredinin®) o la ribavirina (Virazole® y Rebetol®) que, en la actualidad, son ampliamente utilizados en diversos tratamientos quimioterapéuticos [4, 5 y 6].

Además de su potencial terapéutico, la manipulación del gen de la IMPDH puede ser usada para modular el flujo metabólico a través de la ruta de biosíntesis *de novo* de nucleótidos de guanina, mejorando así la producción de metabolitos de interés industrial cuyo precursor directo es el GTP [1]. Por ejemplo, trabajos previos de nuestro grupo de investigación demostraron que, en el hongo filamentoso de uso industrial *Ashbya gossypii*, un sobreproductor natural de riboflavina (vitamina B2), la manipulación del gen de la IMPDH incrementa de forma significativa la producción de riboflavina [7].

En disolución, la IMPDH forma tetrámeros en los que cada monómero está formado por un dominio catalítico y otro regulador. El domino catalítico es un barril $(\beta/\alpha)_8$, representante del plegamiento triosa-fosfato isomerasa (barril TIM). Una característica exclusiva de todas las enzimas IMPDH es la presencia de una lámina-β arqueada que se proyecta desde el dominio catalítico. Esta estructura, denominada *finger,* es esencial tanto para la actividad catalítica como para su regulación [1]. Dentro del *finger* se encuentra un *loop*, denominado *flap* catalítico, que es esencial para la reacción enzimática (figura 2, A) [2].

El dominio regulador, de unos 120 aminoácidos de longitud, está insertado en un *loop* del domino catalítico y está compuesto por dos repeticiones del motivo cistationina β-sintasa (CBS1 y CBS2), constituyendo un dominio Bateman (figura 2, B) [8]. Los dominios Bateman, ampliamente distribuidos, no tienen función por sí mismos, pero actúan como moduladores alostéricos de enzimas de muy diversa naturaleza [9]. La relevancia fisiológica de los dominios Bateman está recalcada por el hecho de que mutaciones en algunos de sus residuos causan una variedad de enfermedades hereditarias en humanos, entre las que se incluyen el síndrome de Wolff-Parkinson-White (proteína quinasa activada por AMP), la miotonia congénita (canal de cloro dependiente de voltaje) o la homocistinuria (CBS) [10]. En IMPDH, se han descrito varias mutaciones dentro del dominio Bateman que se asocian a retinopatías, como la amaurosis congénita de Leber (LCA) y la retinitis pigmentosa (RP) [10, 11 y 12], y a distonia [13]. La mayoría de los dominios Bateman presentan dos sitios canónicos de unión de ligandos, habitualmente nucleótidos de adenina (figura 2, B). En respuesta a la unión de nucleótidos, estos dominios regulan la enzima a la que se asocian [9].

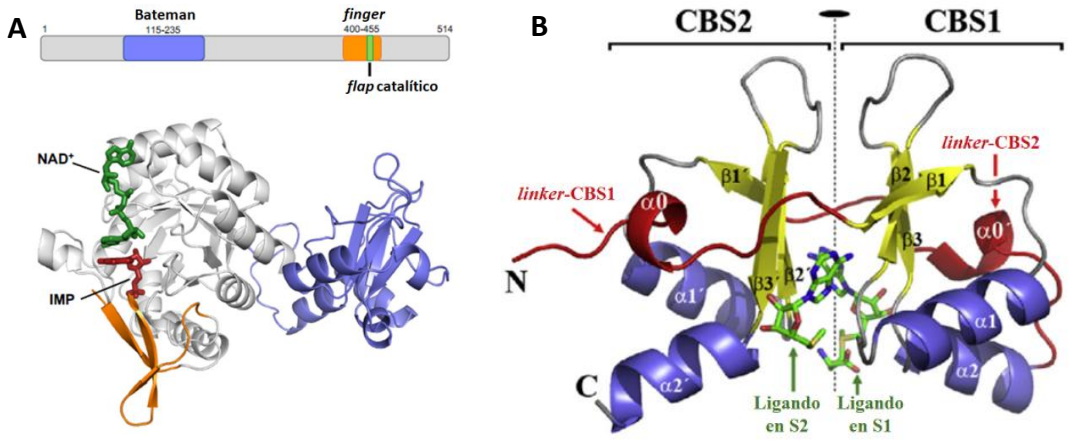


Figura 2. A, Esquema de las distintas regiones de la IMPDH a lo largo de la secuencia (arriba) y estructura típica de un monómero de IMPDH representada en *cartoon* (abajo). El dominio catalítico se muestra en color en gris con su *finger* en naranja y el dominio regulador en azul [tomado de 14]. B, estructura típica de un domino Bateman donde pueden observarse los dos motivos CBS que lo componen y los dos sitios canónicos de unión de nucleótidos [tomado de 9].

En la IMPDH, el dominio Bateman no juega un papel significativo en el mecanismo catalítico *per se*, pero es fundamental para su regulación alostérica [1, 7 y 15]. De hecho, existen diversas pruebas experimentales que indican que los dominios Bateman de las IMPDH son esenciales para la homeostasis del GTP. Por ejemplo, en *Escherichia coli*, el dominio regulador es esencial para mantener el equilibrio intracelular ATP/GTP dentro de su rango fisiológico [16 y 17]. En *Bacillus subtilis*, varias mutaciones en el dominio Bateman suprimen el fenotipo característico generado por la deficiencia de (p)ppGpp (guanosina penta/tetrafosfato), lo que sugiere una relación entre la regulación de la IMPDH y la señalización por estas alarmonas [18, 19 y 20]. Además, el dominio Bateman de la IMPDH también se ha asociado con la regulación de la transcripción y la traducción, a través de su unión a ADN [21, 22 y 23], aunque se desconocen los mecanismos moleculares por los que tiene lugar.

Regulación alostérica de la IMPDH: el *interruptor molecular* conformacional.

En disolución, la unidad básica de la IMPDH es un tetrámero formado por la interacción de los dominios catalíticos (figura 3). Los dominios reguladores de distintos tetrámeros dimerizan en respuesta a la unión de nucleótidos de purina, lo que da lugar a dímeros de tetrámeros (octámeros).

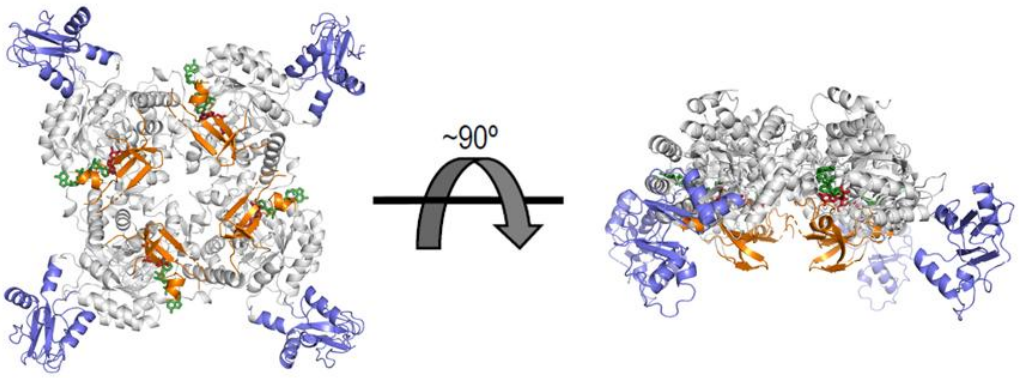


Figura 3. Estructura típica de un tetrámero de IMPDH representada en *cartoon*. El dominio catalítico se muestra en color gris con su *finger* en naranja y el dominio regulador en azul. El NAD^+ y el IMP están representados con *sticks* verdes y rojos, respectivamente [tomada de 14].

Los octámeros de IMPDH oscilan entre dos estados conformacionales, uno compacto con actividad catalítica reducida, y otro extendido con actividad plena. Estas conformaciones se podrían corresponder a los estados T y R del modelo clásico de alosterismo [24]. La unión de nucleótidos de purina al dominio regulador Bateman conduce a la enzima de un estado a otro (figura 4). Es decir, existe un *interruptor conformacional* que regula de manera alostérica la actividad catalítica de la IMPDH [1 y 25].

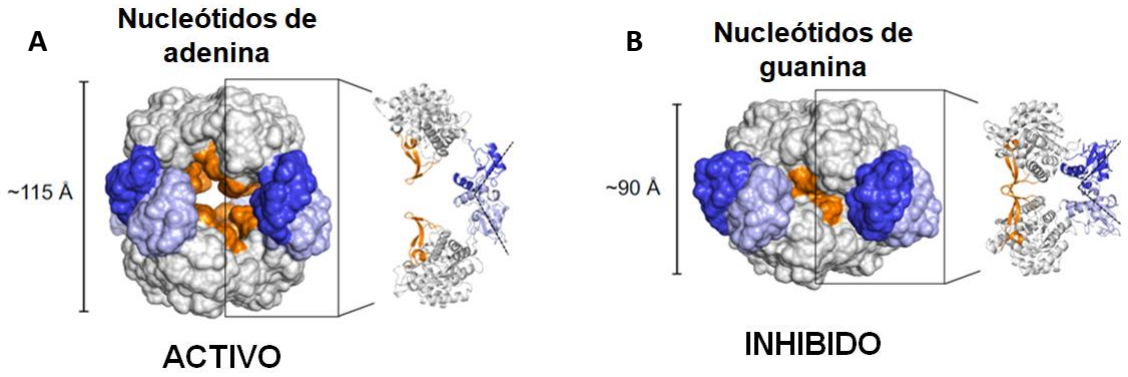


Figura 4. Estructura típica de octámeros de IMPDH en dos estados conformacionales representada en vista de superficie y *cartoon*. El dominio catalítico se muestra en color gris con su *finger* en naranja y el dominio regulador en azul. A, octámero extendido y activo inducido por nucleótidos de adenina. B, octámero compacto e inhibido inducido por nucleótidos de guanina [tomado de 14].

Los octámeros inducidos por nucleótidos de adenina representan el estado relajado de la enzima; tienen una conformación extendida con forma globular hueca en la que los sitios activos, los *fingers* y los *flaps* catalíticos quedan expuestos al disolvente, orientados hacia el interior del octámero y sin interaccionar entre sí (figura 4, A). En esta conformación, la IMPDH retiene la actividad catalítica plena [25].

Por otro lado, la unión de nucleótidos de guanina induce la compactación del octámero en las IMPDHs eucariotas (figura 4, B). Esta conformación compacta, que representa el estado tenso de la enzima, fuerza a los *fingers* de los tetrámeros enfrentados a interaccionar, formando un pseudo barril-β inter-digitado que altera la dinámica conformacional del sitio activo y reduce la afinidad aparente por el sustrato IMP y la actividad catalítica de la enzima (figura 5) [1].

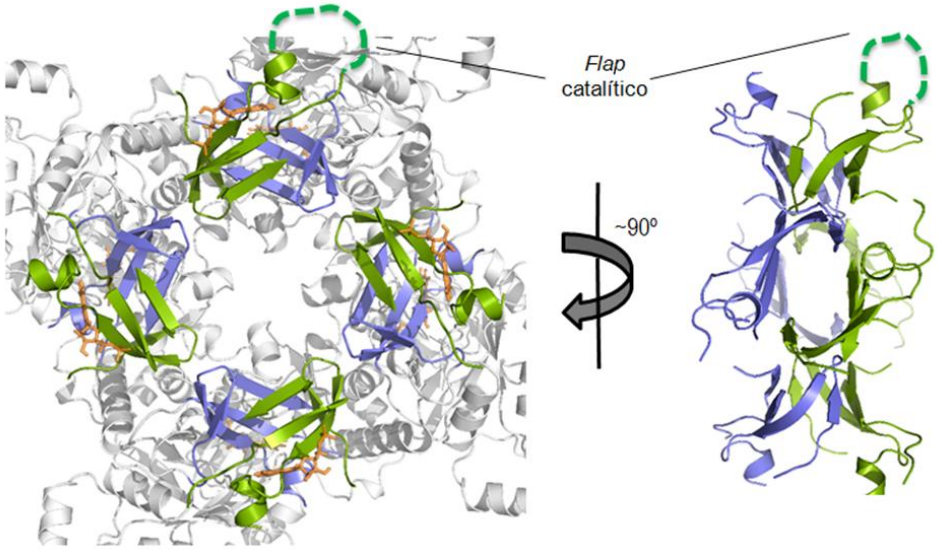


Figura 5. Distintas vistas de la estructura del pseudo barril-β formado por los *fingers* en el octámero compacto. Los *fingers* de distintos tetrámeros están representados en *cartoon* azul y verde [tomado de 1].

La IMPDH de organismos eucariotas.

Nuestro grupo de investigación, usando la enzima del hongo de interés industrial *Ashbya gossypii* (AgIMPDH), demostró que la unión de GTP o GDP a los dominios Bateman induce la formación de dímeros de tetrámeros con actividad catalítica reducida [1]. La unión de tres moléculas de GTP (o GDP) a los sitios alostéricos del dominio Bateman provoca la inhibición de la actividad catalítica de la AgIMPDH. Dos de estas moléculas se unen a los sitios canónicos de nucleótidos (sitios 1 y 2; figura 6), mientras que la tercera molécula de GTP se une a un tercer sitio no canónico exclusivo de las IMPDHs eucariotas (figura 6) y que no está presente en las IMPDHs bacterianas [1].

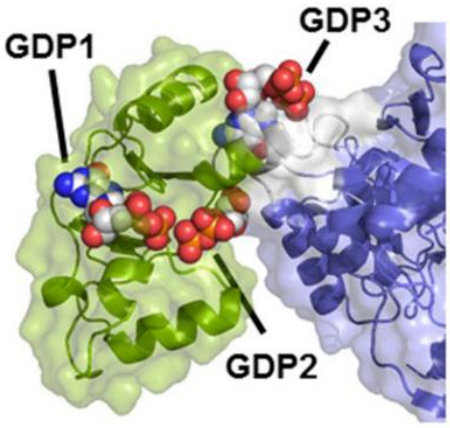


Figura 6. Estructura de un monómero de la IMPDH del hongo *Ashbya gossypii* unido a GDP representada en *cartoon* y vista de superficie. El dominio catalítico está coloreado en azul y el Bateman en verde. Los átomos de los nucleótidos se muestran como esferas [tomada de 25].

Al contrario que la unión de GTP y GDP, la unión de dos nucleótidos de adenina (ATP, ADP y AMP) a los sitios alostéricos canónicos del dominio Bateman, dejando el tercer sitio no canónico desocupado, induce la formación de octámeros extendidos catalíticamente activos. Por tanto, los nucleótidos de adenina y guanina compiten por los sitios canónicos de unión de nucleótidos de los dominios Bateman de la IMPDH, induciendo diferentes conformaciones con diferente actividad catalítica [25]. La relevancia fisiológica de este mecanismo de regulación alostérica se pone de manifiesto por el hecho de que, en humanos, diversas mutaciones que agrupan en los sitios alostéricos en el dominio Bateman se han asociado a retinopatías [10, 11 y 12] y neuropatías [13].

Se ha propuesto que las mutaciones en el gen *IMPDH1* en humanos asociadas a retinopatías podrían interferir con la regulación alostérica de la enzima que codifica, generando mutantes constitutivamente activos. Por tanto, la desregulación de esta enzima podría resultar en unos niveles de nucleótidos de purina alterados, lo que puede causar daño a las células fotorreceptoras. Esta hipótesis es concordante con el carácter hereditario dominante de estas mutaciones, ya que la pérdida de regulación por GTP, o ganancia de función, de uno de los dos alelos sería suficiente para alterar los niveles intracelulares de nucleótidos [1].

La IMPDH de organismos procariotas.

Al contrario que la IMPDH de eucariotas, la IMPDH de organismos procariotas no se inhibe alostéricamente por nucleótidos de guanina (figura 7) [1, 15 y 18]. Además, las alarmonas (p)ppGpp actúan como inhibidores de las IMPDHs procariotas, pero debido a su potencia modesta, probablemente no tengan un efecto relevante *in vivo* [18].

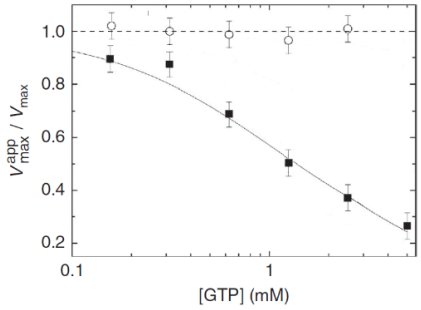


Figura 7. Valores de actividad catalítica normalizada frente concentraciones crecientes de GTP para la enzima IMPDH de *Ashbya gossypii* (cuadrados negros) y de *Escherichia coli* (círculos blancos) [modificada de 1].

Entre las IMPDHs de los organismos eucariotas y procariotas existen divergencias significativas en la secuencia del dominio Bateman que podrían explicar la diferente respuesta ante los nucleótidos de guanina. Una de estas divergencias se encuentra en el tercer sitio no canónico, presente en las enzimas eucariotas y ausente en las procariotas (figura 8) [1].

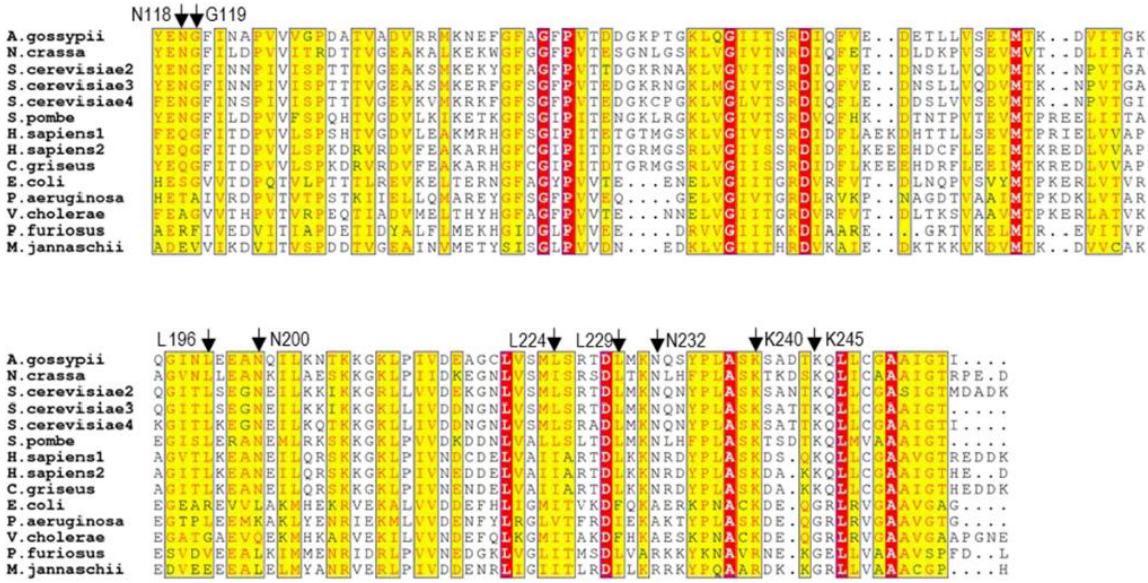


Figura 8. Alineamiento de múltiples secuencias del dominio Bateman de diferentes IMPDHs eucariotas y procariotas. Los residuos clave de la interacción con el GDP en el tercer sitio no canónico en el dominio Bateman de la IMPDH del hongo *Ashbya gossypii* se encuentran indicados con flechas [tomada de 1].

Si bien era plausible que la IMPDH en organismos procariotas pudiera oscilar entre conformaciones compactas (inhibidas) y extendidas (activas) [15, 26 y 27], el mecanismo de inhibición alostérico de estas IMPDHs se desconocía hasta hace poco y es algo que hemos abordado en el laboratorio como parte de este proyecto de tesis doctoral.

Filamentación de la IMPDH.

Actualmente, la filamentación de enzimas está reconocida como un mecanismo relevante de regulación de las propiedades funcionales y estructurales de las proteínas. La filamentación de enzimas puede, por un lado, afectar a la regulación de la actividad enzimática o, por otro lado, jugar un papel estructural, donde las estructuras filamentosas podrían reclutar otras enzimas, facilitando la canalización de sustratos de una misma ruta metabólica [28 y 29]. Se han identificado decenas de proteínas no citoesqueléticas capaces de polimerizar de manera reversible en respuesta a estrés nutricional; entre ellas, las enzimas metabólicas se encuentran sobrerrepresentadas [30]. Los ejemplos más representativos de éstas catalizan los pasos limitantes en la ruta de biosíntesis *de novo* de nucleótidos de pirimidina y purina: la CTP sintasa y la IMPDH, respectivamente [28, 29 y 31].

Las IMPDHs de organismos vertebrados tienen la capacidad de polimerizar *in vivo* en respuesta a condiciones con elevada demanda de GTP, como estados proliferativos o activación de células T [32, 33 y 34], formando estructuras micrométricas denominadas *cytoophidia* (figura 9). Asimismo, la reducción farmacológica de los niveles intracelulares de nucleótidos de guanina también induce *in vivo* la formación reversible de *cytoophidia* [35 y 36].

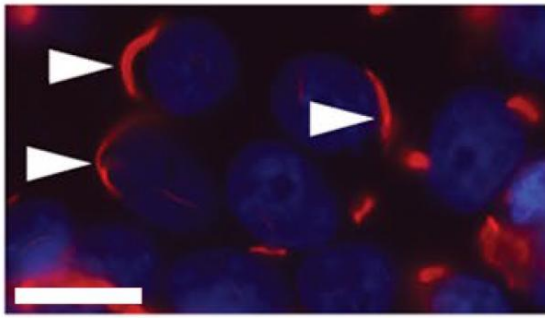


Figura 9. Micrografía obtenida por inmunofluorescencia de células HEK293 transfectadas con la IMPDH2-myc humana tratadas con 10μM ácido micofenólico para inducir la formación de *cytoophidia* (flechas). Los filamentos de IMPDH se muestran en rojo y los núcleos en azul. Barra de escala: 20μm [tomado de 30].

Mediante microscopía electrónica se han caracterizado *in vitro* los filamentos formados por las enzimas IMPDH humanas. La unión de nucleótidos de purina al dominio regulador Bateman induce el apilamiento de octámeros para formar filamentos helicoidales (figura 10) [15, 30 y 35]. Estos filamentos pueden acomodar tanto octámeros compactos como extendidos (figura 10) y la enzima presenta idéntica actividad ya se encuentre incluida en estos polímeros o en su forma no ensamblada [30].

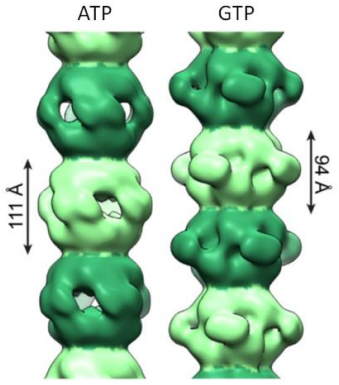


Figura 10. Reconstrucción de microscopía electrónica en tinción negativa de filamentos de la IMPDH2 humana en conformaciones extendida, unida a ATP, y compacta, unida a GTP [tomado de 30].

Se ha propuesto que la IMPDH podría ser más resistente a la inhibición por GTP cuando se encuentra formando filamentos, facilitando así la acumulación intracelular de GTP, pero no se han presentado pruebas experimentales que apoyen esta hipótesis [34]. Además, falta información de los mecanismos moleculares que gobiernan el ensamblaje de la IMPDH. De hecho, los filamentos de IMPDH reconstituidos *in vitro* hasta la fecha consisten en unas pocas partículas organizadas en protofilamentos sencillos cortos [15, 30 y 35] que no se asemejan los *cytoophidia* de IMPDH, compuestos por múltiples protofilamentos y de longitudes micrométricas, observados *in vivo* [33 y 36].

2. Hipótesis de trabajo, objetivos y principales conclusiones.

Artículo 1: A Nucleotide-Dependent Conformational Switch Controls the Polymerization of Human IMP Dehydrogenases to Modulate their Catalytic Activity.

Varias observaciones realizadas en el laboratorio llevaron a plantear la hipótesis de que, en condiciones de *crowding* macromolecular, las IMPDHs humanas ensamblan *in vitro* formando estructuras micrométricas semejantes a los *cytoophidia*. En este artículo, se propuso validar esta hipótesis y caracterizar la dinámica de ensamblaje de *cytoophidia* en relación con la inhibición alostérica por nucleótidos de guanina.

Las principales conclusiones obtenidas son:

- El *interruptor conformacional* controlado por nucleótidos de purina previamente descrito en *A. gossypii* está presente en las IMPDHs humanas, controlando tanto la regulación alostérica como la dinámica de los *cytoophidia*.
- Las IMPDHs humanas ensamblan espontáneamente *in vitro,* formando estructuras micrométricas similares a los *cytoophidia*, bajo condiciones de *crowding* macromolécular en ausencia de nucleótidos.
- En presencia de ATP o GTP en la disolución, desensamblan, de forma similar a lo observado en células.
- Los polímeros de IMPDH reconstituidos *in vitro* son catalíticamente funcionales, con actividad semejante a la IMPDH no ensamblada, pero más resistentes la inhibición alostérica por GTP.
- La mayoría de las mutaciones asociadas a retinopatías mapean en los sitios alostéricos de unión, alterando la unión de nucleótidos y, en consecuencia, anulando la inhibición alostérica inducida por GTP y alterando la dinámica de los *cytoophidia*.

Artículo 2: The Bateman domain of IMP dehydrogenase is a binding target for dinucleoside polyphosphates.

Los dinucleósidos polifosfatos son moléculas ubicuas en las que dos nucleósidos están unidos por una cadena de dos a siete fosfatos. Se ha descrito que el dinucleósido polifosfato Ap_4A puede unirse a las IMPDHs bacterianas, ejerciendo un efecto semejante al del ATP [37 y 38]. Un análisis detallado de la estructura de la

IMPDH unida a GDP, permitió plantear la hipótesis de que los dinucleósidos polifosfatos podrían unirse de manera simultánea a los dos sitios canónicos de los dominios Bateman. Por ello, en este trabajo se propuso corroborar esta hipótesis y evaluar si los dinucleósidos polifosfatos podrían tener efecto sobre el *interruptor conformacional* que controla la actividad catalítica de las IMPDHs.

Las principales conclusiones obtenidas de este artículo fueron:

- Los dinucleósidos polifosfatos de adenina/guanina se unen con afinidades sub-micromolares (en el rango de concentración fisiológico de los dinucleósidos polifosfatos) a los dominios Bateman de IMPDHs eucariotas *in vitro*.
- La estructura cristalográfica de la IMPDH unida al dinucleósido polifosfato Ap5G demuestra que esta molécula ocupa simultáneamente los dos sitios canónicos de unión a nucleótidos del dominio Bateman.
- Los dinucleósidos polifosfatos modulan el *interruptor conformacional* y la actividad catalítica de las IMPDHs eucariotas *in vitro*, compitiendo eficientemente con mononucleótidos de adenina / guanina por los sitios alostéricos.

Artículo 3: Diversity of mechanisms to control bacterial GTP homeostasis by the mutually exclusive binding of adenine and guanine nucleotides to IMP dehydrogenase.

La elevada conservación del dominio Bateman y sus sitios canónicos de unión de nucleótidos en las IMPDHs procariotas nos llevó a plantear la hipótesis de que, muy probablemente, estas enzimas también se controlan de manera alostérica por nucleótidos de purina. En este trabajo se propuso analizar los mecanismos de regulación alostérica de la IMPDH de organismos procariotas, así como caracterizarlos desde un punto de vista estructural y funcional.

Las principales conclusiones obtenidas de este artículo fueron:

- El *interruptor conformacional* controlado por nucleótidos de purina que controla la actividad catalítica de las IMPDHs es universal, es decir, está evolutivamente conservado desde bacterias hasta humanos.
- La mayoría de las IMPDHs bacterianas están alostéricamente moduladas por la unión mutuamente excluyente de ATP y (p)ppGpp al dominio Bateman.
- El (p)ppGpp se une a un sitio, descrito por primera vez en este trabajo, que solapa parcialmente con el sitio canónico 2, donde compite con el ATP.
- La mayoría de las proteobacterias carecen del sitio de unión de (p)ppGpp y su actividad catalítica está controlada por la unión mutuamente excluyente de ATP y GTP al sitio canónico 2 del dominio Bateman.
- Las relaciones ATP/GTP o ATP/(p)ppGpp elevadas favorecen la conformación extendida y activa. Por el contrario, cuando estas *ratios* bajan, se favorece la conformación compacta, con actividad catalítica reducida.

3. Resultados del proyecto de tesis adicionales a los publicados en los 3 artículos que componen la tesis doctoral.

En este apartado se presentan de manera breve algunos resultados adicionales del proyecto de tesis que no están incluidos en los tres artículos que componen esta memoria, pero que están incluidos en los siguientes artículos:

- Plana-Bonamaiso A, Lopez-Begines S, Fernandez-Justel D, Junza A, Soler-Tapia A, Andilla J, Loza-Alvarez P, Rosa JL, Miralles E, Casals I, Yanes O, de la Villa P, Buey RM, Mendez A (2020) Post-translational regulation of retinal IMPDH1 in vivo to adjust GTP synthesis to illumination conditions. Elife 9:e56418 [39].

- Burrell AL, Nie C, Said M, Simonet JC, Fernández-Justel D, Johnson MC, Quispe J, Buey RM, Peterson JR, Kollman JM (2022) IMPDH1 retinal variants control filament architecture to tune allosteric regulation. Nat. Struct. Mol. Biol. 29:47–58 [40].

Filamentación de las enzimas IMPDH humanas.

Los humanos tienen dos enzimas IMPDH (HsIMPDH1 y HsIMPDH2) codificadas en genes diferencialmente expresados. Estas enzimas tienen un 84% de identidad de secuencia y sus propiedades catalíticas son prácticamente idénticas [2 y 41].

Mediante experimentos de crio-microscopía electrónica se demostró que la unión de GTP o GDP a los sitios alostéricos 2 y 3 del dominio Bateman de las enzimas humanas induce la compactación del octámero, así como una leve curvatura de los dos tetrámeros que conforman el octámero (figura 11, A). De este modo la superficie del tetrámero compuesta por los dominios catalíticos queda ligeramente curvada (conformación *bowed*), en contraste con los tetrámeros de los octámeros inducidos por ATP, en los que esta superficie está plana (conformación *flat*) (figura 11, B).

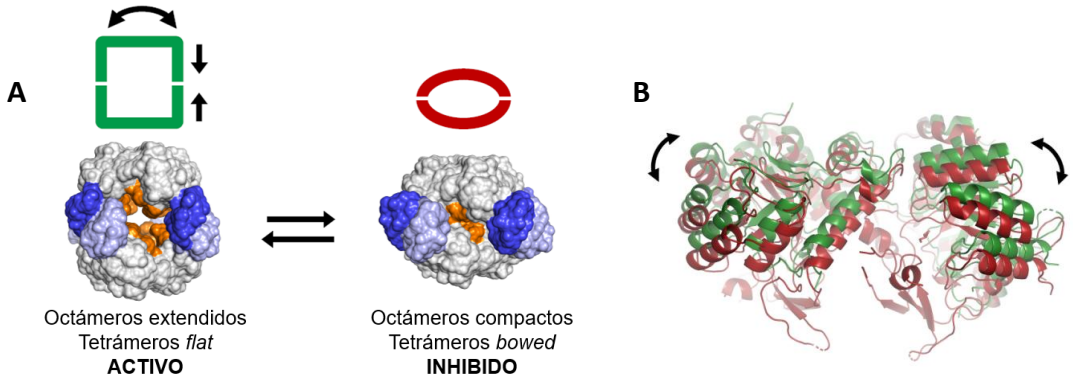


Figura 11. A, estructura típica de octámeros de IMPDH en los estados conformacionales inducidos por ATP (activo) y GTP (inhibido) representada en vista de superficie, junto con una representación esquemática de los dos cambios conformacionales inducidos por el GTP, compactación e incremento de la curvatura. El dominio catalítico se muestra en color gris con su *finger* en naranja y el dominio regulador en azul. B, estructuras superpuestas de los dominios catalíticos de dos tetrámeros de IMPDH en conformación *flat* (verde) y *bowed* (rojo) representadas en *cartoon* [tomada de 14].

En la enzima HsIMPDH2, la unión de ATP induce la formación de polímeros compuestos por octámeros en conformación *flat* y, en su mayoría, extendidos. Por el contrario, la unión de GTP a la enzima filamentada induce la compactación del octámero pero, dado que los contactos en el filamento son sólo compatibles con la

conformación *flat*, no se induce la transición de los tetrámeros a una conformación *bowed*, lo que implica que la HsIMPDH2 polimerizada mantiene parcialmente la actividad catalítica a concentraciones moderadas de GTP. A concentraciones muy elevadas de GTP, los filamentos despolimerizan en octámeros que adquieren la conformación compacta y *bowed* (figura 12, A). Por tanto, el estado filamentado reduce la sensibilidad de la HsIMPDH2 a la inhibición.

Además, en presencia de elevadas concentraciones de IMP, los filamentos de HsIMPDH2 son más resistentes a la despolimerización, permitiendo a esta enzima mantenerse parcialmente activa en estadíos que requieren una elevada síntesis de IMP, a pesar de la acumulación de elevados niveles de GTP [42].

Al contrario que en la enzima HsIMPDH2, en la HsIMPDH1 los contactos en el filamento son compatibles tanto con la conformación *flat* como *bowed*, por lo que no hay diferencias en sensibilidad a la inhibición por GTP entre la enzima en estado octamérico y filamentado (figura 12, B) y, por tanto, se desconoce la función de los polímeros de HsIMPDH1 [40].

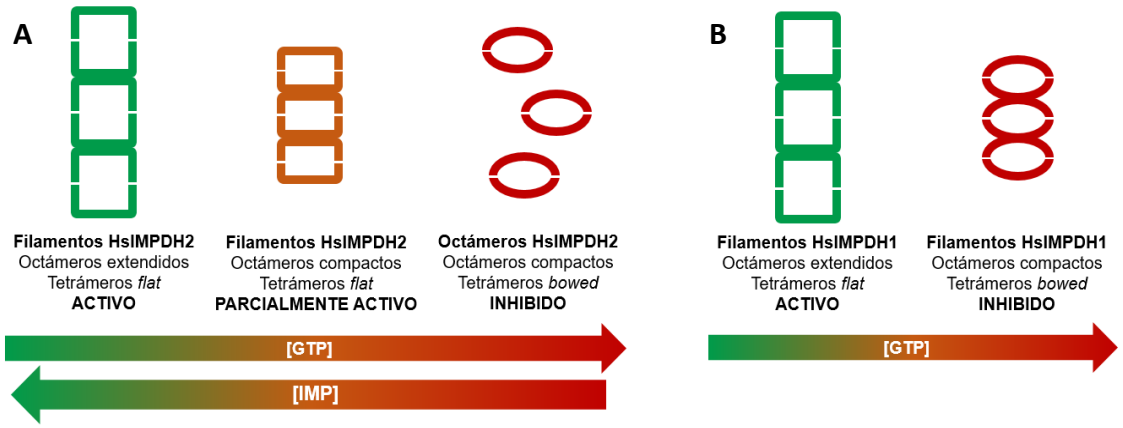


Figura 12. Representación esquemática de los distintos estados conformacionales de las enzimas humanas IMPDH2 (A) e IMPDH1 (B) en función de la concentración de GTP e IMP [tomado de 14].

Variantes específicas de retina.

En las células fotorreceptoras de la retina de mamíferos predominan dos variantes transcripcionales resultantes del procesamiento alternativo del ARN mensajero. Una de estas variantes contiene una extensión en el C-terminal (HsIMPDH1-α de 546 residuos) mientras que la otra contiene extensiones en el N y C-terminales (HsIMPDH1-γ de 595 residuos), con respecto a la variante canónica (HsIMPDH1-β de 514 residuos). La actividad enzimática de estas tres enzimas es idéntica [43] pero poseen diferente sensibilidad a la inhibición por GTP [44].

Mediante experimentos de crio-microscopía electrónica se ha demostrado que la extensión N-terminal presente en la variante γ estabiliza la conformación *flat* cuando la enzima se encuentra formando filamentos. De este modo, la unión de GTP al dominio Bateman induce la compactación de los octámeros, pero no la transición de los tetrámeros a la conformación *bowed*, de forma semejante a lo que ocurre en la HsIMPDH2 (figura 13). Por tanto, la extensión N-terminal reduce la sensibilidad al GTP

cuando la enzima se encuentra polimerizada. No está claro aún qué efecto tiene la extensión C-terminal en la estructura de la enzima, pero, en cualquier caso, ambas extensiones reducen la sensibilidad a la inhibición por GTP, adaptando la regulación alostérica de la enzima IMPDH1 a la elevada demanda de nucleótidos de guanina de la retina [40].

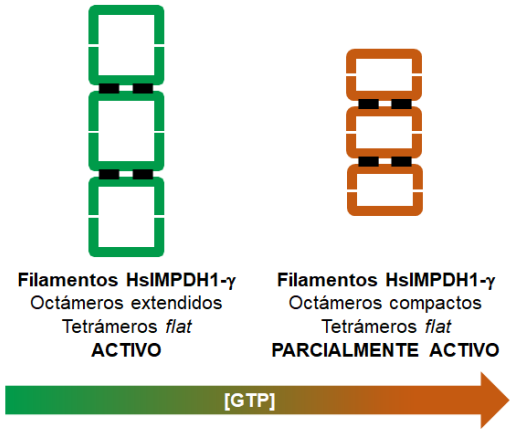


Figura 13. Representación esquemática de los distintos estados conformacionales de la enzima humana IMPDH1-γ en función de la concentración de GTP [tomado de 14].

Modificaciones post-traduccionales.

Las modificaciones post-traduccionales de proteínas son un mecanismo versátil y rápido utilizado para regular la función proteica en respuesta a cambios en las condiciones ambientales [45]. Esto es especialmente relevante en la IMPDH1 de las células de la retina ya que, por un lado, la regulación de la biosíntesis de nucleótidos de guanina es esencial para mantener niveles apropiados de cGMP, una molécula clave para la fototransducción [46] y, por otro lado, la IMPDH1 es la principal responsable del suministro de nucleótidos de guanina, ya que los genes que codifican la enzima IMPDH2 y las enzimas de la ruta de reciclaje de purinas se expresan a niveles bajos en este tejido [40].

Recientemente se ha identificado en células de la retina de mamíferos la fosforilación de varios residuos en la IMPDH1. Dos de estos residuos se encuentran en el dominio Bateman (Thr159 y Ser160 de la HsIMPDH1-β) y son fosforilados *in vivo* en respuesta a la exposición a la luz. Estos residuos se encuentran en el sitio canónico 1 de unión de nucleótidos de la HsIMPDH1 e intervienen de manera directa en la unión de nucleótidos a los sitios alostéricos. Por ello, su fosforilación no afecta a la actividad catalítica, pero sí desensibiliza la enzima a la inhibición alostérica mediada por GTP. Este mecanismo dependiente de la luz facilita alcanzar los elevados niveles de GTP necesarios para la fototransducción [39].

De manera opuesta, otro de los residuos identificados se encuentra en el dominio catalítico (Ser477 de la HsIMPDH1-β) y es fosforilado *in vivo* en oscuridad. Su fosforilación tampoco afecta a la actividad catalítica [39], pero se ha propuesto que podría interferir con el ensamblaje de los filamentos, ya que se encuentra en la interfase entre octámeros en los filamentos de la HsIMPDH1-γ [40]. Por tanto, esta fosforilación incrementa la sensibilidad de la enzima a la inhibición por GTP. En conjunto, estas fosforilaciones permiten adaptar la regulación alostérica de la IMPDH a la demanda cambiante de GTP en las células fotoreceptoras durante el ciclo de luz/oscuridad, necesaria para la fototransducción.

4. Bibliografía.

[1] Buey RM, Ledesma-Amaro R, Velazquez-Campoy A, Balsera M, Chagoyen M, de Pereda JM, Revuelta JL (2015) Guanine nucleotide binding to the Bateman domain mediates the allosteric inhibition of eukaryotic IMP dehydrogenases. Nat. Commun. 6:8923.

[2] Hedstrom L (2009) IMP Dehydrogenase: Structure, Mechanism, and Inhibition. Chem. Rev. 109:2903–2928.

[3] Jayaram HN, Cooney DA, Grusch M, Krupitza G (1999) Consequences of IMP dehydrogenase inhibition, and its relationship to cancer and apoptosis. Curr. Med. Chem. 6:561–574.

[4] Juvale K, Shaik A, Kirubakaran S (2019) Inhibitors of inosine 5′-monophosphate dehydrogenase as emerging new generation antimicrobial agents. Medchemcomm. 10:1290–1301.

[5] Braun-Sand SB, Peetz M (2010) Inosine monophosphate dehydrogenase as a target for antiviral, anticancer, antimicrobial and immunosuppressive therapeutics. Future Med. Chem. 2:81–92.

[6]. Naffouje R, Grover P, Yu H, Sendilnathan A, Wolfe K, Majd N, Smith EP, Takeuchi K, Senda T, Kofuji S, Sasaki AT (2019) Anti-tumor potential of IMP dehydrogenase inhibitors: A century-long story. Cancers (Basel) 11:1346.

[7] Buey RM, Ledesma-Amaro R, Balsera M, de Pereda JM, Revuelta JL (2015) Increased riboflavin production by manipulation of inosine 5′-monophosphate dehydrogenase in Ashbya gossypii. Appl. Microbiol. Biotechnol. 99:9577–9589.

[8] Bateman A (1997) The structure of a domain common to archaebacteria and the homocystinuria disease protein. Trends Biochem. Sci. 22:12–13.

[9] Ereno-Orbea J, Oyenarte I, Martinez-Cruz LA (2013) CBS domains: Ligand binding sites and conformational variability. Arch. Biochem. Biophys 540:70–81.

[10] Scott JW, Hawley SA, Green KA, Anis M, Stewart G, Scullion GA, Norman DG, Hardie DG (2004) CBS domains form energy-sensing modules whose binding of adenosine ligands is disrupted by disease mutations. J. Clin. Invest. 113:274–284.

[11] McGrew DA, Hedstrom L (2012) Towards a pathological mechanism for IMPDH1-linked retinitis pigmentosa. Adv. Exp. Med. Biol. 723:539-45.

[12] Aherne A, Kennan A, Kenna PF, McNally N, Lloyd DG, Alberts IL, Kiang AS, Humphries MM, Ayuso C, Engel PC, Gu JJ, Mitchell BS, Farrar GJ, Humphries P (2004) On the molecular pathology of neurodegeneration in IMPDH1-based retinitis pigmentosa. Hum. Mol. Genet. 13:641–650.

[13] Zech M, Jech R, Boesch S, Škorvánek M, Weber S, Wagner M, Zhao C, Jochim A, Necpál J, Dincer Y, et al. (2020) Monogenic variants in dystonia: an exome-wide sequencing study. Lancet Neurol. 19:908–918.

[14] Buey RM, Fernández-Justel D, Jiménez A, Revuelta JL (2022) The diversity and complexity of the allosteric regulation of IMP dehydrogenase. En revisión.

[15] Labesse G, Alexandre T, Vaupré L, Salard-Arnaud I, Him JLK, Raynal B, Bron P, Munier-Lehmann H (2013) MgATP regulates allostery and fiber formation in IMPDHs. Structure 21:975–985.

[16] Pimkin M, Markham GD (2008) The CBS subdomain of inosine 5'-monophosphate dehydrogenase regulates purine nucleotide turnover. Mol. Microbiol. 68:342–359.

[17] Pimkin M, Pimkina J, Markham GD (2009) A regulatory role of the Bateman domain of IMP dehydrogenase in adenylate nucleotide biosynthesis. J. Biol. Chem. 284:7960–7969.

[18] Kriel A, Bittner AN, Kim SH, Liu K, Tehranchi AK, Zou WY, Rendon S, Chen R, Tu BP, Wang JD (2012) Direct regulation of GTP homeostasis by (p)ppGpp: A critical component of viability and stress resistance. Mol. Cell. 48:231–241.

[19] Bittner AN, Kriel A, Wang JD (2014) Lowering GTP level increases survival of amino acid starvation but slows growth rate for Bacillus subtilis cells lacking (p)ppGpp. J Bacteriol. 196:2067–2076.

[20] Osaka N, Kanesaki Y, Watanabe M, Watanabe S, Chibazakura T, Takada H, Yoshikawa H, Asai K (2020) Novel (p)ppGpp ^{0} suppressor mutations reveal an unexpected link between methionine catabolism and GTP synthesis in Bacillus subtilis. Mol. Microbiol. 113:1155–1169.

[21] Kozhevnikova EN, van der Knaap JA, Pindyurin AV, Ozgur Z, van Ijcken WF, Moshkin YM, Verrijzer CP (2012) Metabolic enzyme IMPDH is also a transcription factor regulated by cellular state. Mol. Cell 47:133−139.

[22] McLean JE, Hamaguchi N, Belenky P, Mortimer SE, Stanton M, Hedstrom L (2004) Inosine 5'-monophosphate dehydrogenase binds nucleic acids in vitro and in vivo. Biochem J. 379:243–251.

[23] Mortimer SE, Xu D, McGrew D, Hamaguchi N, Lim HC, Bowne SJ, Daiger SP, Hedstrom L (2008) IMP dehydrogenase type 1 associates with polyribosomes translating rhodopsin mRNA. J. Biol. Chem. 283:36354–36360.

[24] Monod J, Wyman J, Jean-PierreChangeux JP (1965) On the nature of allosteric transitions: A plausible model. J. Mol. Biol. 12:88–118.

[25] Buey RM, Fernandez-Justel D, Marcos-Alcalde I, Winter G, Gomez-Puertas P, de Pereda JM, Luis Revuelta JL (2017) A nucleotide-controlled conformational switch modulates the activity of eukaryotic IMP dehydrogenases. Sci. Rep. 7:2648.

[26] Labesse G, Alexandre T, Gelin M, Haouz A, Munier-Lehmann H (2015) Crystallographic studies of two variants of Pseudomonas aeruginosa IMPDH with impaired allosteric regulation. Acta Crystallogr. Sect. D Biol. Crystallogr. 71:1890–1899.

[27] Alexandre T, Rayna B, Munier-Lehmann H (2015) Two classes of bacterial IMPDHs according to their quaternary structures and catalytic properties. PLoS One 10:e0116578.

[28] Aughey GN, Liu JL (2016) Metabolic regulation via enzyme filamentation. Crit. Rev. Biochem. Mol. Biol. 51:282–293.

[29] Liu J (2016) The Cytoophidium and Its Kind: Filamentation and Compartmentation of Metabolic Enzymes. Annu. Rev. Cell Dev. Biol. 32:349–372.

[30] Anthony SA, Burrell AL, Johnson MC, Duong-Ly KC, Kuo YM, Simonet JC, Michener P, Andrews A, Kollman JM, Peterson JR (2017) Reconstituted IMPDH polymers accommodate both catalytically active and inactive conformations. Mol. Biol. Cell 28:2600–2608.

[31] Wang H, Saho Q-X (2017) The cytoophidium: A novel intracellular compartmentation formed by metabolic enzymes. Academia Journal of Biotechnology 5:044–050.

[32] Keppeke GD, Chang CC, Peng M, Chen L-Y, Lin W-C, Pai L-M, Andrade LEC, Sung L-Y, Liu J-L (2018) IMP/GTP balance modulates cytoophidium assembly and IMPDH activity. Cell Div. 13:5.

[33] Chang CC, Lin WC, Pai LM, Lee HS, Wu SC, Ding ST, Liu JL, Sung LY (2015) Cytoophidium assembly reflects upregulation of IMPDH activity. J. Cell Sci. 128:3550–3555.

[34] Duong-Ly KC, Kuo YM, Johnson MC, Cote JM, Kollman JM, Soboloff J, Rall GF, Andrews A. J, Peterson JR (2018) T cell activation triggers reversible inosine-5'-monophosphate dehydrogenase assembly. J. Cell. Sci. 131:jcs223289.

[35] Ji YS, Gu JJ, Makhov AM, Griffith JD, Mitchell BS (2006) Regulation of the Interaction of Inosine Monophosphate Dehydrogenase with Mycophenolic Acid by GTP. J. Biol. Chem. 281:206–212.

[36] Carcamo WC, Satoh M, Kasahara H, Terada N, Hamazaki T, Chan JY, Yao B, Tamayo S, Covini G, von Mühlen CA, Chan EK (2011) Induction of cytoplasmic rods and rings structures by inhibition of the CTP and GTP synthetic pathway in mammalian cells. PLoS One 6:e29690.

[37] Despotovic D, Brandis A, Savidor A, Levin Y, Fumagalli L, Tawfik DS (2017) Diadenosine tetraphosphate (Ap4A) – an E. coli alarmone or a damage metabolite? FEBS J. 284:2194–2215.

[38] Guo W, Azhar MA, Xu Y, Wright M, Kamal A, Miller AD (2011) Isolation and identification of diadenosine 5',5'''-P1,P4-tetraphosphate binding proteins using magnetic bio-panning. Bioorg. Med. Chem. Lett. 21:7175–7179.

[39] Plana-Bonamaiso A, Lopez-Begines S, Fernandez-Justel D, Junza A, Soler-Tapia A, Andilla J, Loza-Alvarez P, Rosa JL, Miralles E, Casals I, Yanes O, de la Villa P, Buey RM, Mendez A (2020) Post-translational regulation of retinal IMPDH1 in vivo to adjust GTP synthesis to illumination conditions. Elife 9:e56418.

[40] Burrell AL, Nie C, Said M, Simonet JC, Fernández-Justel D, Johnson MC, Quispe J, Buey RM, Peterson JR, Kollman JM (2022) IMPDH1 retinal variants control filament architecture to tune allosteric regulation. Nat. Struct. Mol. Biol. 29:47–58.

[41] Carr SF, Papp E, Wu JC, Natsumeda Y (1993) Characterization of human type I and type II IMP dehydrogenases. J. Biol. Chem. 268:27286–27290.

[42] Johnson MC, Kollman JM (2020) Cryo-EM structures demonstrate human IMPDH2 filament assembly tunes allosteric regulation. Elife 9:e53243.

[43] Xu D, Cobb GC, Spellicy CJ, Bowne SJ, Daiger SP, Hedstrom L (2008) Retinal Isoforms of Inosine 5′-Monophosphate Dehydrogenase Type I Are Poor Nucleic Acid Binding Proteins. Arch. Biochem. Biophys. 472:100–104.

[44] Andashti B, Yazdanparast R, Barzegari E, Galehdari H (2020) The functional impact of the C/N-terminal extensions of the mouse retinal IMPDH1 isoforms: a kinetic evaluation. Mol. Cell. Biochem. 465:155–164.

[45] Lin H, Caroll KS (2018) Introduction: Posttranslational Protein Modification. Chem. Rev. 118:887–888.

[46] Bowne SJ, Liu Q, Sullivan LS, Zhu J, Spellicy CJ, Rickman CB, Pierce EA, Daiger SP (2006) Why do mutations in the ubiquitously expressed housekeeping gene IMPDH1 cause retina-specific photoreceptor degeneration? Investig. Ophthalmol. Vis. Sci. 47:3754–3765.

Artículo 1

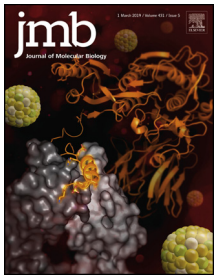
Título:

Un interruptor conformacional dependiente de nucleótidos controla la polimerización de las IMP deshidrogenasas humanas para modular sus actividades catalíticas.

Resumen:

La IMPDH cataliza el paso limitante en la ruta biosintética *de novo* del GTP y tiene papeles esenciales en la proliferación celular. Como diana terapéutica, la IMPDH ha sido estudiada durante décadas, pero sólo durante los últimos años hemos comenzado a entender la complejidad de los mecanismos de su regulación fisiológica. En este trabajo, se propuso evaluar si el *interruptor conformacional* controlado por nucleótidos de purina presente en algunas IMPDH eucariotas está también presente en las IMPDHs humanas y cómo este puede estar vinculado a la dinámica de los *cytoophidia*. Para ello se hizo uso de múltiples metodologías de biología estructural como cristalografía de macromoléculas, SAXS y microscopía electrónica; así como metodologías de biología celular y bioquímica e ingeniería de proteínas.

Aquí, presentamos información estructural y funcional sobre cómo los nucleótidos de adenina y guanina controlan un *interruptor conformacional* que modula el ensamblaje las dos enzimas IMPDHs humanas en *cytoophidia* y regula alostéricamente sus actividades catalíticas. Estructuras micrométricas semejantes a los *cytoophidia* reconstituidas *in vitro* muestran actividad catalítica comparable a la IMPDH no ensamblada, pero, por otro lado, son más resistentes a la inhibición alostérica por GTP/GDP. Por último, demostramos que la mayoría de las mutaciones en la IMPDH asociadas a retinopatías eliminan la inhibición alostérica inducida por GTP/GDP y alteran la dinámica de los *cytoophidia*. Por tanto, la formación de *cytoophidia* de IMPDH facilita la acumulación de altos niveles de nucleótidos de guanina cuando la célula lo requiere; además, nuestros resultados sugieren que la alteración en la dinámica de los *cytoophidia* causada por las mutaciones asociadas a retinopatías podría jugar un papel en el desarrollo de la enfermedad.



A Nucleotide-Dependent Conformational Switch Controls the Polymerization of Human IMP Dehydrogenases to Modulate their Catalytic Activity

David Fernández-Justel [1], Rafael Núñez [2], Jaime Martín-Benito [3], David Jimeno [4], Adrián González-López [1], Eva María Soriano [1], José Luis Revuelta [1] and Rubén M. Buey [1]

1 - Metabolic Engineering Group, *Dpto. Microbiología y Genética, Universidad de Salamanca, Campus Miguel de Unamuno, 37007, Salamanca, Spain*
2 - Centro de Investigaciones Biológicas (CIB), *Spanish National Research Council (CSIC), Ramiro de Maeztu 9, 28040 Madrid, Spain*
3 - Centro Nacional de Biotecnología (CNB), *Spanish National Research Council (CSIC), Darwin 3, 28039 Madrid, Spain*
4 - Instituto de Biología Molecular y Celular del Cáncer (CSIC-Universidad de Salamanca), *Campus Miguel de Unamuno, 37007 Salamanca, Spain*

Correspondence to José Luis Revuelta and Rubén M. Buey: *Lab 233, Edificio Departamental, Campus Miguel Universidad de Salamanca, de Unamuno, 37007 Salamanca, Spain. revuelta@usal.es, ruben.martinez@usal.es*
https://doi.org/10.1016/j.jmb.2019.01.020
Edited by Georg Schulz

Abstract

Inosine 5′-monophosphate dehydrogenase (IMPDH) catalyzes the rate-limiting step in the *de novo* GTP biosynthetic pathway and plays essential roles in cell proliferation. As a clinical target, IMPDH has been studied for decades, but it has only been within the last years that we are starting to understand the complexity of the mechanisms of its physiological regulation. Here, we report structural and functional insights into how adenine and guanine nucleotides control a conformational switch that modulates the assembly of the two human IMPDH enzymes into cytoophidia and allosterically regulates their catalytic activity. *In vitro* reconstituted micron-length cytoophidia-like structures show catalytic activity comparable to unassembled IMPDH but, in turn, are more resistant to GTP/GDP allosteric inhibition. Therefore, IMPDH cytoophidia formation facilitates the accumulation of high levels of guanine nucleotides when the cell requires it. Finally, we demonstrate that most of the IMPDH retinopathy-associated mutations abrogate GTP/GDP-induced allosteric inhibition and alter cytoophidia dynamics.

© 2019 Elsevier Ltd. All rights reserved.

Introduction

Inosine 5′-monophosphate dehydrogenase (IMPDH) is the enzyme that catalyzes the rate-limiting step in the *de novo* guanine nucleotide biosynthetic pathway, which plays a crucial role in the regulation of the cellular pools of purine nucleotides. Therefore, IMPDH is a key enzyme involved in the control of cell viability, division and proliferation. Indeed, IMPDH is the target of a diverse number of drugs presently used in clinical chemotherapy such as immunosupressors, antivirals, anticancer or antibiotics [1].

IMPDH is composed of an archetypal TIM barrel catalytic domain and a Bateman regulatory domain, which is inserted within a loop of the catalytic module. In solution, the basic units of most IMPDHs are homotetramers that can dimerize in different ways to form octamers or higher-order oligomers [2–7].

Using the IMPDH enzyme from the industrial fungus *Ashbya gossypii* as a model, we have recently reported a molecular mechanism by which purine nucleotides allosterically modulate the catalytic activity. The competition of adenine or guanine nucleotides for their binding sites within the regulatory Bateman domain controls a conformational switch that modulates the catalytic activity by shifting from extended to compacted IMPDH octamers. Extended, ATP-induced octamers are fully active, while the catalytic activity of GTP/GDP-induced compacted octamers is significantly reduced [6,7]. The relevance of this allosteric mechanism of regulation is stressed by the observation that most of the described missense mutations in

human IMPDH isoform 1 associated with severe retinopathies, such as retinitis pigmentosa and leber congenital amaurosis [8], map into the nucleotide binding sites of the Bateman regulatory domain. Based on these results, it was proposed that the retinopathy-associated mutations might interfere with nucleotide binding and disrupt the allosteric regulation of human IMPDH isoform 1, generating constitutively active IMPDH mutants, which is in agreement with the dominant hereditary character of these mutations [7].

Adding more complexity to the mechanisms of IMPDH regulation, the two human enzymes have been reported to polymerize into mesoscale intracellular assemblies such as purinosomes [9] and micrometric structures denoted as *rod and rings* or *cytoophidia* [4,10,11]. Thereby, human IMPDH, as well as CTP synthase (CTPS) and some other metabolic enzymes, possesses the particular ability to self-assemble into higher-order structures. This macromolecular organization has been suggested to modulate enzyme activity and play important roles in regulating cell metabolism by controlling intracellular nucleotide homeostasis [12,13]. The two human IMPDH enzymes, in response to intracellular guanine-nucleotide depletion, assemble into micron-length cytoophidia that disappear once the guanine-nucleotide levels are restored. Remarkably, the physiological functions of IMPDH cytoophidia remain unclear, although it has been reported that polymerization correlates with rapid cell proliferation [11,14,15]. Nonetheless, the *in vitro* reconstituted polymers show identical activity for polymerized and non-assembled human IMPDH isoform 2 [5]. To reconcile these results, it has been recently speculated that filamentous IMPDH might be more resistant to GTP/GDP inhibition, facilitating the intracellular accumulation of GTP when required [15], but no experimental evidence supporting this hypothesis has been obtained. Moreover, there is an evident lack of information regarding the structural details and the molecular mechanisms governing the dynamics of IMPDH cytoophidia assembly *in vitro*. Indeed, to our best knowledge, the *in vitro* reconstituted IMPDH filaments studied so far consist of a few particles organized into chains polymerized by a back-to-back assembly mechanism [2,4,5] that do not resemble the micrometer-long fibrillar IMPDH cytoophidia that are observed in cells [10,11,16–21].

In this study, we report the *in vitro* reconstitution of the assembly of the two human IMPDH enzymes into cytoophidia-like polymers and their structural and functional characterization. We show that micron-length human IMPDH cytoophidia-like structures spontaneously assemble *in vitro* under macromolecular crowding conditions in the absence of nucleotides but disassemble when either GTP or ATP is present in the solution, resembling what is observed within cells. The *in vitro* reconstituted IMPDH cytoophidia-like polymers are catalytically functional, with similar activity to non-assembled IMPDH, but they are significantly more resistant to GTP/GDP allosteric inhibition. Our results show that the cytoophidia dynamics and the allosteric regulation of the catalytic activity are tightly linked to the purine nucleotide-controlled conformational switch that we have previously reported for the *A. gossypii* fungal IMPDH [6,7]. They further provide a plausible structural mechanism for the nucleotide-dependent dynamics of cytoophidia assembly. Finally, we present the high-resolution crystal structures of human IMPDH isoform 2 complexed to GTP and GDP and demonstrate that most of the retinopathy-associated missense mutations map into the allosteric binding sites, altering nucleotide binding and subsequently abrogating GTP/GDP-induced allosteric inhibition of human IMPDH isoform 1. In addition, these mutations also alter cytoophidia dynamics, suggesting a potential pathological role for these assemblies that deserves to be further investigated.

Results

A nucleotide-controlled conformational switch operates in both human IMPDH isoforms

By using the IMPDH enzyme from the industrial fungus *A. gossypii,* we have recently reported a conformational switch that modulates the catalytic activity in response to the binding of purine nucleotides within the Bateman regulatory domain: adenine nucleotides (ATP, ADP and AMP) induce active IMPDH octamers in an extended (~115 Å long) conformation, while guanine nucleotides (GTP and GDP) induce inhibited octamers in a compact (~95 Å long) conformation [6]. Experimental evidence of the existence of this conformational switch in the isoform 2 of human IMPDH (HsIMPDH2) was recently reported by using electron microscopy (EM) on ATP and GTP-induced helical protofilaments [5]. Here, we have further investigated the nucleotide-conformational switch in both human IMPDH isoforms (HsIMPDH1 and HsIMPDH2) *in vitro* by using small-angle x-ray solution scattering (SAXS).

HsIMPDH1 and HsIMPDH2 wild-type proteins at the concentration used for the SAXS experiments (2.5 mg/mL) are mostly octamers in solution, but the addition of nucleotides induces stochastic oligomerization (see below) that results in poly-disperse solutions [2,4,5], which are not appropriate for SAXS analysis. Thereby, we made use of the missense mutation Y12A that has been previously reported to abrogate polymerization of HsIMPDH2 *in vitro* and in cultured cells [5]. Indeed, in the absence of nucleotides, HsIMPDH1-Y12A and HsIMPDH2-Y12A mutant enzymes remained as monodisperse tetramers in solution, as demonstrated by size-exclusion chromatography (Supplemental Fig. 1A). This observation

indicates that the octamers that exist in solution in the absence of nucleotides are most probably formed by the back-to-back interaction of the catalytic domains of two tetramers with a crucial role for residue Y12, as suggested in previous reports [2,5].

The addition of ATP or GDP to HsIMPDH1/2-Y12A induces the association of two tetramers to form octamers (Fig. 1A and B). Remarkably, the SAXS profiles of both human IMPDH isoforms resemble those described for the *A. gossypii* ATP or GDP-induced octamers (Supplemental Fig. 1B–D), demonstrating that the conformational switch previously proposed for the fungal *A. gossypii* AgIMPDH [6] is also present in both isoforms of the human IMPDH enzyme.

As shown in Supplemental Fig. 1E–F, ATP induces the formation of octamers more potently than GDP for both HsIMPDH1 and HsIMPDH2. Interestingly, significant differences are observed between both isoforms. In HsIMPDH1, the GDP-induced inhibition of the catalytic activity correlates with octamer compaction (Fig. 1C). In contrast, GDP-induced compact octamers of HsIMPDH2 are formed before inhibition occurs (Fig. 1D), highlighting mechanistic differences between both human isoforms that might be relevant *in vivo*. Nonetheless, when ATP is present in the solution, GDP-induced octamers of both HsIMPDH1 and HsIMPDH2 are formed before catalytic inhibition occurs (Fig. 1C and D).

In summary, our data show that the nucleotide-controlled conformational switch initially described for the *A. gossypii* enzyme also operates in both human IMPDH isoforms, where the binding of ATP or GDP induces octamers, formed by the interaction of the Bateman domains of two tetramers. The presence of adenine nucleotides in the solution induces octamers with an extended conformation that are catalytically active, while guanine nucleotides induce the compaction of these octamers, significantly inhibiting their enzymatic activity.

Retinopathy-associated mutations abrogate the allosteric inhibition of human IMPDH

To gain insights into the binding modes of purine nucleotides to the Bateman domain of human IMPDH, we attempted to obtain high-resolution structural information by x-ray crystallography. This issue is

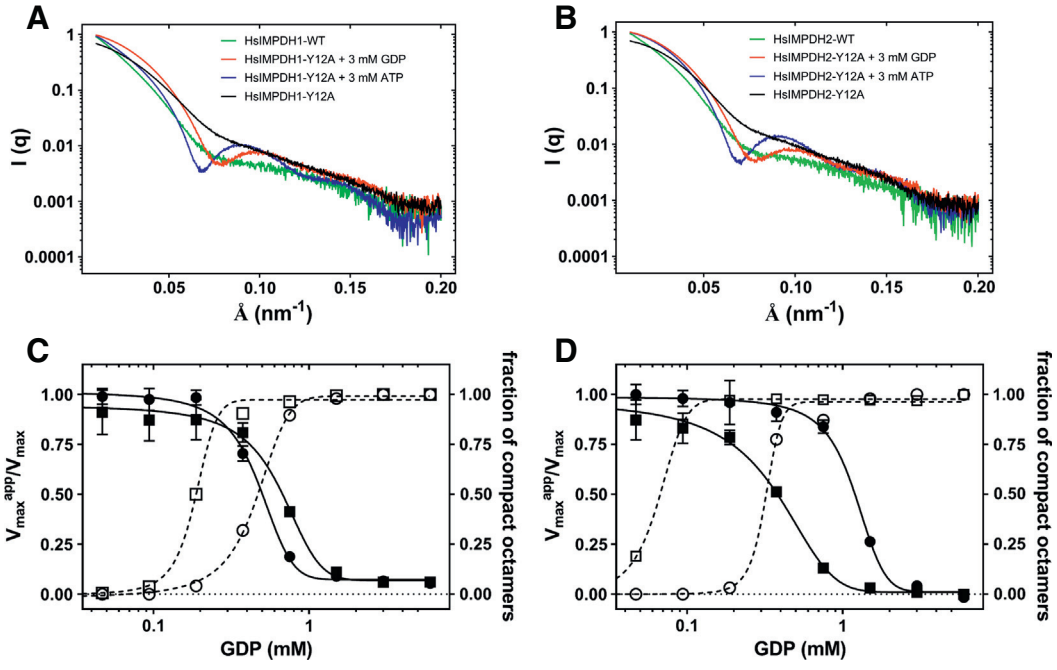


Fig. 1. The conformational switch of HsIMPDH controls its catalytic activity. (A and B) Experimental SAXS profiles of HsIMPDH1 (A) and HsIMPDH2 (B) wild-type and mutant Y12A (2.5 mg/mL) in the absence and presence of the indicated purine nucleotides. (C and D) Plots representing the fraction of compact octamers, as determined by SAXS, (empty symbols and dashed lines) and the catalytic activity (V_{max}^{app}/V_{max}; filled symbols and continuous lines) *versus* GDP concentration for HsIMPDH1-Y12A (C) and HsIMPDH2-Y12A (D). Squares: 3 mM ATP fixed concentration *versus* increasing concentrations of GDP. Circles: increasing concentrations of GDP in the absence of ATP. Data points represent the mean value and the standard errors. Lines represent the non-linear regression analysis of the experimental data, according to a standard allosteric sigmoidal equation (GraphPad Prism). At the fixed concentrations of ATP (3 mM) and GDP (3 mM) used for these experiments, HsIMPDH1-Y12A and HsIMPDH2-Y12A proteins remained as octamers with no detectable fraction of tetramers, as determined by SAXS.

especially relevant since, based on the *A. gossypii* fungal IMPDH structure, we have previously proposed that most of the retinopathy-associated missense mutations in HsIMPDH1 alter GTP/GDP-mediated allosteric inhibition [7]. Thereby, we solved the high-resolution crystal structures of HsIMPDH2 in complex with GTP and GDP, which are essentially identical (Supplemental Fig. 2A). A detailed description of these structures can be found in the Supplemental Information. Both structures unequivocally demonstrate that most of the retinopathy-associated mutations either (i) placed at the interface of two interacting Bateman domains: R224P, L227P and R231P (Supplemental Fig. 2C) or (ii) are directly involved in nucleotide binding at the allosteric sites of the Bateman domain: D226N for GTP/GDP2 (Supplemental Fig. 3B) and N198K and K238E for GTP3/GDP3 (Supplemental Fig. 3C).

We then introduced most of the missense mutations described in the literature [8] into HsIMPDH1 and purified the mutant enzymes for their analyses *in vitro*. Our results showed that the mutants had catalytic activity *in vitro* that fell within the same range (between 1.1- and 0.6-fold the activity of the WT; Fig. 2) as the WT enzyme. ATP showed no significant effect on the catalytic activity of both the WT and the mutant enzymes (between 1.0- and 0.6-fold the activity of the enzyme without nucleotide; Fig. 2). On the other hand, those mutations that map within the Bateman domain nucleotide binding sites (N198K, D226N and K238E; Supplemental Fig. 3) or at the interphase between the Bateman domains (R224P, L227P and R231P; Supplemental Fig. 2C) cannot be allosterically inhibited *in vitro* neither by GTP/GDP (Fig. 2), which thereby results in constitutively activated mutant enzymes.

In vitro reconstitution of micron-length human IMPDH cytoophidia assembly

We then investigated *in vitro* the ability of IMPDH to reversibly assemble into mesoscale structures that have been described to form within cells in response to the depletion of the intracellular guanine nucleotide pool [10,19,21]. It is important to stress here that several reports have shown that ATP and GTP induce the formation of IMPDH polymers *in vitro* [3–5], but these polymers consist of a few IMPDH octamers stacked back-to-back and organized into single filaments. Thereby, these polymers do not represent the IMPDH micron-length filamentous bundles that have been reported to form in cells [10,18,19,21].

These data suggest that an important factor is missing *in vitro*, but what could be this factor? An initial hint came from the published purification protocol of recombinant human IMPDH enzymes from *Escherichia coli* [21]. This protocol uses 1.5 M urea to keep the protein "soluble" in the supernatant after the initial centrifugation of the bacterial cell extracts. However, 1.5 M urea concentration is much lower than the midpoint of the urea-induced denaturation curve (approximately 5 M [22]), which indicates that there is no need to denature the IMPDH to "solubilize" it. We then hypothesized that IMPDH properly folds in the cytoplasm of *E. coli*; however, the high background concentration of macromolecules in the initial cell extracts favored the formation of large IMPDH assemblies that readily pelleted during a soft centrifugation.

We therefore tested the influence of macromolecular crowding on IMPDH filament assembly *in vitro* under different experimental conditions by monitoring protein assembly with turbidimetry. Our results showed that at high Ficoll-70 concentrations, both human IMPDH isoforms (HsIMPDH1 and HsIMPDH2) spontaneously assemble into large polymers, as indicated by the large increase in the turbidity of the solution (Fig. 3A and Supplemental Fig. 4A), and further corroborated by EM (upper panels of Fig. 3B and Supplemental Fig. 4B). At Ficoll-70 concentrations $\geq$150 mg/mL, most of the IMPDH is included within these polymers. These results led us to conclude that the formation of micron-length cytoophidia-like structures is due to the

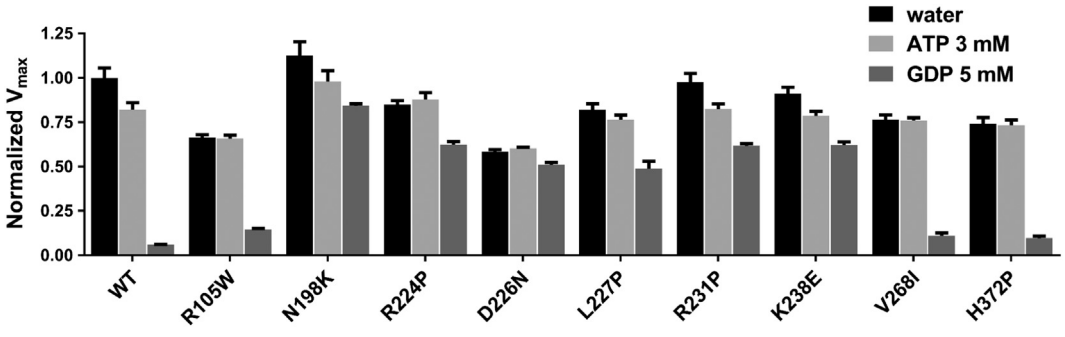


Fig. 2. Retinopathy-associated missense mutations disrupt GTP/GDP-mediated allosteric inhibition *in vitro*. Normalized catalytic activity (V_{max} derived from the Michaelis–Menten analysis of the experimental data) of HsIMPDH1-WT and retinopathy-associated mutants in the absence or presence of purine nucleotides. The error bars represent SEM.

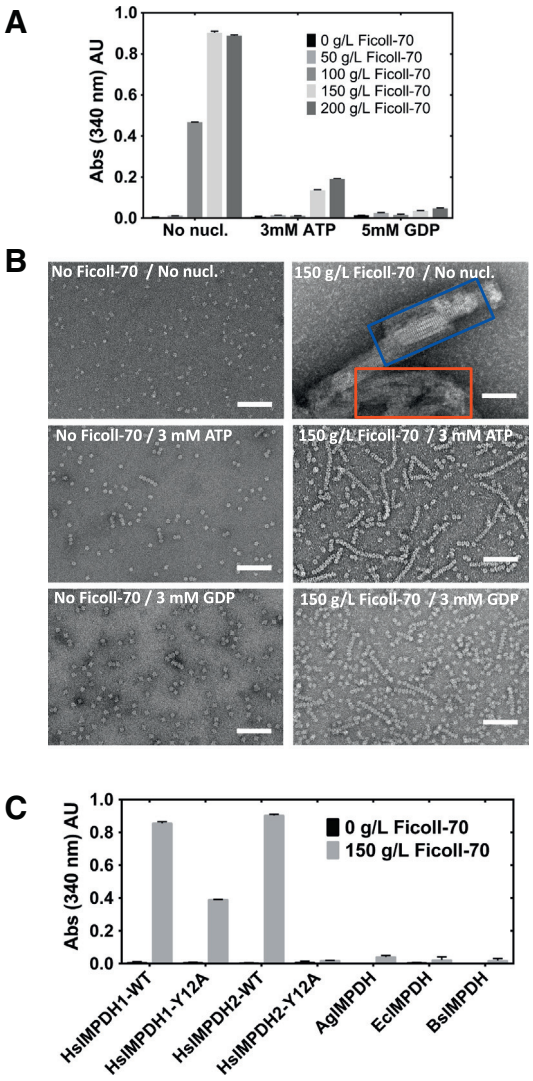


Fig. 3. *In vitro* reconstitution of human IMPDH cytoophidia assembly. (A) Turbidity measurements, indicating the formation of large polymers of HsIMPDH2, at different Ficoll-70 concentrations in the presence or absence of purine nucleotides. (B) EM analysis of the samples in the absence and presence Ficoll-70. The scale bars represent 100 nm. The red rectangle in the upper right panel shows bundles of twisted and curved filaments that intricate into the three dimensions without apparent regular or defined structure, while the blue rectangle shows ordered bundles of parallel protofilaments that were sporadically observed. (C) Turbidity measurements of purified IMPDH from different organisms. HsIMPDH1, *Homo sapiens* isoform 1; HsIMPDH2: *H. sapiens* isoform 2; AgIMPDH: *A. gossypii*; EcIMPDH: *E. coli*; BsIMPDH: *B. subtilis*. The error bars represent SEM.

macromolecular crowding conditions, since mesoscale polymerization can be detected neither at low crowding agent concentrations nor in its absence.

As a negative control, we used the Y12A missense mutation that has been previously reported to abrogate polymerization of HsIMPDH2 in cultured cells [5]. In accordance with this report, we were not able to detect significant assembly of the HsIMPDH2-Y12A mutant *in vitro* in dilute solutions or in crowding conditions (Fig. 3C). In contrast, we observed significant polymerization of the HsIMPDH1-Y12A mutant under macromolecular crowding conditions, although to a lower extent than the wild-type protein (Fig. 3C). These results agree with previous reports that describe a higher tendency to polymerize of HsIMPDH1 than HsIMPDH2 [23]. In addition, we tested whether the IMPDH enzymes from different organisms, other than humans, can also form cytoophidia-like polymers *in vitro*. Within Fig. 3C, it can be observed in that, in contrast to the two human isoforms, the eukaryotic *A. gossypii* (AgIMPDH), the bacterial *E. coli* (EcIMPDH) and *Bacillus subtilis* (BsIMPDH) enzymes are unable to form cytoophidia-like structures in our experimental conditions.

To further corroborate that eukaryotic AgIMPDH does not form cytoophidia, we ectopically overexpressed this gene in HeLa and HEK293T cells. As it is shown in Supplemental Fig. 4C, in contrast to HsIMPDH2 that showed a large amount of cytoophidia in essentially all the transfected cells, no detectable polymer formation was observed for AgIMPDH, despite the large amount of protein observed into the cytoplasm. Thereby, our results demonstrate that the ability of human IMPDH to form cytoophidia is not universal, since not all—eukaryotic or prokaryotic—IMPDH enzymes are able to assemble into large aggregates. In agreement with our results, other authors could neither find IMPDH polymers in the model yeast *Saccharomyces cerevisiae* [24].

The huge polymers of human IMPDH that formed *in vitro* under macromolecular crowding conditions are composed of octamers that associate into bundles of twisted and curved filaments that intricate into three dimensions without apparent regular or defined structure (red rectangle in the upper right panel of Fig. 3B and upper right panel of Supplemental Fig. 4B). Nonetheless, ordered bundles of parallel protofilaments were eventually observed within the huge polymers in some of the HsIMPDH2 micrographs (blue rectangle in the upper right panel in Fig. 3B). Direct distance measurements and power spectra analysis by fast Fourier transform of the protofilaments within these bundles showed a repetitive longitudinal spacing of 58.2 ± 0.4 Å. This longitudinal spacing is compatible with the expanded ATP-induced ~115-Å-long octamers previously observed by x-ray crystallography for AgIMPDH [6] and by SAXS for human IMPDH.

Remarkably, when ATP or GDP was present, the turbidity of the solution was significantly lower than in their absence (Fig. 3A and Supplemental Fig. 4A), indicating that these nucleotides inhibited the assembly of IMPDH into cytoophidia-like structures. The EM analysis of the polymers formed in the presence of purine nucleotides revealed either isolated octamers or

helical oligomers, extended for ATP and compacted for GDP (Fig. 3B and Supplemental Fig. 4B). A detailed analysis of the polymers formed in the presence of purine nucleotides can be found in the Supplemental Information, including the 3D reconstructions of ATP and GDP-induced protofilaments formed under macromolecular crowding conditions (Supplemental Fig. 5).

Moreover, once the cytoophidia-like polymers were spontaneously formed *in vitro*, the addition of either ATP or GDP depolymerized them, but the extent of this depolymerization strongly depended on the incubation time before nucleotide addition, that is, the maturation time [18]. The more mature the cytoophidia-like polymers are, the longer it takes to depolymerize them by GDP or ATP (Supplemental Fig. 6).

In summary, both human IMPDH isoforms spontaneously assemble *in vitro* into micron-length cytoophidia-like structures under macromolecular crowding conditions that resemble the cytoophidia found in cells. Under these conditions, the presence of purine nucleotides in the solution strongly reduces IMPDH cytoophidia formation, by both inhibiting assembly and inducing disassembly. Thus, our experimental setup reconstitutes *in vitro* the reversible guanine nucleotide-controlled cytoophidia assembly phenomenon previously reported to occur in cells. Our results also indicate a similar role for adenine nucleotides *in vitro*, although this observation remains to be corroborated *in vivo*.

Retinopathy-associated missense mutations in IMPDH1 alter the nucleotide-dependent cytoophidia dynamics *in vitro*

We next studied the nucleotide-dependent dynamics of the assembly of cytoophidia-like polymers *in vitro* for the HsIMPDH1 enzymes containing the retinopathy-associated mutations. All the mutants have the ability to spontaneously assembly into cytoophidia-like polymers to a similar extent than the wild-type enzyme (Fig. 4). Nonetheless, those mutants where the GTP/GDP allosteric inhibition is abrogated have also altered nucleotide-controlled regulation of cytoophidia-like assembly (Fig. 4) and disassembly (Supplemental Fig. 7A). The only exception is the mutant N198K that cannot be allosterically inhibited by GTP/GDP but possesses assembly dynamics comparable to the wild-type enzyme (Fig. 4 and Supplemental Fig. 7A). These data might indicate that the non-canonical guanine nucleotide binding site is needed for allosteric inhibition mediated by GTP/GDP, but is not implied in the regulation of assembly by nucleotides.

Remarkably, our data on cytoophidia-like structures assembled *in vitro* perfectly agree with a recent report that showed that HsIMPDH1 mutant enzymes R224P, D226N and R231P formed irreversible cytoophidia in transfected HEK293T cells when treated with guanosine [14].

IMPDH cytoophidia are catalytically active in vitro but more resistant to GTP/GDP inhibition

We next studied the effects of the polymerization into micron-length cytoophidia-like structures on the catalytic activity *in vitro.* To perform these experiments, we used as control the Y12A mutants that have compromised polymerization ability (Fig. 3C). Remarkably, we observed no significant differences between the catalytic activities of the Y12A mutants and the wild-type enzymes, neither in crowded nor in non-crowded solutions (Supplemental Table 2, Fig. 5A and B). The slight increase in the $K_{1/2}$ values between crowded and non-crowded conditions is most probably due to excluded volume and substrate limited diffusion effects, produced by the high concentrations of Ficoll-70. Indeed, similar differences in the $K_{1/2}$ values have

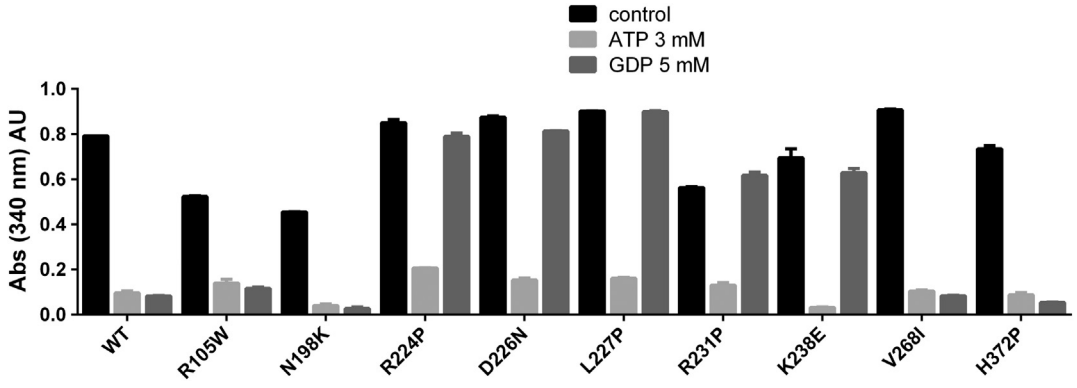


Fig. 4. Retinopathy-associated missense mutations alter IMPDH cytoophidia assembly *in vitro.* Turbidity measurements, indicating the formation of large polymers *in vitro*, at 150 g/L Ficoll-70 of HsIMPDH1 wild-type and retinopathy-associated mutants (0.25 mg/mL) in the absence or presence of purine nucleotides. Data were measured 10 min after dilution of the proteins into a solution containing Ficoll-70 and the indicated nucleotides. The error bars represent SEM.

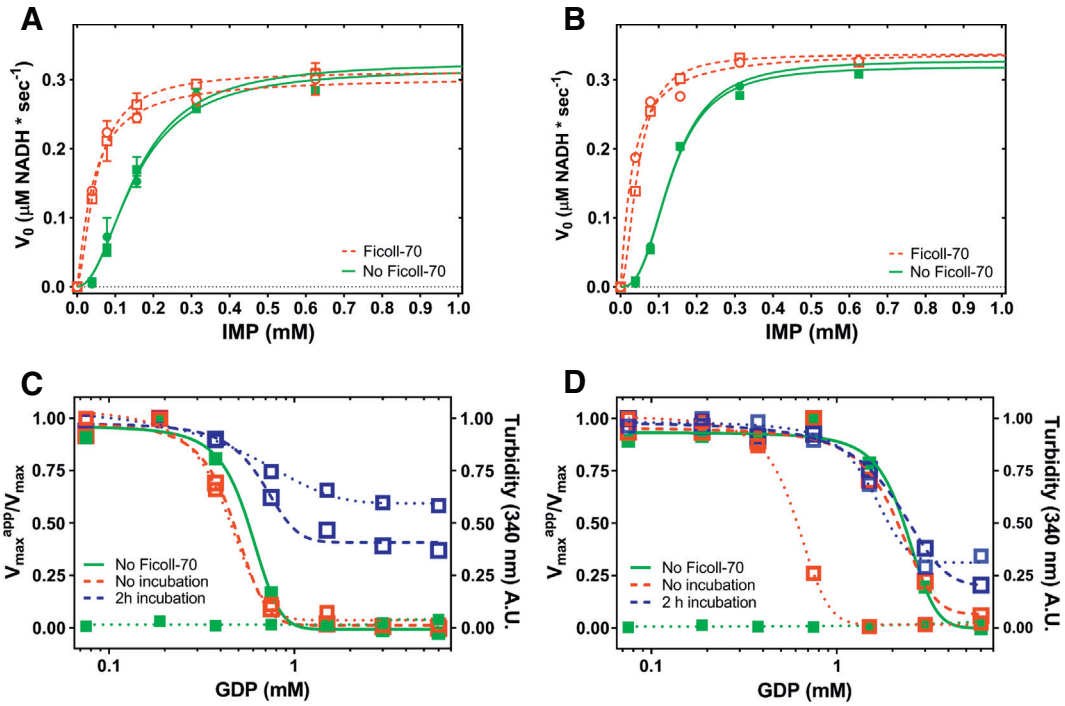


Fig. 5. Human IMPDH cytoophidia are catalytically active and resistant to GDP allosteric inhibition. (A and B) Michaelis–Menten representation of the catalytic activity of HsIMPDH1 (A) and HsIMPDH2 (B) wild-type (squares) and Y12A mutant (circles) in a dilute solution (solid figures and continuous green lines) and in the presence of 150 g/L Ficoll-70 (empty figures and discontinuous red lines). (C and D) Plots representing normalized solution turbidity (dotted lines) and catalytic activity (V_{max}^{app}/V_{max}; solid figures and continuous green line in the absence of Ficoll-70, empty figures and dashed red line for the short incubation with Ficoll-70, and empty figures and dashed blue line for the long incubation with Ficoll-70) at different GDP concentrations for HsIMPDH1-WT (C) and HsIMPDH2-WT (D). In our experimental setup, the measurements were performed approximately 30 min after GDP addition. Lines represent the non-linear regression analysis of the experimental data, according to a standard allosteric sigmoidal equation (GraphPad Prism). The error bars represent SEM.

been reported for a number of enzymes using similar crowding agents [25].

As an additional control, just before the measurements, we centrifuged the samples (5.000*g* for 10 min), so that the cytoophidia-like polymers were pelleted and the tetramers, octamers and small oligomers remained in the supernantant. The catalytic activity in the supernatant of the wild-type enzymes under crowding conditions was significantly reduced (Supplemental Fig. 7B), demonstrating that most of the catalytic activity comes from the IMPDH cytoophidia. In addition, most of the Y12A mutant enzyme that have compromised polymerization (Supplemental Fig. 7C) cannot be pelleted using these centrifugation conditions, therefore leaving the activity in the supernatant comparable to the activity prior to centrifugation (Supplemental Fig. 7B). From these experiments, we can conclude that IMPDH polymerization into micron-length cytoophidia-like structures did not significantly affect the catalytic activity in our *in vitro* experimental conditions.

Since GTP and GDP promote both cytoophidia disassembly and catalytic activity inhibition, it can be hypothesized that IMPDH polymerization might serve to fine-tune the allosteric regulation of the enzyme. To test this hypothesis, we studied how GDP affects the catalytic activity of the cytoophidia-like structures assembled in our *in vitro* system. As observed in Fig. 5C, non-mature polymers (without incubation before GDP addition) demonstrated inhibition of the catalytic activity while being depolymerized (red data) that showed no significant differences to the inhibition of the unassembled protein (green data). In contrast, the cytoophidia-like polymers that had been pre-incubated for 2 h before GDP addition, were more resistant to GDP-induced depolymerization (see also Supplemental Fig. 5) and, to a certain extent, were resistant to GDP allosteric inhibition (blue data). As expected, this behavior can also be observed for HsIMPDH2 but to a lesser extent (Fig. 5D), given that HsIMPDH2 is more sensitive to GDP-induced depolymerization than HsIMPDH1 (Supplemental Fig. 5). Moreover, HsIMPDH2 was depolymerized at lower GDP concentrations than those required to inhibit its catalytic activity (Fig. 5D). This observation agrees with the data presented above showing that GDP

induces octamer compaction at lower concentrations than those required for catalytic activity inhibition (Fig. 1D).

Discussion

Although there is wide knowledge on the enzymatic reaction mechanisms of IMPDH and its inhibition by a variety of molecules, there is an evident lack of information on its physiological mechanisms of regulation. Indeed, it has only been since the last few years that we have obtained the first experimental evidences on how the signal triggered by the binding of nucleotides to the regulatory Bateman domain is transmitted to the catalytic domain to modulate the enzymatic activity of IMPDH. To this respect, it has been recently described a conformational switch—controlled by purine nucleotides—that modulates the catalytic activity of eukaryotic IMPDH enzymes. The switch was first proposed by crystallography and x-ray scattering using the enzyme AgIMPDH from the industrial fungus *A. gossypii* [6] and was recently observed by EM with HsIMPDH2, the second isoform of human IMPDH [5]. We further demonstrate here that this conformational switch operates in both human IMPDH isoforms, suggesting that it might be conserved within all eukaryotic IMPDH enzymes. Moreover, a similar conformational switch, modulated by adenine nucleotides, has also been reported for some prokaryotic IMDPHs [2], despite the fact that these enzymes are not regulated by guanine nucleotides [7]. This observation suggests that the conformational switch is inherent to the acquisition of the Bateman regulatory domain, before the divergence of prokaryotic and eukaryotic enzymes. Nevertheless, the latter evolved separately to generate an additional non-canonical nucleotide binding site that allows the inhibition of the enzyme by GTP and GDP, the end products of the IMPDH's metabolic pathway.

Remarkably, we have found functional differences between the two human isoforms of IMPDH, where GTP/GDP-mediated allosteric inhibition of the catalytic activity is nicely correlated with octamer compaction in HsIMPDH1. In contrast, HsIMPDH2 octamer compaction occurs at lower GTP/GDP concentrations than those required for catalytic inhibition. These data, observed both in HsIMPDH2-Y12A (Fig. 1D) and HsIMPDH2-WT (Fig. 5D), indicate that additional features, other than octamer compaction itself, are required to inhibit HsIMPDH2. Possibly, the catalytic inhibition of IMPDH requires the binding of GTP/GDP to the three allosteric sites within the Bateman domain, while octamer compaction can happen with only a partial occupancy of these sites. Thereby, distinct affinities of GTP/GDP among the three nucleotide-binding sites of HsIMPDH1 and HsIMPDH2 might be the cause of the observed differences. In addition, our data show that HsIMPDH1 has a significantly higher tendency to filament than HsIMPDH2, in accordance with previous reports [23]. Future experimental studies will elucidate whether the different sensitivities to GTP/GDP-mediated allosteric inhibition and/or the different propensities to polymerize of the human IMPDH isoforms might have physiological consequences.

Presently, it is clearly accepted that the filamentation of enzymes to form cytoophidia serves as a general mechanism for the regulation of metabolism by fine-tuning protein functional and structural properties [12,13]. Indeed, enzyme filamentation seems to be rather extended with more than 20 metabolic enzymes reported to filament in *S. cerevisiae* [24]. Perhaps the most representative examples of cytoophidia-forming enzymes are those that catalyze the limiting steps in the *de novo* biosynthetic pathways of pyrimidine and purine nucleotides, CTPS and IMPDH, respectively.

Human CTPS filaments lock the enzyme into an active conformation, providing a mechanism for increasing the catalytic activity in response to metabolic state [26]. Similarly, human IMPDH cytoophidia formation correlates with rapid cell proliferation [11,14,15]; however, the *in vitro* reconstituted polymers show identical activity for both polymerized and non-assembled IMPDH [5]. In any case, the reported structural and functional data for IMPDH cytoophidia *in vitro* are based on polymers, induced by ATP or GTP, that are formed by the repeated back-to-back stacking of tetramers and octamers into single filaments [4,5], which do not represent the micrometer long and thick bundles observed in cells [10,19]. The results presented here demonstrate that these polymers do not represent cytoophidia but rather the remnants of their depolymerization. Our experimental conditions yield IMPDH polymer bundles *in vitro* with similar dimensions to the micron-length cytoophidia found in cells. Moreover, the dynamics of these polymers is modulated by guanine nucleotides *in vitro* in the same way as it has been observed in cells, as it will be discussed below. Thereby, our conditions allow a much better biochemical and structural characterization of this biological process.

The nucleotide-mediated steric self-compatibility of the Bateman interface and the highly symmetric structure of the octamers promote the assembly of IMPDH into the relatively thin and extended filaments that have been previously reported to form *in vitro* [4,5]. Nonetheless, once these filaments are formed, they are not able to significantly associate side by side to form the bundles that constitute cellular cytoophidia. The higher-order assembly into bundles of filaments proceeds only in the absence of nucleotides and seems to be a cooperative process, much less favorable than the nucleotide-induced single filament assembly is. Consistent with these observations, IMPDH assembly into micron-length cytoophidia-like structures depends on macromolecular crowding conditions, indicating that this assembly reaction is not only driven by enthalpy

due to specific interface interactions, but rather is also driven by entropy as a consequence of excluded volume effects [27]. Indeed, in a crowded *milieu*, oligomerization is greatly favored to minimize the overall crowding by enhancing protein association, which can thereby reduce the excluded volume [28]. The cytoophidia-like polymers assembled under these conditions are constituted by IMPDH octamers associated without an apparent order, although highly ordered specimens are also observed in the HsIMPDH2 micrographs. This observation indicates that the association of IMPDH octamers under crowding conditions confers high flexibility and dynamicity to the polymers, which is in further agreement with the observed variety of shapes that easily inter-convert in cells.

Our *in vitro* results reconstitute what it is observed in cells: IMPDH assemble into micron-length cytoophidia-like structures upon guanine nucleotide depletion but cytoophidia disassemble after guanine levels recover. This observation might also apply for the adenine nucleotides, because it is assumed that the levels of the adenine and guanine nucleotide pools rise or decrease in parallel, at least to a certain extent. Several mechanisms explain the parallel changes in adenine and guanine nucleotide levels. First, lowering the GTP levels might provoke a decrease in the adenine nucleotide levels through a dual action by (i) a reduced synthesis of AMP through adenylosuccinate synthetase, for which GTP serves as cofactor, and (ii) a greater degradation of AMP by AMP deaminase, which is inhibited by GTP. Second, an interplay exists between the syntheses of AMP/ATP and GMP/GTP from IMP, where ATP is required for the synthesis of GMP at the level of GMP synthase.

In addition, it will be interesting to study how the presence of substrates and products affect cytoophidia dynamics, as it has been very recently reported that the intracellular IMP accumulation promotes cytoophidia assembly, whereas elevated GTP level triggers the disassociation of aggregates [14]. Therefore, the balance GTP/IMP might be an additional important factor in regulating cytoophidia dynamics that definitively deserves to be investigated. For instance, it can be expected that IMP, bound to the active site, might somehow affect GTP-induced octamer compaction, given that this compaction implies the interaction of the finger domains, which place adjacent to—and interact with—the active site.

How do adenine and guanine nucleotides modulate IMPDH polymerization? A plausible explanation is that these nucleotides induce IMPDH octamer conformations that allow a few octamers to stack back-to-back and form short lineal filaments [4,5], but these filaments do not significantly associate laterally to form the large bundles that constitute the cytoophidia-like polymers. In contrast, in the absence of purine nucleotides, human IMPDH adopts a conformation that under crowding conditions favors both filament formation and filament bundling. A schematic representation of this hypothesis is shown in Fig. 6. In support of this hypothesis, three different conformations for eukaryotic IMPDHs have been reported (Fig. 6): (i) ATP-induced extended active octamers (5MCP, [6]), (ii) GTP/GDP-induced compacted inhibited octamers (6I0O, 6I0M in this work and 4Z87 [7]), and (iii) extended octamers with no nucleotide bound at the Bateman domain (1NF7 and 1NFB). The structures of the apo-enzyme and the ATP-induced IMPDH octamers have similar dimensions, but they significantly differ in the bending of the Bateman module that increases upon ATP binding (Fig. 6). Therefore, it is then tempting to speculate that the less bent Bateman module of the apo-enzyme octamers favors the lateral packing of the single filaments that result in large micrometric bundles. On the contrary, the increased bending of the Bateman module, induced by the binding of either ATP or GTP/GDP to the allosteric sites, avoids the lateral association of octamers and single protofilaments that consequently avoids the formation of cytoophidia-like structures (Fig. 6). Indeed, the crystal packing of 1NF7 (Supplemental Fig. 8A) would be compatible with the repetition pattern observed in the ordered bundles of HsIMPDH2 found in some of the micrographs of the *in vitro* reconstituted cytoophidia-like polymers (Fig. 3B) and in a previous report [19], suggesting that this crystal might be mimicking the packing of IMPDH within the cytoophidia.

Our results demonstrate that assembly into cytoophidia-like structures does not significantly change the catalytic activity of purified IMPDH *in vitro*. These results agree with a previous report that could neither find differences in catalytic activity between a mutant unable to polymerize (HsIMPDH2-Y12A) and the wild-type enzyme, both *in vitro* and in cultured cells [5]. In turn, IMPDH assembly modulates the sensitivity of the enzyme to allosteric inhibition. Remarkably, the more mature the cytoophidia-like polymers (longer incubation times) are, the more resistant to GTP/GDP-induced octamer compaction they become and thereby more resistant to depolymerization and subsequent inhibition of the catalytic activity. In other words, the more mature a cytoophidia-like polymer is, the longer it takes to depolymerize by GTP/GDP. At this point, it remains unknown how maturation time correlates to resistance to GDP-induced octamer compaction *in vitro*, but it is clear that it might have important physiological implications. The longer a cell remains in a state of guanine nucleotide deprivation, the longer it will take to recover, that is, the longer IMPDH should work actively in the absence of negative feedback inhibition. Therefore, IMPDH cytoophidia formation and maturation might constitute a mechanism to temporal and spatially regulate the ability of IMPDH polymers to maintain especially high intracellular levels of guanine nucleotides when required, for example, for active cell proliferation or after a pharmacological depletion of the guanine nucleotide pools. At this point, it is important to

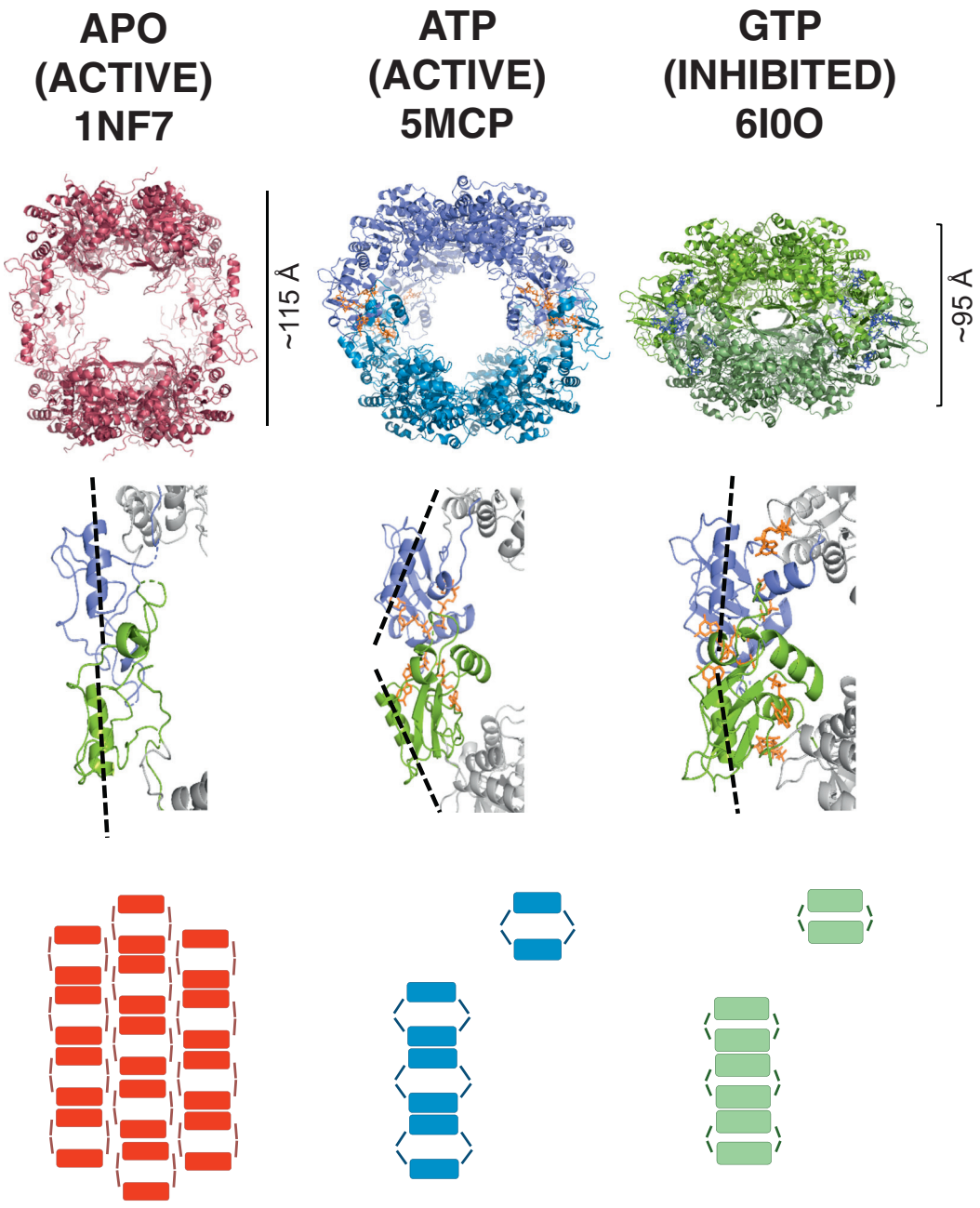


Fig. 6. The nucleotide controlled-conformational switch of human IMPDH. Upper panels: the three different octamer conformations observed in eukaryotic IMPDH enzymes and their respective PDB codes. IMPDH protein is shown in cartoons and nucleotides in sticks. The approximate longitudinal dimensions of the octamers are indicated on their side. Middle panels: close-up view of two interacting Bateman domains from adjacent tetramers within the octameric arrangement. The black dashed lines show the approximate longitudinal axis of helices comprising residues 194–204. Lower panels: schematic representation of the assembly of human IMPDH into different polymers.

stress that this study was performed *in vitro*, from purified components, but it is envisaged that *in vivo* post-translational modifications and interaction partners will play an important role in the regulation of the dynamics of IMPDH cytoophidia assembly.

Finally, we demonstrate that the mutations in HsIMPDH1 associated with human retinopathies map into the allosteric nucleotide binding sites, which therefore alter the nucleotide-controlled conformational switch. Subsequently, they also disrupt allosteric inhibition mediated by GTP/GDP and modify the dynamics of the cytoophidia-like polymers *in vitro*. Thereby, our data indicate that the HsIMPDH1 mutations within the first instance will affect the intracellular

levels of the purine nucleotide pools in retinal cells that, in a medium/long term, will lead to visual receptor cell death and subsequent retinal degeneration. Future studies are needed to elucidate the molecular details on how the alterations in the nucleotide pools develop into retinopathies. Moreover, it will also be very interesting to explore the potential physiological roles that cytoophidia play in retinal development. Indeed, in preliminary experiments, we were able to detect IMPDH cytoophidia in the retina of adult mice as 1- to 2-μm-long structures, mostly localized in the periphery of the retina, although they were detected throughout this organ (Supplemental Fig. 8B). Altogether, these data indicate that cytoophidia form in the retina *in vivo* under normal developmental conditions and suggest a potential physiological role of cytoophidium that might be altered by the retinopathy-associated missense mutations of human IMPDH1.

The data presented in this manuscript show that the effective concentrations of GDP that affect the IMPDH conformational switch, the polymerization dynamics, and the inhibition of the catalytic activity, lie roughly in the same range than the expected intracellular GTP/GDP concentrations, this is, in the 0.1- to 1-mM range [29]. Therefore, our *in vitro* data suggest that the molecular mechanisms we propose might be relevant *in vivo* at the expected physiological intracellular nucleotide concentrations, although this hypothesis awaits experimental confirmation.

In summary, our results provide novel and valuable information for understanding the physiological regulation of IMPDH as well as deciphering the putative roles of IMPDH cytoophidia *in vivo*, both under physiological and pathological conditions. Moreover, given that IMPDH is a widely validated drug target in several types of diseases, the reported results might eventually support future studies to determine the therapeutic potential of the cytoophidium as a useful target and/or biomarker.

Materials and Methods

Proteins and nucleotides

Expression and purification of IMPDH proteins was performed as previously described [7,21]. Nucleotides were purchased from Sigma-Aldrich and Jena Bioscience. Missense mutations were introduced into the bacterial expression vectors by using QuickChange II Site-directed mutagenesis protocol (Agilent Technologies).

Protein polymerization analysis *in vitro*

In vitro polymerization was monitored by turbidimetry at 340 and 410 nm on a spectrophotometer by using proteins, purified to homogeneity, at a concentration of 0.1–0.25 mg/mL in buffer 100 mM Tris–HCl, 100 mM KCl, 2 mM DTT and 1 mM $MgCl_2$ (final free Mg^{+2} concentration; pH 8.0) and in the presence of the indicated amounts of Ficoll-70 and/or nucleotides.

Control experiments were also performed by pelleting the polymers by centrifugation and determining the protein concentration in pellets and supernatants by spectrophotometry and/or SDS-PAGE densitometry. Samples of protein polymers were taken from each experiment for further analysis by EM (see below).

Enzyme kinetics assay

IMPDH activity was assayed, as previously reported [6], at 32 °C using 96 or 384-well microtiter plates by monitoring the reduction of NAD^+ and the subsequent increase in absorbance at 340 nm. All the enzyme kinetics and inhibition experiments were performed by using a fixed concentration of enzyme (100 μg/mL) and NAD^+ (0.5 mM), while IMP varied from 0.04 to 5 mM. The reaction buffer was 100 mM Tris–HCl, 100 mM KCl, 2 mM DTT and 1 mM $MgCl_2$ (final free Mg^{+2} concentration; pH 8.0).

Initial velocities (V_0) were extracted from the time-course reaction progress curves, which were then fitted by non-linear regression analysis to an allosteric sigmoidal equation using GraphPad Prism (GraphPad Prism Software, Inc.) to estimate the $K_{1/2}$ and V_{max} values. It must be stated here that, given the high concentration of enzyme used for these experiments, the steady state in the lowest substrate concentrations cannot be ensured, which might influence the precision of the calculated $K_{1/2}$ values.

To monitor enzyme kinetics under macromolecular crowding conditions, where turbidity might interfere with the measurement at λ = 340 nm, the catalytic reaction was stopped by incubating the samples with 4 M urea (final concentration) to disaggregate protein assemblies and avoid the turbidity of the solution. These experiments demonstrated that the constant background at λ = 340 nm due to the presence of turbidity in the solution could be easily subtracted from the raw measurements, without affecting the precise estimation of the kinetic parameters.

For control experiments, HsIMPDH1/2-WT and HsIMPDH1/2-Y12A mutant enzymes under macromolecular crowding conditions were centrifuged at 5000*g* for 10 min at 25 °C, to pellet the cytoophidia-like polymers, and the catalytic activity of the supernatants was measured as described above.

SAXS

SAXS measurements were performed at the B21 beamline at the Diamond Light Source. Protein samples at 2.5 mg/mL in buffer 20 mM Tris–HCl, 300 mM KCl, 1 mM $MgCl_2$ (final free Mg^{+2} concentration) and 3 mM DTT (pH 8.0) were measured in the presence of increasing amounts of nucleotides (total concentration of nucleotides ranging from 0.02 to

3 mM). Experimental data were reduced following standard methodologies by using the program PRIMUS. The fractions of tetramers, and expanded and compacted octamers were calculated with the program OLIGOMER and the theoretical solution scattering profiles with CRYSOL. All these programs are found within the ATSAS software suite [30].

Crystallization and structure determination

Crystals of the complexes HsIMPDH2-GTP and HsIMPDH2-GDP were grown at 22 °C using the vapor diffusion method by mixing a protein solution at 7.5 mg/mL in 10 mM Tris–HCl, 150 mM KCl, 1 mM DTT, 7.5 mM GTP (or GDP) and 5 mM total $MgCl_2$ (pH 8.0), with an equal volume of mother liquor consisting of 25% PEG-1500 and 0.1 M buffer MIB (malonic acid, imidazole and boric acid) at pH 9.0 for HsIMPDH-GTP and 0.1 M sodium citrate at pH 5.5, 0.2 M lithium sulfate and 15% ethanol for HsIMPDH2-GDP. Protein crystals were flashed-cooled in liquid nitrogen, and data were collected at 100 K, using monochromatic x-rays of ≈1 Å wavelength, at the MX beamlines of the Diamond Light Source synchrotron (UK) or the XALOC beamline in the ALBA synchrotron (Spain). Crystals of HsIMPDH2-GDP were cryo-protected by immersion in NVH oil before being flashed-cooled in liquid nitrogen. Diffraction intensities were indexed and integrated by using the software autoPROC [31].

The experimental data were phased by molecular replacement using the program PHASER [32] using as template the structure of the complex AgIMPDH-GDP (PDB code 4Z87). The structures were iteratively refined by alternating manual modeling with COOT [33] with the automated refinement utility of the PHENIX crystallographic software suite [34]. Rigid body, gradient-driven positional, restrained individual isotropic B-factor and TLS were used for structure refinement.

EM

Samples were analyzed by EM after being adsorbed to glow-discharged carbon coated grids and stained with 2% uranyl acetate. Grids were observed using a JEOL JEM-1230 transmission electron microscope operated at 100 kV and a nominal magnification of 40.000. Images were taken under low-dose conditions with a CMOS Tvips TemCam-F416 camera, at 2.84 Å per pixel. Image processing was performed using SCIPION package [35]. The contrast transfer function of the microscope for each micrograph was estimated using CTFFIND4 [36]. Helical segments were picked from the micrographs using the Xmipp3 manual-picking routine implemented inside SCIPION.

In the initial step, images of the helical segments were extracted and horizontally pre-aligned using a multi-reference pattern-free alignment protocol [37]. After pre-alignment, images were two-dimensional classified using RELION software [38] limiting in-plane rotations, allowing bimodal search and using a rectangular mask to focus the classification process in the helix. Classes containing the straightest particles were selected for 3D reconstruction. Initial model was built by assigning random rotation angles to the images and 3D reconstructed. This procedure generates featureless tubular structures suitable as a starting model for 3D classification in RELION; this classification was performed with no symmetry application to avoid initial bias in the reconstructions. Afterward, the selected classes were also refined without the application of helical symmetry. When the angular assignment of the images reached convergence, symmetry parameters of the volumes were determined using the "xmipp_volume_find_symmetry" utility and applied. Finally, a new cycle of refinement, applying symmetry, was carried out to generate the final structures.

Figures of protein structures, electron density maps and EM maps were rendered by using PyMOL (The PyMOL Molecular Graphics System, Version 2.0 Schrödinger, LLC).

Immunofluorescence

HeLa cells were grown onto poly-L-Lysine coated glass coverslips and fixed with 2.5% paraformaldehyde for 30 min at room temperature, washed three times with PBS, permeabilized for 10 min with Triton 0.1% X100 and blocked with 1% BSA for another 10 min. The primary antibody (mouse anti-HA 12CA5, Roche) was used at a 1:5000 dilution and incubated for 2 h at room temperature. The secondary antibody (Alexa-488 anti-mouse) was used at a 1:2000 dilution and incubated overnight at 4 °C. Cells were then washed with 1% BSA, and the nuclei were stained with DAPI.

Mice retinas were fixed by immersion in 4% paraformaldehyde for 4 h at 4 °C. The tissue was cryo-protected in 30% sucrose and embedded in OCT, and 16-μm sections were obtained. Sections were washed in PBS and blocked with 5% BSA, 2% goat serum and 0.1% Triton X100. Primary antibody (IMPDH, H-300; Santa Cruz; sc-50510) was incubated at a 1:30 dilution overnight at 4 °C and detected with a secondary antibody anti-rabbit Alexa-488 used at a 1:300 dilution, for 1 h at room temperature. Nuclei were stained with DAPI.

Accession numbers

The atomic coordinates and the structure factors described in this work have been deposited in the Research Collaboratory for Structural Bioinformatics Protein Data Bank under the codes PDB ID: 6I0O (HsIMPDH2-GTP) and PDB ID: 6I0M (HsIMPDH2-GDP). The EM-derived maps have been deposited in the Electron Microscopy Data Bank under the accession codes EMD ID: 4402 (HsIMPDH1-GDP) and EMD ID: 4403 (HsIMPDH1-ATP).

Acknowledgments

This work was supported by the Spanish Ministerio de Ciencia, Innovación y Universidades (grants BFU2016-79237-P to R.M.B. and BIO2014-56930-P to J.L.R.). D.F.J. was supported by a pre-doctoral contract from the "Junta de Castilla y León". We thank María Dolores Sánchez, Silvia Domínguez and Marta Santos for excellent technical help; Ángel Hernández for help with cell cultures; and Germán Rivas, José M de Pereda and Kyle B del Valle for their valuable comments and suggestions to the manuscript. Protein crystallography experiments were performed at the i03 beamline (Diamond Light Source, UK) and XALOC (ALBA Synchrotron, Spain) beamlines with the collaboration of Diamond and ALBA staff. X-ray scattering experiments were performed at the B21-Solution State SAXS beamline (Diamond Light Source, UK).

Appendix A. Supplementary data

Supplementary data to this article can be found online at https://doi.org/10.1016/j.jmb.2019.01.020.

Received 12 November 2018;
Received in revised form 9 January 2019;
Accepted 10 January 2019
Available online 18 January 2019

Keywords:
IMP dehydrogenase;
cytoophidia;
conformational switch;
allosteric regulation;
x-ray crystallography and scattering

Present address: E.M. Soriano, Institute for Cardiovascular and Metabolic Research, School of Biological Sciences, Harborne building, University of Reading, Whiteknights, Reading, RG6 6AS, United Kingdom.

Abbreviations used:
IMPDH, inosine 5′-monophosphate dehydrogenase; CTPS, CTP synthase; HsIMPDH2, isoform 2 of human IMPDH; SAXS, small-angle x-ray solution scattering; EM, electron microscopy; HsIMPDH1, isoform 1 of human IMPDH.

References

[1] L. Hedstrom, IMP dehydrogenase: structure, mechanism, and inhibition, Chem. Rev. 109 (2009) 2903–2928.
[2] G. Labesse, T. Alexandre, L. Vaupré, I. Salard-Arnaud, J. Him, B. Raynal, et al., MgATP regulates allostery and fiber formation in IMPDHs, Structure 21 (2013) 975–985.
[3] G. Labesse, T. Alexandre, M. Gelin, A. Haouz, H. Munier-Lehmann, Crystallographic studies of two variants of *Pseudomonas aeruginosa* IMPDH with impaired allosteric regulation, Acta Crystallogr. D Biol. Crystallogr. 71 (2015) 1890–1899.
[4] Y. Ji, J. Gu, A. Makhov, J. Griffith, B. Mitchell, Regulation of the interaction of inosine monophosphate dehydrogenase with mycophenolic acid by GTP, J. Biol. Chem. 281 (2006) 206–212.
[5] S.A. Anthony, A.L. Burrell, M.C. Johnson, K.C. Duong-Ly, Y.M. Kuo, J.C. Simonet, et al., Reconstituted IMPDH polymers accommodate both catalytically active and inactive conformations, Mol. Biol. Cell 28 (2017) 2600–2608.
[6] R.M. Buey, D. Fernandez-Justel, I. Marcos-Alcalde, G. Winter, P. Gomez-Puertas, J.M. de Pereda, et al., A nucleotide-controlled conformational switch modulates the activity of eukaryotic IMP dehydrogenases, Sci. Rep. 7 (2017) 2648.
[7] R.M. Buey, R. Ledesma-Amaro, A. Velazquez-Campoy, M. Balsera, M. Chagoyen, J.M. de Pereda, et al., Guanine nucleotide binding to the Bateman domain mediates the allosteric inhibition of eukaryotic IMP dehydrogenases, Nat. Commun. 6 (2015) 8923.
[8] D.A. McGrew, L. Hedstrom, Towards a pathological mechanism for IMPDH1-linked retinitis pigmentosa, Adv. Exp. Med. Biol. 723 (2012) 539–545.
[9] A.M. Pedley, S.J. Benkovic, A new view into the regulation of purine metabolism: the purinosome, Trends Biochem. Sci. 42 (2017) 141–154.
[10] W.C. Carcamo, M. Satoh, H. Kasahara, N. Terada, T. Hamazaki, J.Y. Chan, et al., Induction of cytoplasmic rods and rings structures by inhibition of the CTP and GTP synthetic pathway in mammalian cells, PLoS One 6 (2011), e29690.
[11] C.C. Chang, W.C. Lin, L.M. Pai, H.S. Lee, S.C. Wu, S.T. Ding, et al., Cytoophidium assembly reflects upregulation of IMPDH activity, J. Cell Sci. 128 (2015) 3550–3555.
[12] G.N. Aughey, J.L. Liu, Metabolic regulation via enzyme filamentation, Crit. Rev. Biochem. Mol. Biol. 51 (2015) 282–293.
[13] H. Wang, Q.-X. Saho, The cytoophidium: a novel intracellular compartmentation formed by metabolic enzymes, Acad. J. Biotechnol. 5 (2017) 7.
[14] G.D. Keppeke, C.C. Chang, M. Peng, L.Y. Chen, W.C. Lin, L.M. Pai, et al., IMP/GTP balance modulates cytoophidium assembly and IMPDH activity, Cell Div 13 (2018) 5.
[15] K.C. Duong-Ly, Y.M. Kuo, M.C. Johnson, J.M. Cote, J.M. Kollman, J. Soboloff, et al., T cell activation triggers reversible inosine-5′-monophosphate dehydrogenase assembly, J. Cell Sci. 131 (2018).
[16] S.J. Calise, W.C. Carcamo, C. Krueger, J.D. Yin, D.L. Purich, E.K. Chan, Glutamine deprivation initiates reversible assembly of mammalian rods and rings, Cell. Mol. Life Sci. 71 (2014) 2963–2973.
[17] S.J. Calise, D.L. Purich, T. Nguyen, D.A. Saleem, C. Krueger, J.D. Yin, et al., 'Rod and ring' formation from IMP dehydrogenase is regulated through the one-carbon metabolic pathway, J. Cell Sci. 129 (2016) 3042–3052.
[18] C.C. Chang, G.D. Keppeke, L.Y. Sung, J.L. Liu, Interfilament interaction between IMPDH and CTPS cytoophidia, FEBS J. 285 (2018) 3753–3768.
[19] P. Juda, J. Smigova, L. Kovacik, E. Bartova, I. Raska, Ultrastructure of cytoplasmic and nuclear inosine-5′-monophosphate dehydrogenase 2 "rods and rings" inclusions, J. Histochem. Cytochem. 62 (2014) 739–750.

[20] J.L. Liu, The cytoophidium and its kind: filamentation and compartmentation of metabolic enzymes, Annu. Rev. Cell Dev. Biol. 32 (2016) 349–372.
[21] E. Thomas, J. Gunter, J. Webster, N. Schieber, V. Oorschot, R. Parton, et al., Different characteristics and nucleotide binding properties of inosine monophosphate dehydrogenase (IMPDH) isoforms, PLoS One 7 (12) (2012).
[22] E. Nimmesgern, T. Fox, M.A. Fleming, J.A. Thomson, Conformational changes and stabilization of inosine 5′-monophosphate dehydrogenase associated with ligand binding and inhibition by mycophenolic acid, J. Biol. Chem. 271 (1996) 19421–19427.
[23] J.H. Gunter, E.C. Thomas, N. Lengefeld, S.J. Kruger, L. Worton, E.M. Gardiner, et al., Characterisation of inosine monophosphate dehydrogenase expression during retinal development: differences between variants and isoforms, Int. J. Biochem. Cell Biol. 40 (2008) 1716–1728.
[24] Q.J. Shen, H. Kassim, Y. Huang, H. Li, J. Zhang, G. Li, et al., Filamentation of metabolic enzymes in *Saccharomyces cerevisiae*, J. Genet. Genomics 43 (2016) 393–404.
[25] T. Vopel, G.I. Makhatadze, Enzyme activity in the crowded milieu, PLoS One 7 (2012), e39418.
[26] E.M. Lynch, D.R. Hicks, M. Shepherd, J.A. Endrizzi, A. Maker, J.M. Hansen, et al., Human CTP synthase filament structure reveals the active enzyme conformation, Nat. Struct. Mol. Biol. 24 (2017) 507–514.
[27] G. Rivas, A.P. Minton, Macromolecular crowding in vitro, in vivo, and in between, Trends Biochem. Sci. 41 (2016) 970–981.
[28] A.P. Minton, The influence of macromolecular crowding and macromolecular confinement on biochemical reactions in physiological media, J. Biol. Chem. 276 (2001) 10577–10580.
[29] T.W. Traut, Physiological concentrations of purines and pyrimidines, Mol. Cell. Biochem. 140 (1994) 1–22.
[30] D. Franke, M.V. Petoukhov, P.V. Konarev, A. Panjkovich, A. Tuukkanen, H.D.T. Mertens, et al., ATSAS 2.8: a comprehensive data analysis suite for small-angle scattering from macromolecular solutions, J. Appl. Crystallogr. 50 (2017) 1212–1225.
[31] C. Vonrhein, C. Flensburg, P. Keller, A. Sharff, O. Smart, W. Paciorek, et al., Data processing and analysis with the autoPROC toolbox, Acta Crystallogr. D Biol. Crystallogr. 67 (2011) 293–302.
[32] A.J. McCoy, R.W. Grosse-Kunstleve, P.D. Adams, M.D. Winn, L.C. Storoni, R.J. Read, Phaser crystallographic software, J. Appl. Crystallogr. 40 (2007) 658–674.
[33] P. Emsley, B. Lohkamp, W.G. Scott, K. Cowtan, Features and development of Coot, Acta Crystallogr. D Biol. Crystallogr. 66 (2010) 486–501.
[34] P.D. Adams, P.V. Afonine, G. Bunkoczi, V.B. Chen, I.W. Davis, N. Echols, et al., PHENIX: a comprehensive Python-based system for macromolecular structure solution, Acta Crystallogr. D Biol. Crystallogr. 66 (2010) 213–221.
[35] J.M. de la Rosa-Trevin, A. Quintana, L. Del Cano, A. Zaldivar, I. Foche, J. Gutierrez, et al., Scipion: a software framework toward integration, reproducibility and validation in 3D electron microscopy, J. Struct. Biol. 195 (2016) 93–99.
[36] A. Rohou, N. Grigorieff, CTFFIND4: fast and accurate defocus estimation from electron micrographs, J. Struct. Biol. 192 (2015) 216–221.
[37] C.O. Sorzano, J.R. Bilbao-Castro, Y. Shkolnisky, M. Alcorlo, R. Melero, G. Caffarena-Fernandez, et al., A clustering approach to multireference alignment of single-particle projections in electron microscopy, J. Struct. Biol. 171 (2010) 197–206.
[38] S.H. Scheres, RELION: implementation of a Bayesian approach to cryo-EM structure determination, J. Struct. Biol. 180 (2012) 519–530.

SUPPLEMENTAL INFORMATION

A nucleotide-dependent conformational switch controls the polymerization of human IMP dehydrogenases to modulate their catalytic activity

David Fernández-Justel[1], Rafael Núñez[2], Jaime Martín-Benito[3], David Jimeno[4], Adrián González-López[1], Eva María Soriano[1,5], José Luis Revuelta[1*] & Rubén M Buey[1*]

[1]Metabolic Engineering Group, Dpto. Microbiología y Genética. Universidad de Salamanca. Campus Miguel de Unamuno, 37007, Salamanca, Spain

[2]Centro de Investigaciones Biológicas (CIB), Spanish National Research Council (CSIC), Ramiro de Maeztu 9, 28040 Madrid, Spain

[3]Centro Nacional de Biotecnología (CNB), Spanish National Research Council (CSIC), Darwin 3, 28039 Madrid, Spain

[4]Instituto de Biología Molecular y Celular del Cáncer (CSIC-Universidad de Salamanca). Campus Miguel de Unamuno, 37007, Salamanca. Spain

[5]Present address: Institute for Cardiovascular and Metabolic Research, School of Biological Sciences, Harborne building, University of Reading, Whiteknights, Reading, RG6 6AS, United Kingdom

[*]Correspondence: J.L.R. (revuelta@usal.es) or R.M.B. (ruben.martinez@usal.es)

Crystal structures of HsIMPDH2 in complex with GTP and GDP. We solved the high-resolution crystal structures of HsIMPDH2 in complex with GTP and GDP at 2.6 Å resolution. Both crystals belong to the space group I422 (Supplemental Table 1) with two monomers in the asymmetric unit (AU), located around a quaternary symmetry axis that generates the octameric biological assembly, composed by a dimer of tetramers that interact head-to-head. There are no significant differences between the structures of IMPDH bound to GTP or GDP (Supplemental Figure 2A). The electron density for most of the protein residues was clearly visible, with the exception of the N and C-terminal residues, and some short exposed loops. Additionally, in our structures, there was no interpretable electron density for the residues that compose the catalytic flap, suggesting that they are disordered within the crystal lattice. Three nucleotide molecules were bound in the regulatory Bateman domain: two GTP/GDP molecules were bound into the canonical sites (GTP1/GDP1 and GTP2/GDP2, bound to the first and second binding sites) while a third GTP/GDP molecule was bound into the third non-canonical site (GTP3/GDP3) that we have previously described for the IMPDH from *Ashbya gossypii* [1]. The nucleotide conformations are essentially identical for both GTP and GDP structures in all the three nucleotide binding sites. Furthermore, there are no significant differences in the protein residues that interact with both nucleotides (Supplemental Figure 2B). These data demonstrate that the structural and the functional effects of GTP and GDP are essentially identical.

The octamers of IMPDH are stabilized by the interface that involves the Bateman domains from the upper and the lower tetramers, alongside the interaction of the finger domains that are forced to interact, which results in the inhibition of the catalytic activity that we have previously proposed [1]. The interface between the two Bateman domains is mostly stabilized by hydrogen bonds between the side chain atoms of residues K205 and R224 in a monomer with the respective side chains of residues D162 and D164 in the adjacent Bateman domain. The side chain of residue R161 also contacts the phosphates of the GTP in the adjacent monomer, further stabilizing the interface. Additional hydrophobic interactions, such as L227 in one monomer and F165 in the adjacent monomer, also contribute to stabilize this interface (Supplemental Figure 2C).

GTP/GDP1 nucleotides adopt an extended conformation where the specificity for the guanine ring is conferred by the side chain of residues D184 and K206 and the ribose moiety is mostly stabilized through hydrogen bonds of the ribose hydroxyls with the side chain of D162. The phosphates are coordinated by the backbone of residues of G207, S159 and S160, as well as the side chain of R161 from the adjacent tetramer (Supplemental Figure 3A).

In contrast to GTP1/GDP1, GTP2/GDP2 adopt a compact conformation in which both the guanine ring and the β-phosphate fold back to interact with the backbone of residue G141 (Supplemental Figure 3B). The guanine ring is significantly stabilized by a π-π interaction with the side chain of F139 and by hydrogen bonding with the backbone atoms of V119. The ribose moiety is mostly stabilized through hydrogen bonds of the ribose hydroxyls with the side chain of residues D226 and K229 while the phosphates interact with the side chain of K208 as well as the backbone atoms of C140 (Supplemental Figure 3B).

GTP3/GDP3 bind to the cleft formed by the α6 and α7 helices and the α2-α3 loop, which is connected to the second canonical binding site by the strictly conserved residue D226. The guanine moiety forms a hydrogen bond with the backbone atoms of residue Gln112 as well as to the side chains of N198 and K238 (Supplemental Figure 3C). The phosphates of GDP adopt several alternative conformations within the binding site, whereas the phosphates of GTP adopt a well-defined conformation stabilized by the interaction of the γ-phosphate with the side chain of N230 (Supplemental Figure 3C).

Electron microscopy analysis of the polymers formed in the presence of purine nucleotides under macromolecular crowding conditions. The EM analysis of the polymers formed in the presence of purine nucleotides revealed either isolated octamers or helical oligomers (Figure 4B and Supplementary Figure 4B), as suggested by the turbidity measurements. In HsIMPDH1, some of these protofilaments associate laterally to form bundles of up to 3-5 protofilaments (Supplementary Figure 4B). Remarkably, the axial repetition of these single protofilaments and small protofilament bundles are perfectly compatible with the dimensions of the ATP and GDP-induced octamers (HsIMPDH1: 58.4 ± 0.3 Å for ATP and 49.7 ± 0.2 Å for GDP; HsIMPDH2: 57.7 ± 0.4 Å for ATP and 50.1 ± 0.2 Å for GDP). These data are further corroborated by single-particle 3D

reconstructions of HsIMPDH1 filaments, which showed a helix turn and a Z-rise of about 31º and 115Å for ATP, and 16º and 97Å for GDP-induced polymers (Supplementary Figure 5). Remarkably, the crystallographic contacts of our structures of HsIMPDH2 bound to GTP and GDP showed two interacting octamers rotated about 15º around the quaternary symmetry axis that perfectly agree with our HsIMPDH1 EM reconstructions (right panel in Supplementary Figure 6). Nonetheless, these parameters differ from a previous report that used EM reconstructions of HsIMPDH2 filaments (35.5º for compact-GDP and 30.5º for extended-ATP induced protofilaments under non-macromolecular crowding conditions [2]).

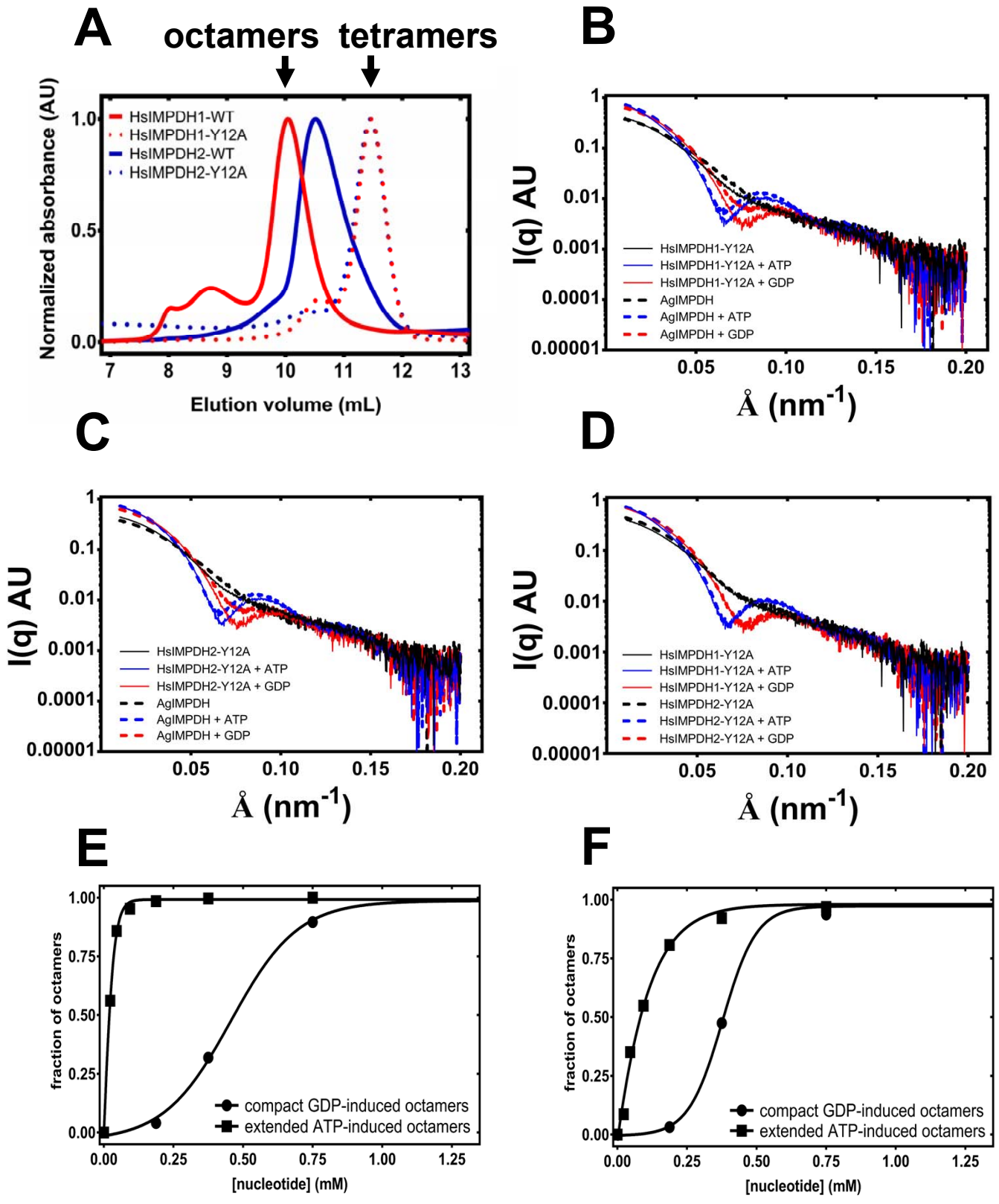
Supplemental Table 1. X-ray crystallography data collection and refinement statistics.

	HsIMPDH2-GTP	HsIMPDH2-GDP
PDB code	6I0O	6I0M
Resolution range (Å)	81.95 - 2.62 (2.72 - 2.62)	162 - 2.57 (2.66 - 2.57)
Ellipsoidal resolution limits (Å)	2.83 2.83 2.62	2.82 2.82 2.52
Space group	I 4 2 2	I 4 2 2
Unit cell (Å, α, β, γ)	134.12 134.12 325.70 90 90 90	134.73 134.73 324.08 90 90 90
Unique reflections	36419 (1821)	39038 (1951)
Multiplicity	6.5 (7.0)	25.8 (27.1)
Completeness spherical (%)	81.1 (20.5)	81.2 (21.8)
Completeness elipsoidal (%)	92.6 (47.0)	94.9 (64.2)
Mean I/sigma(I)	10.6 (1.5)	14.6 (1.6)
R-merge	0.14 (1.56)	0.19 (2.65)
R-meas	0.16 (1.69)	0.20 (2.70)
R-pim	0.06 (0.63)	0.04 (0.52)
CC1/2	0.997 (0.408)	0.997 (0.629)
R-work	0.23 (0.32)	0.23 (0.33)
R-free	0.25 (0.29)	0.25 (0.35)
Number of non-hydrogen atoms	6744	6893
macromolecules	6331	6527
ligands	322	274
solvent	91	92
Protein residues	863	900
RMS_{bonds}	0.012	0.004
RMS_{angles}	1.27	0.93
Ramachandran outliers (%)	0.00	0.34
Rotamer outliers (%)	2.04	6.57
Clashscore	11.41	5.69
Average B-factor	75.65	79.94

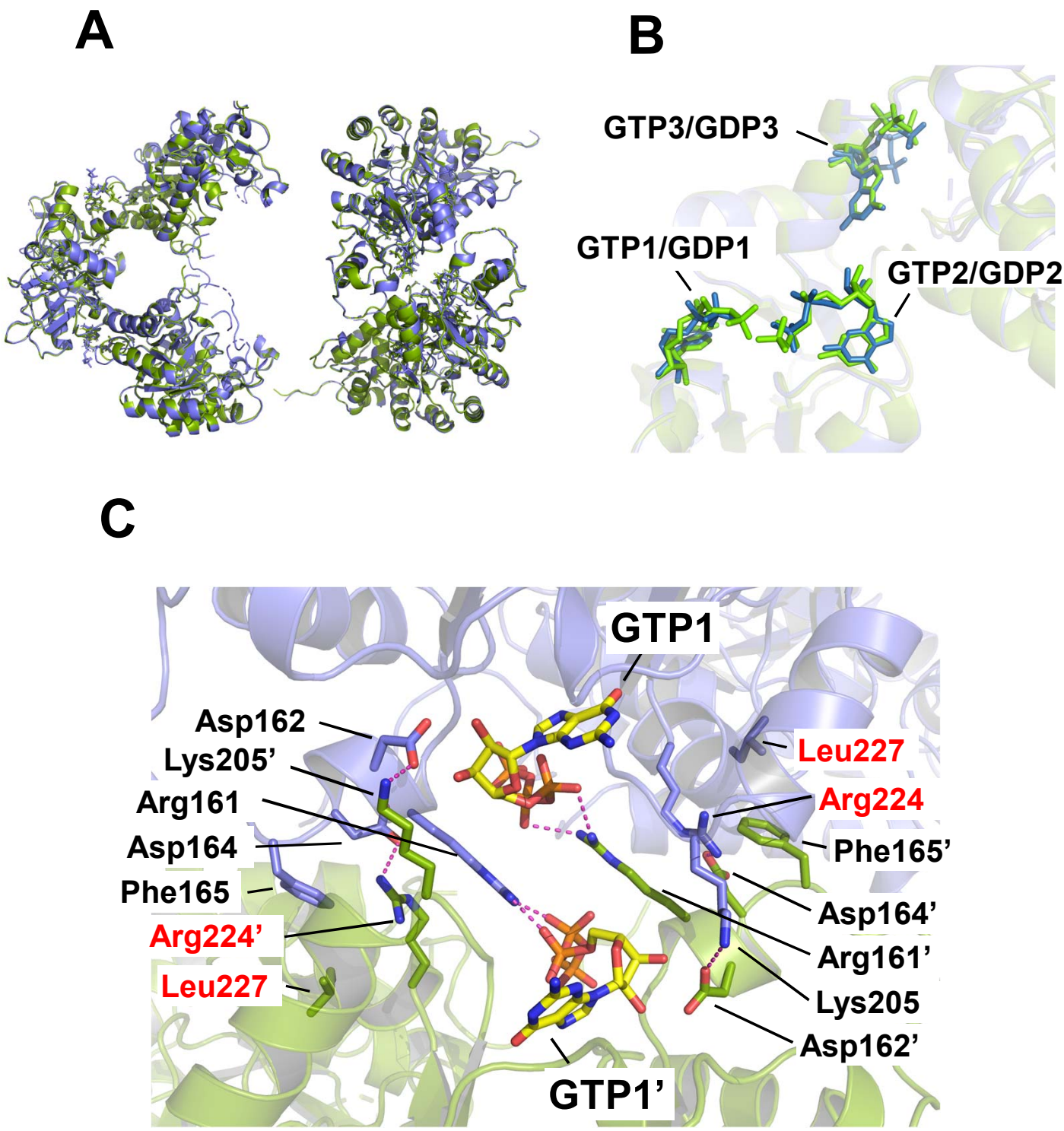
Statistics for the highest-resolution shell are shown in parentheses. Diffraction intensities were indexed and integrated by using the autoPROC toolbox [3], which makes use of the STARANISO software to deal with data anisotropy [4].

Supplemental Table 2. Enzyme kinetic parameters of human IMPDH enzymes under macromolecular crowding conditions.

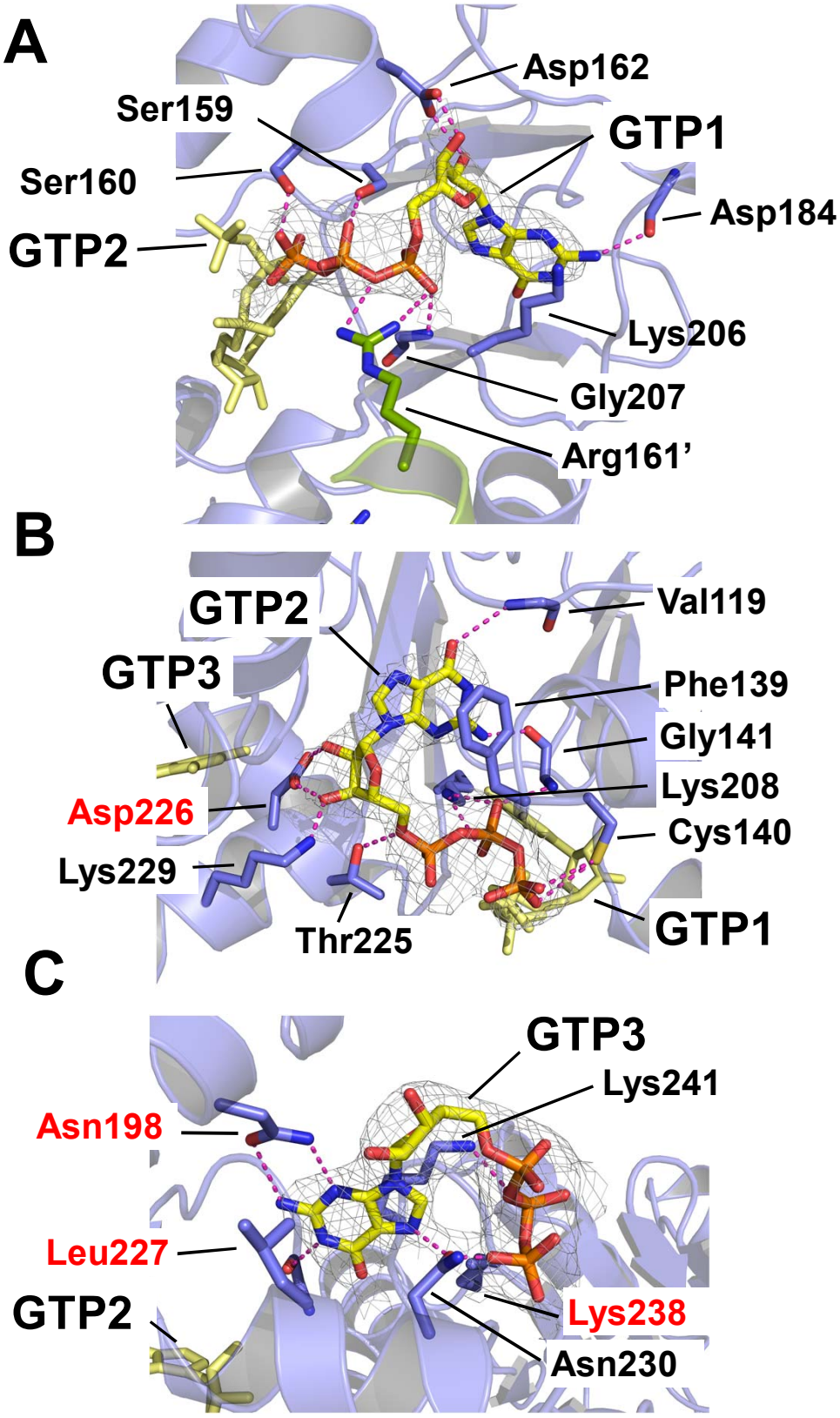
		No Ficoll-70		150 g/L Ficoll-70	
		$K_{1/2}$ (μM)	V_{max} (μM NADH*sec^{-1})	$K_{1/2}$ (μM)	V_{max} (μM NADH*sec^{-1})
HsIMPDH1	WT	153 ± 8	$3.2 \times 10^{-4} \pm 6 \times 10^{-6}$	50 ± 4	$3.1 \times 10^{-4} \pm 4 \times 10^{-6}$
	Y12A	155 ± 8	$3.2 \times 10^{-4} \pm 6 \times 10^{-6}$	42 ± 5	$3.0 \times 10^{-4} \pm 4 \times 10^{-6}$
HsIMPDH2	WT	133 ± 8	$3.2 \times 10^{-4} \pm 6 \times 10^{-6}$	45 ± 2	$3.4 \times 10^{-4} \pm 3 \times 10^{-6}$
	Y12A	135 ± 10	$3.3 \times 10^{-4} \pm 7 \times 10^{-6}$	30 ± 6	$3.4 \times 10^{-4} \pm 6 \times 10^{-6}$



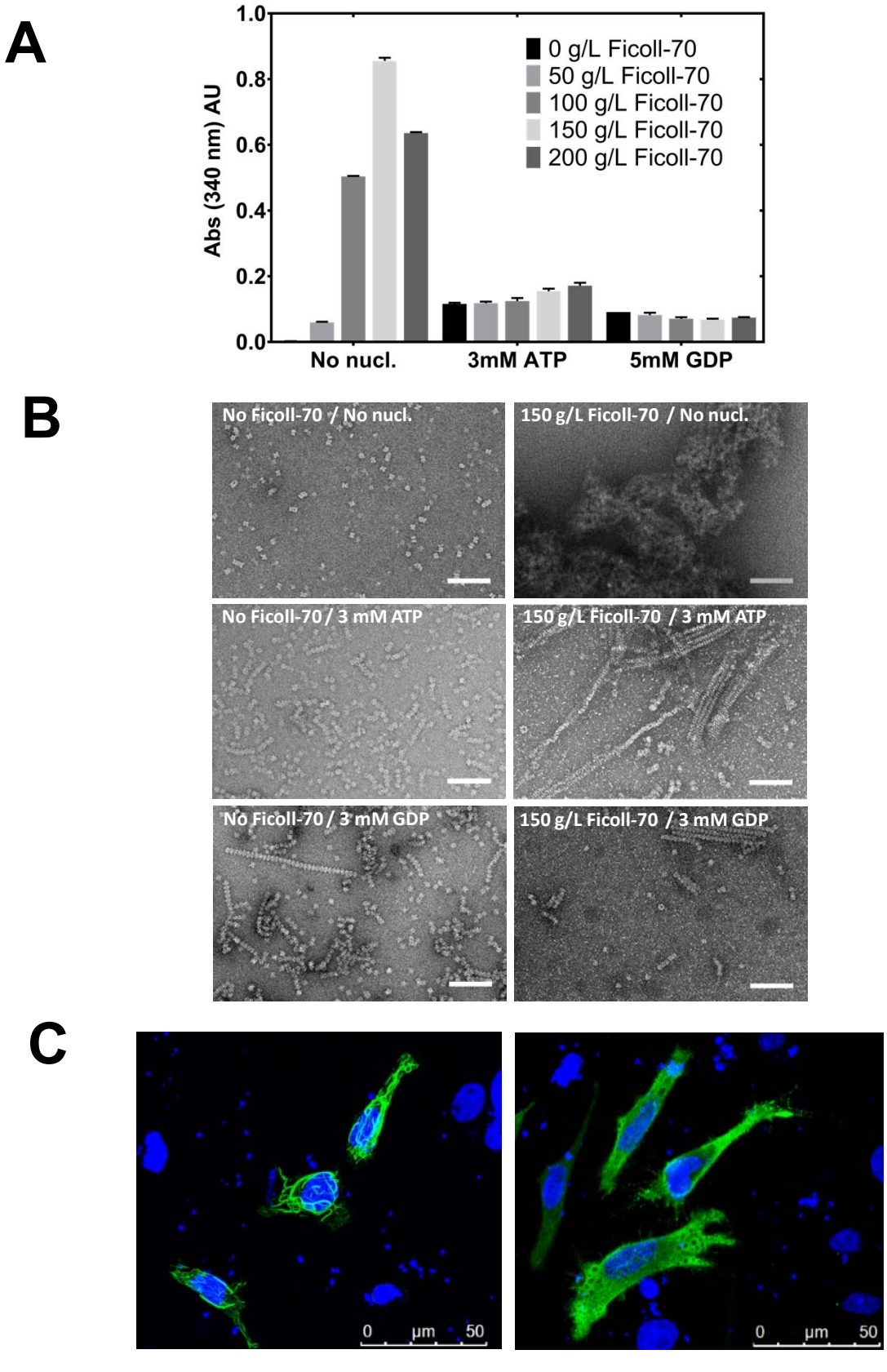
Supplemental Figure 1. *The conformational switch is identical in A. gossypii and H. sapiens*. **A**. Size exclusion chromatograph of the HsIMPDH1/2-WT and Y12A mutants. The approximate elution volumes corresponding to the Stoke´s radius of IMPDH octamers and tetramers are indicated. **B-D.** Comparison of the experimental SAXS profiles of IMPDH from humans and *A. gossypii* in the absence and presence of nucleotides. **E-F.** Fraction of compact and extended octamers at different nucleotide concentrations for HsIMPDH1-Y12A (**E**) and HsIMPDH2-Y12A (**F**), measured by SAXS and estimated by OLIGOMER. Squares: ATP. Circles: GDP.



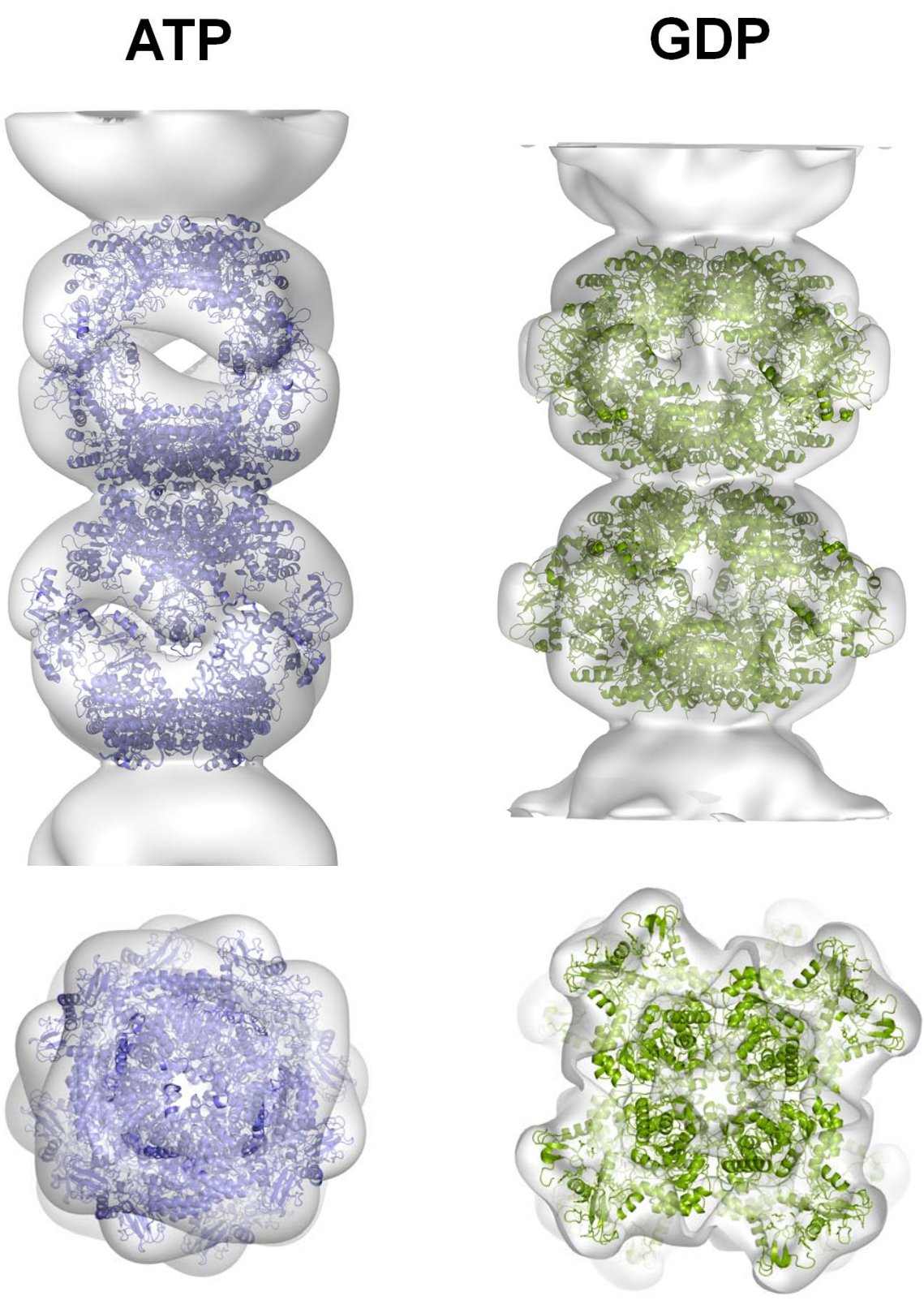
Supplemental Figure 2. *Crystal structures of HsIMPDH2 in complex to GTP and GDP* **A**. Structural superposition of HsIMPDH2 bound to GTP (green cartoons) and GDP (blue cartoons). **B**. Close-up view of the nucleotide conformations, shown as green and blue sticks for GTP and GDP, respectively. **C.** Close-up view of the Bateman domains of the two tetramers (green and blue) of a HsIMPDH2 octamer. Protein is represented in semi-transparent cartoons with the side chain of key interacting residues and GTP molecules shown in sticks. Key protein-nucleotide interactions are represented as magenta dashed lines. Residues mutated in retinopathies are labelled with red letters and numbers.



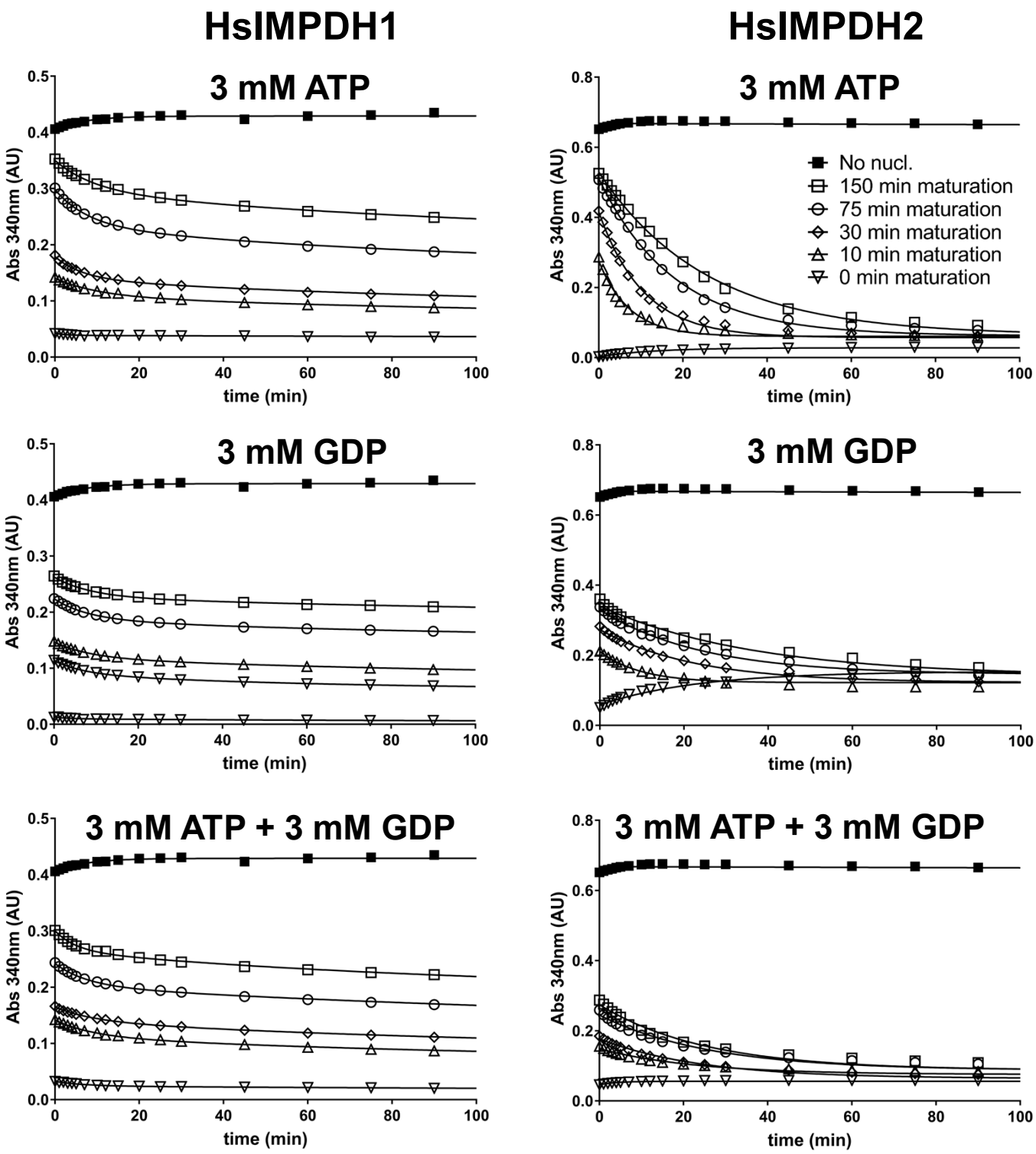
Supplemental Figure 3. *The Bateman domains of HsIMPDH bind three GTP molecules.* Close-up view of the GTP1 (**A**) and GTP2 (**B**) bound to the canonical, and GTP3 (**C**), bound to the non-canonical nucleotide binding sites of the Bateman domain of HsIMPDH2-WT. HsIMPDH2 protein is represented in blue semi-transparent cartoons with the side chain of key interacting residues and GTP molecules shown in sticks. In panel **A**, the side chain of residue Arg161' from the adjacent monomer is shown in green sticks. Key protein-nucleotide interactions are represented as magenta dashes. Residues mutated in retinopathies are labelled with red letters and numbers. The faint grey meshes around the nucleotides show the electron density map ($2F_o$-F_c), contoured at the 1σ level.



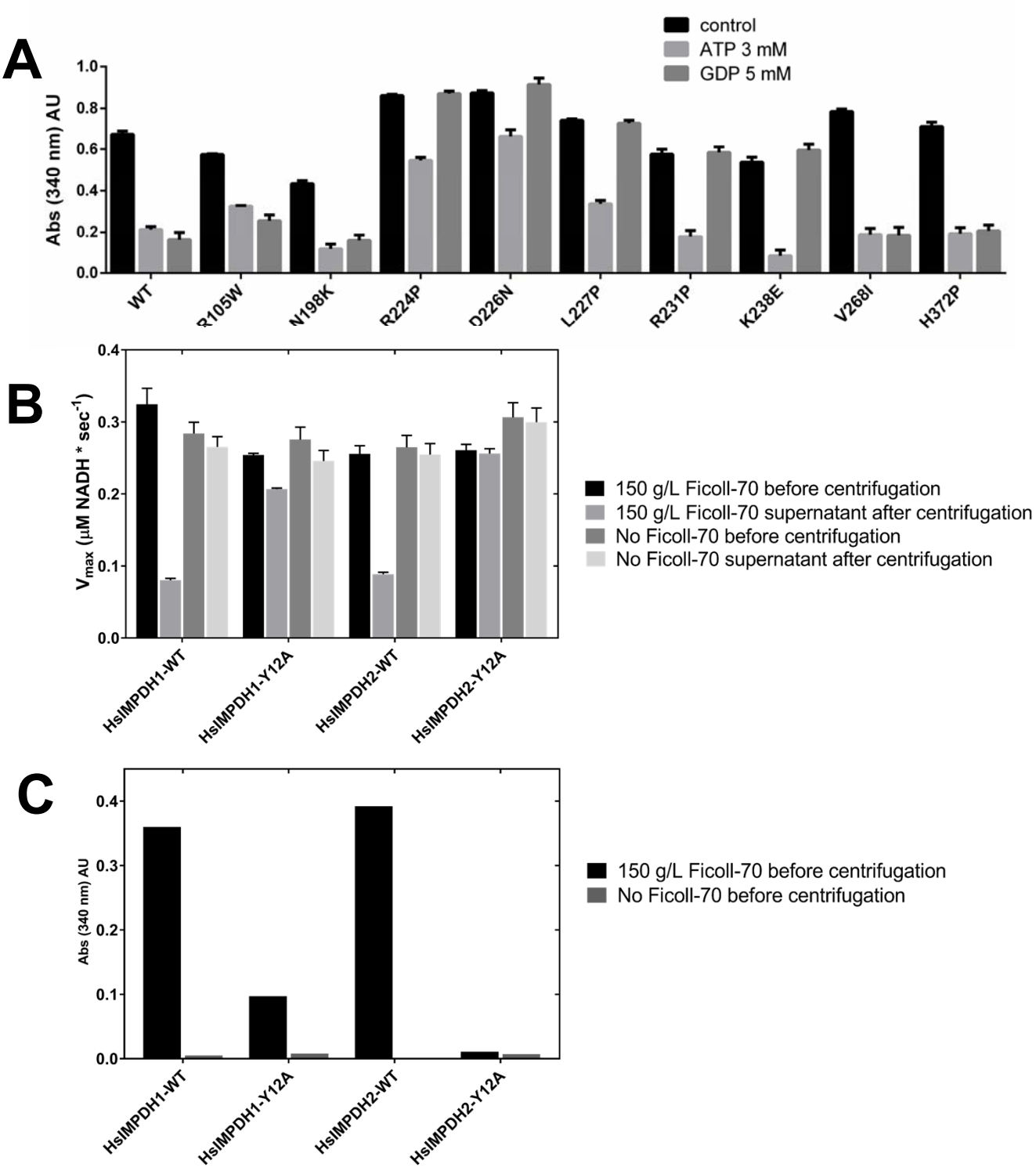
Supplemental Figure 4. *In vitro reconstitution of IMPDH cytoophidia assembly of HsIMPDH1.* **A**. Turbidity measurements, indicating the formation of large polymers, at different Ficoll-70 concentrations of HsIMPDH1-WT in the absence or presence of the indicated purine nucleotides. **B**. Electron microscopy analysis of the samples in the absence (left panels) and presence (right panels) of 150 g/L Ficoll-70. Upper panels: no nucleotide; middle panels: 3 mM ATP; lower panels: 5 mM GDP. Scale bar = 100 nM. **C.** Inmunofluorescence of HeLa cells transfected with HA-tagged HsIMPDH2 (left) and AgIMPDH (right), shown in green colour. Nuclei (in blue) were stained with DAPI.



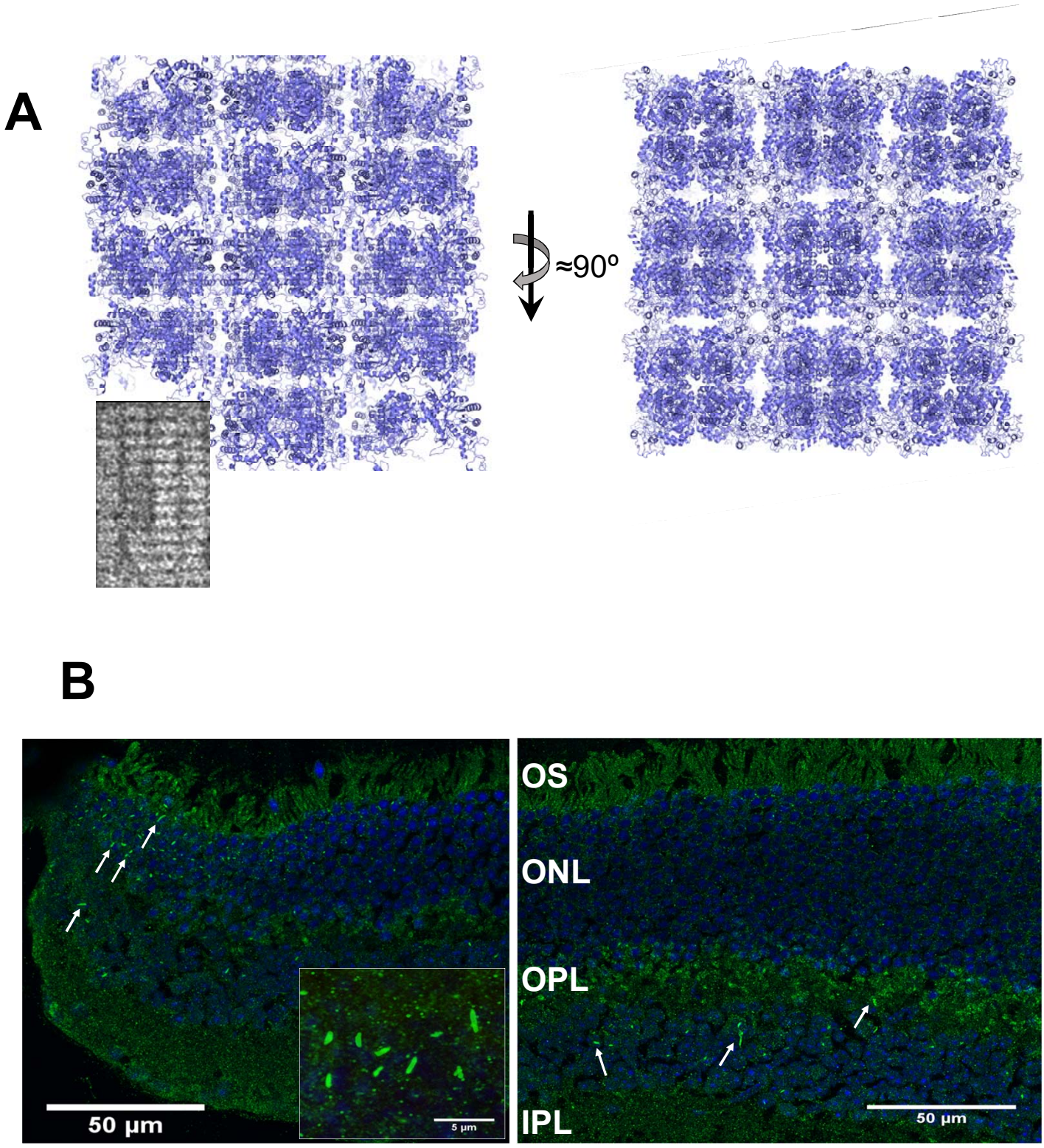
Supplemental Figure 5. *ATP and GDP-induced protofilaments of HsIMPDH1 are composed by octamers with different conformations*. 3D reconstructions of protofilaments of HsIMPDH1 formed in the presence of ATP (left) or GDP (right) at 150 g/L Ficoll-70. Two independent octamers of AgIMPDH-ATP (blue cartoons; PDB code 5MCP) were docked into the EM map. Two interacting octamers (green cartoons) as found within the crystal lattice of our HsIMPDH2-GDP structure were docked into the EM map.



Supplemental Figure 6. *Cytoophidia maturation confers resistance to GDP-induced depolymerization*. Time-course measurement of solution turbidity of HsIMPDH1 (right panels) and HsIMPDH2 (left panels) upon addition of the indicated nucleotides. Before nucleotide addition, samples were incubated at 25ºC for different times in a solution containing 150 g/L Ficoll-70, as indicated in the legend of the upper left panel. Lines represent the best fitting to a single exponential decay function. Significant depolymerization within the dead time of the measurements (estimated in 3 minutes) was observed in all plots.



Supplemental Figure 7. A. Turbidity measurements of HsIMPDH1-WT and retinopathy-associated mutants in the absence or presence of purine nucleotides. Cytoophidia were first formed by incubating the proteins in a solution containing 150 g/L Ficoll-70 at 25ºC for 5 minutes. Measurements were performed 120 minutes after adding the indicated amount of purine nucleotides. Error bars represent standard errors. **B.** Control experiments showing that the catalytic activity (V_{max}) of IMPDH cytoophidia formed in conditions of macromolecular crowding (150 g/L Ficoll-70) is dramatically reduced after a soft centrifugation that pellets only the large polymers. The HsIMPDH2-Y12A mutant with compromised polymerizing ability remains in the supernatant and maintains the inherent catalytic activity. The HsIMPDH1-Y12A mutant partially polymerizes and, thereby, only a partial loss of catalytic activity is observed after centrifugation. **C.** Turbidity measurements showing the large extent of polymerization for the WT proteins and the significantly compromised polymerization for the Y12 mutants.



Supplemental Figure 8. A. Ribbon representation of the packing of a protein crystal of HsIMPDH2 with ribavirin monophosphate and C2-mycophenolic adenine dinucleotide bound to the active site, but no molecules bound in the Bateman domain. To facilitate visualization, below the left panel, it is shown a zoom of one of the ordered bundles formed by HsIMPDH2-WT under macromolecular crowding conditions. **B.** Immunohistochemistry of adult mice retinas showing 1-2 µm long structures, corresponding to IMPDH cytoophidia, localized mainly in the periphery of the retina (white arrows, left panel). In the central regions of the retina scarce cytophidia are also detected (white arrows, right panel). The inset of the left panel shows a higher magnification of cytophidia in the mouse retina. In the right panel the outer segments (OS), outer nuclear layer (ONL), outer plexiform layer (OPL), inner nuclear layer (INL) and inner plexiform layer (IPL) are indicated.

References

[1] Buey RM, Ledesma-Amaro R, Velazquez-Campoy A, Balsera M, Chagoyen M, de Pereda JM, et al. Guanine nucleotide binding to the Bateman domain mediates the allosteric inhibition of eukaryotic IMP dehydrogenases. Nat Commun. 2015;6:8923.
[2] Anthony SA, Burrell AL, Johnson MC, Duong-Ly KC, Kuo YM, Simonet JC, et al. Reconstituted IMPDH polymers accommodate both catalytically active and inactive conformations. Molecular biology of the cell. 2017.
[3] Vonrhein C, Flensburg C, Keller P, Sharff A, Smart O, Paciorek W, et al. Data processing and analysis with the autoPROC toolbox. Acta crystallographica Section D, Biological crystallography. 2011;67:293-302.
[4] Tickle IJ, Flensburg C, Keller P, Paciorek W, Sharff A, Vonrhein C, et al. STARANISO. Cambridge, United Kingdom: Global Phasing Ltd. 2018.

Artículo 2

Título:

El dominio Bateman de la IMP deshidrogenasa es una diana de unión para los dinucleósidos polifosfatos.

Resumen:

La IMP deshidrogenasa es una enzima esencial que cataliza el paso limitante en la ruta biosintética *de novo* de nucleótidos de guanina. Debido a que está involucrada en el control de la división celular y proliferación, la IMPDH representa una diana terapéutica para el tratamiento de diversas enfermedades, incluyendo infecciones microbianas y cáncer. La IMPDH debe estar firmemente regulada, pero los mecanismos moleculares responsables de su regulación fisiológica permanecen sin caracterizar. Con este propósito, recientemente publicamos que los mononucleótidos de adenina y guanina juegan un importante papel uniéndose a dominio regulador Bateman para modular alostéricamente la actividad catalítica de las IMPDHs eucariotas. En este trabajo, se propuso evaluar si los dinucleósidos polifosfatos pueden unirse a IMPDHs eucariotas y tener efecto sobre el mecanismo alostérico de regulación de la actividad; así como caracterizar sus posibles modos de unión. Para ello, hemos empleado metodologías de cinética enzimática, cristalografía de rayos-X y SAXS.

Hemos demostrado que los dinucleósidos polifosfatos de adenina/guanina se unen a los dominios Bateman de la IMPDH del hongo *Ashbya gossypii* con afinidad submicromolar. Estos dinucleósidos polifosfatos modulan la actividad catalítica de las IMPDHs *in vitro* compitiendo eficientemente con los mononucleótidos de adenina y guanina por los sitios alostéricos. Por tanto, estos resultados sugieren que los dinucleósidos polifosfatos juegan importantes papeles fisiológicos en la regulación alostérica de las IMPDHs añadiendo un mecanismo adicional para regular finamente la actividad de estas enzimas. Además, estos descubrimientos pueden tener importantes implicaciones para el diseño de estrategias terapéuticas para inhibir las IMPDHs.

The Bateman domain of IMP dehydrogenase is a binding target for dinucleoside polyphosphates

Received for publication, July 3, 2019, and in revised form, August 13, 2019 Published, Papers in Press, August 15, 2019, DOI 10.1074/jbc.AC119.010055

David Fernández-Justel[‡1], **Rafael Peláez**[§], **José Luis Revuelta**[‡2], **and Rubén M. Buey**[‡3]

From the [‡]*Metabolic Engineering Group, Departamento de Microbiología y Genética and* [§]*Laboratorio de Química Orgánica y Farmacéutica, Departamento de Ciencias Farmacéuticas, Universidad de Salamanca, Campus Miguel de Unamuno, 37007 Salamanca, Spain*

Edited by Wolfgang Peti

IMP dehydrogenase (IMPDH) is an essential enzyme that catalyzes the rate-limiting step in the *de novo* guanine nucleotide biosynthetic pathway. Because of its involvement in the control of cell division and proliferation, IMPDH represents a therapeutic for managing several diseases, including microbial infections and cancer. IMPDH must be tightly regulated, but the molecular mechanisms responsible for its physiological regulation remain unknown. To this end, we recently reported an important role of adenine and guanine mononucleotides that bind to the regulatory Bateman domain to allosterically modulate the catalytic activity of eukaryotic IMPDHs. Here, we have used enzyme kinetics, X-ray crystallography, and small-angle X-ray scattering (SAXS) methodologies to demonstrate that adenine/guanine dinucleoside polyphosphates bind to the Bateman domain of IMPDH from the fungus *Ashbya gossypii* with submicromolar affinities. We found that these dinucleoside polyphosphates modulate the catalytic activity of IMPDHs *in vitro* by efficiently competing with the adenine/guanine mononucleotides for the allosteric sites. These results suggest that dinucleoside polyphosphates play important physiological roles in the allosteric regulation of IMPDHs by adding an additional mechanism for fine-tuning the activities of these enzymes. We propose that these findings may have important implications for the design of therapeutic strategies to inhibit IMPDHs.

Dinucleoside polyphosphates are ubiquitous molecules in which two nucleosides are linked by a chain of two to seven phosphate moieties. Dinucleoside polyphosphates naturally found in biological systems are those formed by two adenosines (Ap_nA), two guanines (Gp_nG), or the combination of adenine and guanine in the same molecule (Ap_nG), most commonly linked by three to five phosphates ($p_n = 3–5$).

These compounds were originally discovered in the late sixties (1, 2), but the first indication of their putative physiological role came a decade later when a correlation between the concentration of Ap_4A and the proliferative status of mammalian cells was demonstrated (3). At present, dinucleoside polyphosphates have been described to participate in an increasing variety of cellular processes, including DNA replication and repair (4), cell division (5), neurotransmission (6), apoptosis (7), analgesia (8), vasoconstriction (9), and platelet aggregation (10) among others. Accordingly, dinucleoside polyphosphates have been described to interact with several target proteins, including adenylate kinase (11), purinergic receptors (12), heat shock proteins (13), 5′-nucleotidase II (14), and poly(A) polymerase (4) among others. Interestingly, diadenosine polyphosphates have also been recently reported to bind to the Bateman domains of some bacterial pyrophosphatases (15) as well as to bacterial IMP dehydrogenases (16, 17), which raises the interesting question of whether Bateman domains are physiological targets of dinucleoside polyphosphates *in vivo*.

Bateman domains are regulatory protein modules composed of pairs of cystathionine β-synthase motifs, which are present in organisms belonging to all kingdoms of life. They either exist as isolated proteins or associated to a variety of enzymes where they allosterically modulate their functions in response to the binding of different molecules. Thereby, Bateman domains sense the cellular energy status, metal ion concentration, or ionic strength and regulate protein function accordingly (18). The physiological relevance of Bateman domains is stressed by the fact that missense mutations within them have been associated to a variety of human hereditary diseases that include the Wolff–Parkinson–White syndrome, congenital myotonia, homocystinuria, and certain retinopathies such as Leber congenital amaurosis and retinitis pigmentosa (19).

Among the proteins that contain Bateman domains, IMP dehydrogenase (IMPDH)[4] is the enzyme that catalyzes the rate-limiting step in the *de novo* guanine nucleotide biosynthetic pathway and, thereby, is involved in the control of cell division and proliferation. IMPDH is composed of an archetypal triose-phosphate isomerase (TIM) barrel catalytic domain that contains a Bateman regulatory module inserted within a loop. The basic units of IMPDH in solution are homotetramers that can dimerize in different ways to form octamers, linear oligomers, and mesoscale polymers,

This work was supported by Spanish Ministerio de Ciencia, Innovación y Universidades Grants BFU2016-79237-P (to R. M. B.) and BIO2017-88435-R (to J. L. R.). The authors declare that they have no conflicts of interest with the contents of this article.

This article contains Table S1 and Figs. S1–S4.

The atomic coordinates and structure factors (code 6RPU) have been deposited in the Protein Data Bank (http://wwpdb.org/).

[1] Supported by a predoctoral contract from the "Junta de Castilla y León."

[2] To whom correspondence may be addressed. E-mail: revuelta@usal.es.

[3] To whom correspondence may be addressed. E-mail: ruben.martinez@usal.es.

[4] The abbreviations used are: IMPDH, IMP dehydrogenase; SAXS, small-angle X-ray scattering; PDB, Protein Data Bank; Hs, *Homo sapiens*; Ag, *A. gossypii*; Ec, *E. coli*; Pa, *P. aeruginosa*; r.m.s.d., root mean square deviation.

© 2019 Fernández-Justel et al. Published under exclusive license by The American Society for Biochemistry and Molecular Biology, Inc.

denoted as cytoophidia (20). Despite the fact that IMPDH is a widely studied therapeutic target, it has been only since the last few years that we are beginning to understand its molecular mechanisms of allosteric regulation.

The Bateman domain of eukaryotic IMPDHs has three nucleotide-binding sites that operate coordinately to allosterically modulate the catalytic activity. Canonical sites 1 and 2 are present in all IMPDH Bateman domains and can be occupied by either adenine (ATP, ADP, and AMP) or guanine (GTP and GDP) nucleotides. In contrast, the noncanonical site 3 is exclusive of eukaryotic IMPDHs and can only be occupied by guanine (GTP and GDP) nucleotides (Fig. 1). Adenine nucleotide binding to sites 1 and 2 induces catalytically active, extended octamers, whereas the coordinated binding of GTP/GDP to sites 2 and 3 induces the compaction of these octamers into an inhibited conformation (Fig. 1).

Strong cooperativity between allosteric sites 2 and 3 must exist because the incubation of IMPDH with a mixture of ATP and GDP resulted in a complex with ATP bound to site 1 and GDP bound to sites 2 and 3. GDP binding to site 3 is obvious because this site is exclusive for GTP/GDP, but GDP binding to site 2 must be favored by the occupancy of site 3 given that GDP has 20-fold less apparent affinity than ATP (21). These data imply that sites 2 and 3 are linked.

Moreover, given that site 3 is exclusive for guanine nucleotides and the binding of these to site 2 is tightly linked to the occupancy of site 3, ATP cannot efficiently displace GTP/GDP from sites 2 and 3, and thereby the nucleotide-controlled conformational switch of IMPDH has been reported to be unidirectional. That is, GTP/GDP are able to inhibit the active octamers induced by ATP, but in contrast, ATP cannot activate the inhibited octamers induced by GTP/GDP (20, 21). Altogether, the occupancy of the second canonical and the third noncanonical nucleotide-binding sites of the Bateman domain determines the conformation of IMPDH octamers and, therefore, their catalytic activity.

In this work, we demonstrate that adenine/guanine dinucleoside polyphosphates bind with submicromolar affinities to the Bateman domains and modulate the catalytic activity of IMPDHs *in vitro* by efficiently competing with the adenine/guanine mononucleotides for the canonical sites. We further report the crystallographic structure of the inhibited ternary complex of IMPDH bound to Ap5G and GDP that indicates that dinucleoside polyphosphates occupy both canonical sites simultaneously. Altogether, our results strongly suggest that dinucleoside polyphosphates might play important physiological roles by adding an extra level for fine-tuning the allosteric regulation of IMPDHs. Furthermore, the reported data might have important implications for the design of novel therapeutic strategies to inhibit IMPDHs.

Results and discussion

Adenine/guanine dinucleoside polyphosphates efficiently bind to the Bateman domain of IMPDH

An analysis of the published structures of the human (HsIMPDH) and *Ashbya gossypii* IMPDH (AgIMPDH) enzymes bound to GTP (20), ATP, ATP/GDP (21), and GDP (22) showed that the β- and γ-phosphates of the mononucleotides bound at canonical sites 1 and 2 are facing each other (Fig. 1*B*). Thus, we speculated that adenine/guanine dinucleoside polyphosphates could bind simultaneously to canonical sites 1 and 2 and, thereby, could efficiently compete with adenine and guanine mononucleotides. Following this hypothesis, we tested the effects of several commercially available dinucleoside polyphosphates on the catalytic activity of AgIMPDH.

First, we assayed Ap4A, Ap5A, and Ap6A and compared them side-by-side with ATP. All these nucleotides bind to AgIMPDH and slightly activate its catalytic activity. Ap6A and Ap5A bind to AgIMPDH with high affinity with an approximate $K_{1/2}$ value of 0.3 μM, which is about 2 orders of magnitude higher than that of ATP (Fig. 2*A*).

Remarkably, both Ap5A and Ap6A are able to revert the strong allosteric inhibition of AgIMPDH mediated by millimolar amounts of GDP (3 mM) in contrast to Ap4A and ATP (Fig. 2*B*), which cannot activate the GDP-inhibited enzyme even when Ap4A and ATP bind to AgIMPDH 2 orders of magnitude more efficiently than GDP (21). This observation is indeed interesting because it implies that submicromolar concentrations of Ap5A and Ap6A could activate the enzyme even at high concentrations of GTP and GDP. We speculate that this might constitute a mechanism that can be used by the cell to maintain higher steady-state levels of guanine nucleotides that might be required under certain circumstances, such as high cell proliferation rates (23).

The high binding affinity of Ap5A and Ap6A to AgIMPDH suggests that these are occupying both canonical sites simultaneously, in contrast to Ap4A that seems to bind as a surrogate of ATP, that is, one molecule of Ap4A per canonical site. These results agree with those previously reported stating that Ap4A binds the *Escherichia coli* and *Pseudomonas aeruginosa* IMPDH enzymes (EcIMPDH and PaIMPDH) with only 5-fold higher affinity than ATP, and thereby this interaction is physiologically irrelevant (16). In contrast, our results suggest that Ap5A and Ap6A might bind with much higher affinity than ATP (and Ap4A) to these bacterial enzymes. We corroborated this hypothesis by monitoring the ATP-induced activation of PaIMPDH and observed a potent activation mediated by Ap6A and partially Ap5A but not Ap4A and ATP that needed much higher concentrations to activate the enzyme (Fig. S1). Altogether, these data demonstrate that adenine dinucleotides are *in vitro* common ligands of the Bateman domains of bacterial and eukaryotic IMPDHs.

We next assayed the effects of Ap5G and Gp5G on the enzymatic activity of AgIMPDH *in vitro* and observed a slight activator effect of Ap5G and no effect at all for Gp5G (Fig. 2*C*). However, submicromolar amounts of Ap5G were able to significantly inhibit the enzyme in combination with a subsaturating concentration of GDP (300 μM), which lies within the expected range of nucleotide intracellular concentrations (24); Gp5G, in contrast, showed no effect at all (Fig. 2*D*). Thereby, our data show that submicromolar amounts of Ap5G, but not Gp5G, are able to hypersensitize AgIMPDH to GTP/GDP-mediated allosteric inhibition.

These observations suggest that the guanine moieties of Gp5G cannot bind simultaneously to the two canonical sites of

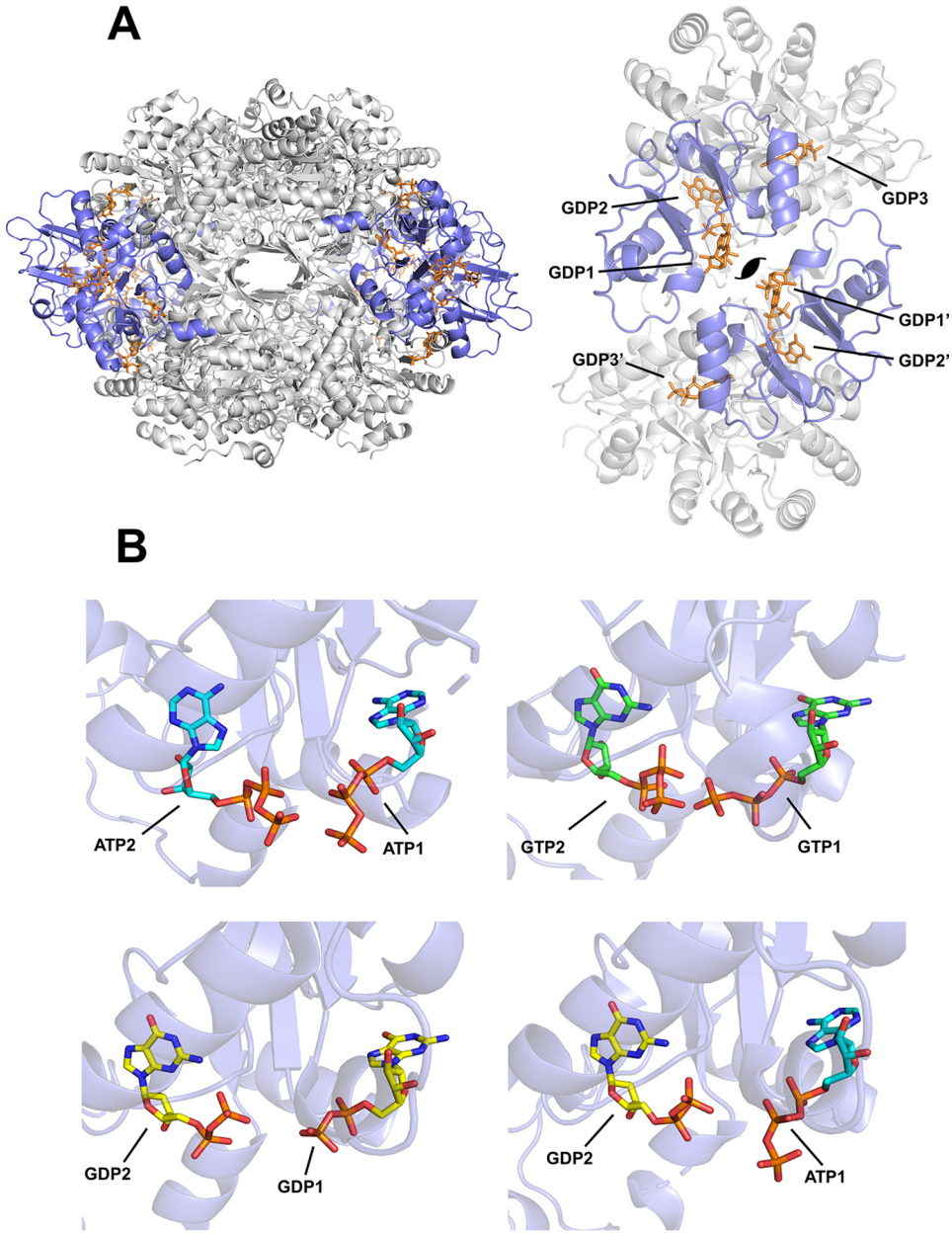


Figure 1. Nucleotide binding to the Bateman domain of IMDPH. *A*, cartoon representation of the structure of AgIMPDH octamers formed in the presence of GDP (*orange sticks*). The catalytic domain is shown in *light gray*, and the Bateman regulatory domain is colored in *blue*. The *right panel* corresponds to a close-up view of two interacting Bateman domains within the octamer, showing the disposition of the three bound GDP molecules. The approximate position of the symmetry axis is indicated. *B*, close-up views of the adenine and guanine nucleotides (shown in *sticks*) bound to the two canonical sites of AgIMPDH (represented in *semitransparent blue cartoons*). *Upper left panel*, AgIMPDH–ATP (PDB code 5MCP). *Upper right panel*, HsIMPDH–GTP (PDB code 6I0O). *Lower left panel*, AgIMPDH–GDP (PDB code 4Z87). *Lower right panel*, AgIMPDH–ATP/GDP (PDB code 5TC3). In all cases, it can be observed that the β- and γ-phosphates of the nucleotides bound to the canonical sites face each other. The canonical binding sites (1 and 2) are indicated after the corresponding nucleotides; *i.e.* ATP1 means ATP bound to the canonical site 1.

the Bateman domain of AgIMPDH, opposite to Ap5G that occupies both canonical sites simultaneously with submicromolar affinity. Nonetheless, Ap5G alone has no effect on the catalytic activity because the noncanonical binding site 3 needs to be occupied by GTP/GDP to inhibit the enzyme; that is, all three allosteric sites must be occupied to inhibit efficiently the enzyme (22).

Structure of the ternary complex AgIMPDH–Ap5G–GDP

The biochemical data reported in the previous section suggest that Ap5A, Ap6A, and Ap5G bind simultaneously to the two canonical nucleotide-binding sites of the Bateman domain. To corroborate this hypothesis, we aimed to determine the crystal structure of IMPDH bound to a dinucleoside polyphosphate and succeeded at solving the ternary complex AgIMPDH–Ap5G–GDP at a maximum resolution of 2.1 Å despite the strong anisotropy of the experimental data (details are given under "Experimental procedures" and in Table 1). The crystal belongs to space group I 4 2 2 and contains only one IMPDH monomer in the asymmetric unit, but the octameric species, expected from the small-angle X-ray scattering (SAXS) experiments, can be reconstructed from the crystallographic

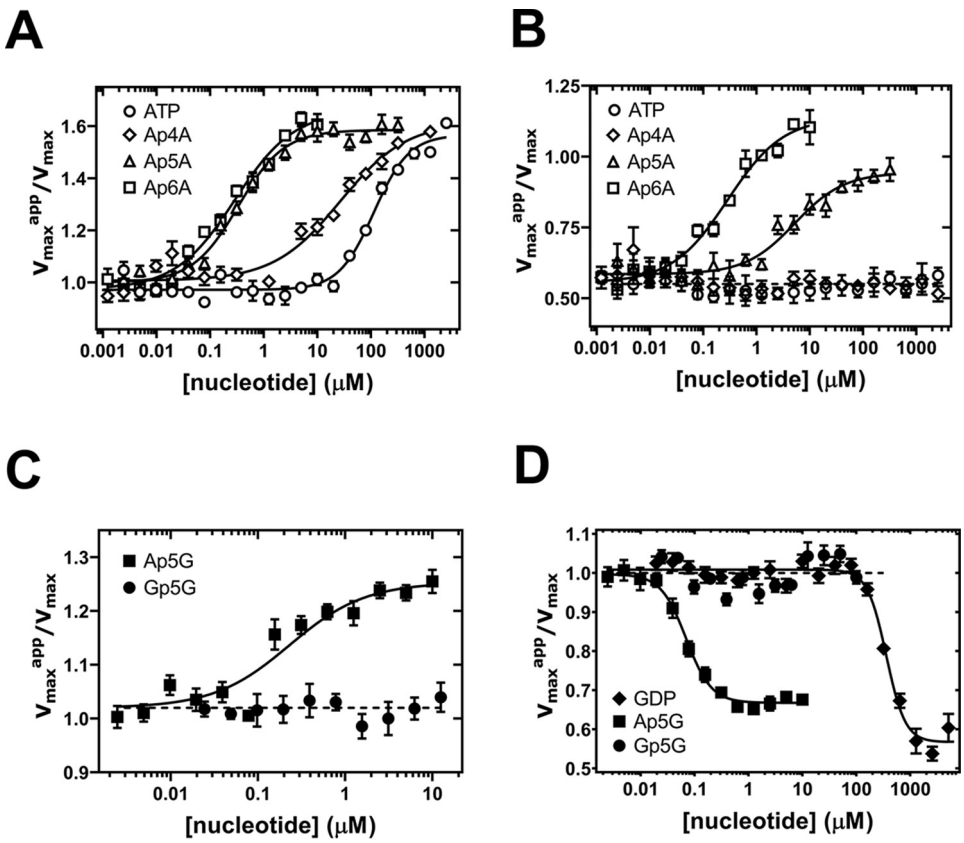


Figure 2. Effects of dinucleoside polyphosphates on the catalytic activity of AgIMPDH *in vitro*. Graphs show the normalized V_{max} values (V_{max}^{app} in the presence of nucleotide divided by the V_{max} in the absence of nucleotide) *versus* nucleotide concentration. *A* and *C* show the effects of the indicated dinucleoside polyphosphates alone on the AgIMPDH enzyme, whereas *B* and *D* show their effects on the enzyme in the presence of GDP (*B*, inhibited enzyme at 3 mM GDP (21); *D*, subsaturating GDP concentration of 0.3 mM, which cannot inhibit the enzyme significantly (21)). Experimentally determined V_{max} values were fitted to a dose-response function (four parameters, variable slope) as implemented in GraphPad Prism software (*continuous lines*). *Error bars* represent S.E.

contacts (Fig. S2*A*). The overall protein structure is essentially identical to that of AgIMPDH–GDP (PDB code 4Z87; all-atom r.m.s.d., 1.08 Å) and AgIMPDH–ATP/GDP (PDB code 5TC3; all-atom r.m.s.d., 0.78 Å); both of them compacted and inhibited octamers (21) as shown in Fig. S2*B*. The electron density for Ap5G and GDP is clear and allows modeling these nucleotides unequivocally.

Remarkably, Ap5G binds simultaneously to the two canonical sites, with the adenine and guanine moieties bound to sites 1 and 2, respectively (Figs. 3*A* and S3) and the polyphosphate chain buried in a highly charged positive groove (Fig. S3*B*). The binding modes for the adenosine and guanosine moieties of Ap5G are identical to those observed for ATP and GDP in the ATP/GDP complex structure (Fig. 3*B*), as it happens with the GDP molecule that occupies the noncanonical site 3 (21).

The structure demonstrates that purine dinucleoside polyphosphates can bind simultaneously the two canonical binding sites in the Bateman domain, which explains why their affinities are 2 orders of magnitude higher than the corresponding adenine and guanine mononucleotides. The large increase in affinity presumably comes from the simultaneous reduction of the entropic penalty of binding, due to the molecularity change, and the electrostatic repulsion.

This structure, together with the biochemical data reported above, further corroborates our previous observation that the canonical site 2 and the noncanonical site 3 are tightly linked. This is also evidenced by their spatial proximity and the common residues that both sites share (20, 21). Thereby, the occupancy of site 3 facilitates the binding of guanine mononucleotides to site 2, but the binding of adenine mononucleotides is difficulted (21, 22). Given that Ap5A/Ap6A occupy both canonical sites 1 and 2 with affinities that are 3 orders of magnitude higher than GTP/GDP, they can readily displace GTP/GDP from site 2 and, subsequently, from site 3, reverting the GTP/GDP-mediated inhibition of IMPDH. Moreover, the fact that Ap5G hypersensitizes the IMPDH enzyme to the GDP-mediated allosteric inhibition indicates that the occupancy of site 2 by the guanosine moiety of Ap5G favors the binding of GDP to site 3.

Dinucleoside polyphosphates binding to IMPDH is highly specific in the sense that it requires an appropriate polyphosphate chain length to allow the two purine nucleoside moieties to be accommodated simultaneously into the canonical binding sites. In this respect, the binding of the guanine ring at the canonical site 1 occurs with a shift of about 3 Å with respect to adenine (Fig. S4*A*), thus imposing a different register to the polyphosphate chain. This observation explains the lack of effect of Gp5G, in contrast to Ap5G, on the catalytic activity of AgIMPDH. We speculate that Gp6G might efficiently bind to AgIMPDH, but this remains to be experimentally demon-

Table 1

X-ray crystallography data collection and refinement statistics

Statistics for the highest-resolution shell are shown in parentheses. Diffraction intensities were indexed and integrated by using the autoPROC toolbox (28), which makes use of the STARANISO software to deal with data anisotropy (29). CC, Pearson correlation coefficient.

	AgIMPDH–Ap5G–GDP
Crystal parameters	
PDB code	6RPU
Resolution range (Å)	85.10–2.11 (2.26–2.11)
Ellipsoidal resolution limits (Å)	2.10, 2.10, 3.13[a]
Resolution $I/I\sigma > 2.0$ (overall)	2.43
Resolution $I/I\sigma > 2.0$ (along h)	2.26
Resolution $I/I\sigma > 2.0$ (along k)	2.26
Resolution $I/I\sigma > 2.0$ (along l)	3.30
Resolution $CC_{1/2} > 0.3$ (overall)	2.16
Resolution $CC_{1/2} > 0.3$ (along h)	2.08
Resolution $CC_{1/2} > 0.3$ (along k)	2.08
Resolution $CC_{1/2} > 0.3$ (along l)	3.05
Space group	I 4 2 2
Unit cell $a, b, c/\alpha, \beta, \gamma$(Å/°)	148.54, 148.54, 103.83/90, 90, 90
Unique reflections	22,408 (1,106)
Multiplicity	23.3 (23.4)
Completeness spherical (%)	66.4 (17.8)
Completeness ellipsoidal (%)	95.8 (68.4)
Mean $I/\sigma(I)$	21.5 (1.7)
R_{merge}	0.09 (2.41)
R_{meas}	0.10 (2.46)
R_{pim}	0.02 (0.51)
$CC_{1/2}$	0.999 (0.704)
Refinement statistics	
R_{work}	0.27 (0.40)
R_{free}	0.29 (0.31)
Number of non-hydrogen atoms	3,325
Macromolecules	3,171
Ligands	102
Solvent	52
Protein residues	432
r.m.s.$_{bonds}$	0.013
r.m.s.$_{angles}$	1.78
Ramachandran outliers (%)	0.00
Rotamer outliers (%)	3.34
Clashscore	29.79
Average B-factor	61.69
Macromolecules	61.97
Ligands	65.05
Solvent	38.22

[a] Experimental data showed strong anisotropy with ellipsoidal resolution limits defined at 2.10 (a), 2.10 (b), and 3.13 (c) Å by STARANISO using as threshold $I/\sigma I \geq 1.2$.

strated (Gp6G is not commercially available so far). Additionally, slight variations in the primary sequence among organisms and/or isoforms might completely change the binding specificity as will be discussed below.

Dinucleoside polyphosphates modulate the conformational switch of AgIMPDH

We studied next the effects of the dinucleoside polyphosphates on the quaternary structure and conformation of AgIMPDH in solution by using SAXS. AgIMPDH has been extensively characterized by using this methodology, and it has been reported that AgIMPDH exists as a tetramer in solution in the absence of nucleotides (profile *1*), and the binding of adenine (ATP, ADP and AMP) and guanine (GTP and GDP) nucleotides in the Bateman domain induces extended-active (profile *3*, ATP) and compacted-inhibited octamers (profile *6*, GDP), respectively (Ref. 21 and Fig. 3*C*).

We then corroborated that Ap6A (profile *4*) induces the association of AgIMPDH tetramers to form octamers highly similar to those induced by ATP (profile *3*). Moreover, Ap6A (profile *5*), but not Ap4A (profile *8*) or ATP (profile *9*), is able

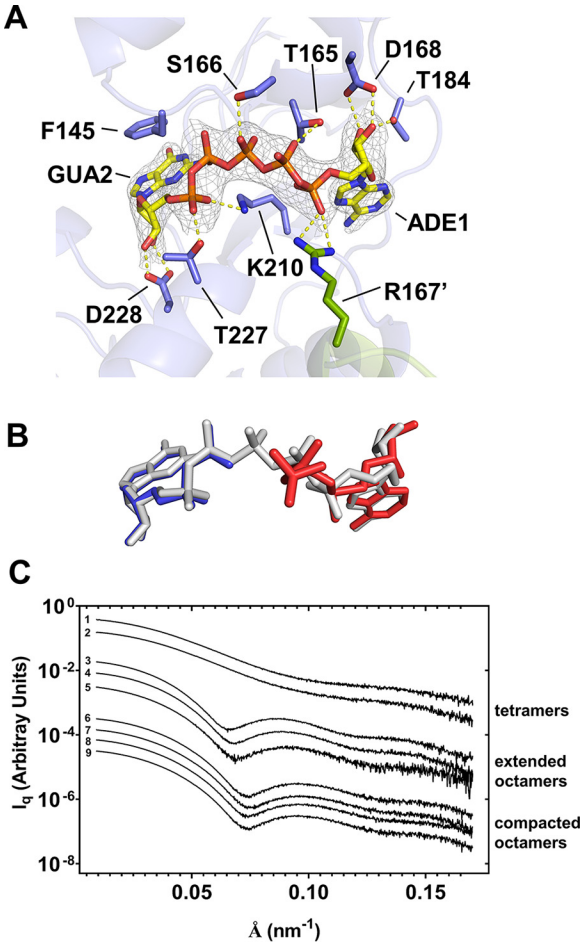


Figure 3. Structure of AgIMPDH bound to dinucleoside polyphosphates. *A*, crystal structure of the ternary complex AgIMPDH–Ap5G–GDP. Shown is a close-up view of Ap5G (shown in *sticks*) simultaneously bound to the two canonical sites of the Bateman domain. The protein is represented in *semitransparent blue cartoons* with the side chain of key interacting residues shown in *sticks*. The adjacent monomer and the side chain of residue Arg-167′ are shown in *green cartoon* and *sticks*, respectively. The *gray mesh* around Ap5G represents the $2mF_o - DF_c$ electron density map contoured at the 1.3σ level (a stereoview of the final $F_o - F_c$ omit map is shown in Fig. S2*A*). Key protein–nucleotide atomic interactions are represented as *yellow dashed lines*. *B*, ATP and GDP mononucleotide structures bound to AgIMPDH (PDB code 5TC3 (21)) compared with the bound structure of Ap5G (PDB code 6RPU, this work). The structural alignment was generated by superimposing the backbone atoms of the Bateman domains (residues 130–210) of both structures. *C*, SAXS profiles of AgIMPDH in the presence of different mononucleotides and dinucleoside polyphosphates. To facilitate visualization, the plots have been conveniently displaced along the *y axis* and grouped according to three different conformations: tetramers, extended, and compacted octamers. The profiles shown correspond to: (i) tetramers: *1*, control; *2*, 0.3 mM GDP; (ii) extended octamers: *3*, 3 mM ATP; *4*, 0.1 mM Ap6A; *5*, 0.1 mM Ap6A + 3 mM GDP; (iii) compacted octamers: *6*, 3 mM GDP; *7*, 0.1 mM Ap5G + 0.3 mM GDP; *8*, 0.1 mM Ap4A + 3 mM GDP; *9*, 3 mM ATP + 3 mM GDP.

to expand the compacted octamers formed in the presence of millimolar amounts of GDP (Fig. 3*C*), reverting the GDP-induced inhibition of the catalytic activity. Additionally, as expected, Ap5G (profile *7*) in the presence of a subsaturating concentration of GDP (0.3 mM GDP (profile *2*); unable to induce a significant proportion of octamers) induces compacted, inhibited octamers identical to those formed in the presence of millimolar amounts of GDP (profile *6*; Fig. 3*C*). A more detailed SAXS-data analysis, including the estimated

structural parameters for each profile, can be found in Table S1.

Thereby, as for the mononucleotides, the conformations of AgIMPDH induced by the binding of dinucleoside polyphosphates correlate with their catalytic activities. Ap6A induces the formation of extended octamers that are catalytically active, whereas Ap5G in combination with subsaturating concentrations of GTP/GDP induces the formation of compacted octamers that show a significant reduction of the catalytic activity. Moreover, Ap6A is able to revert the GDP-mediated inhibition of the IMPDH catalytic activity by expanding the GDP-induced compacted octamers.

Dinucleoside polyphosphates modulate the activity of the human IMPDH isoforms

Several lines of experimental evidence indicating that the mechanism for allosteric regulation, initially described for AgIMPDH (22), also operates in other eukaryotic IMPDHs, including the two human isoforms, have been reported (20, 23, 25). We therefore tested next whether dinucleoside polyphosphates might also modulate the catalytic activity of human IMPDHs *in vitro*.

We first assayed the effects of diadenosine polyphosphates on HsIMPDH1 and observed no significant effect on its catalytic activity (Fig. 4*A*). However, Ap5A was able to efficiently revert the GDP-induced inhibition of HsIMPDH1, in contrast to Ap6A that showed no effect (Fig. 4*A*). These results are in contrast to those found for AgIMPDH where Ap6A efficiently activates the GDP-inhibited enzyme (Fig. 2*B*). These data are indeed unexpected given the high similarity between the structures of both organisms (20, 22). Nonetheless, the comparison of the human and fungal structures of IMPDH bound to GDP showed a displacement of about 2 Å in the guanine ring bound to the canonical site 1, which might thus impose a different optimal polyphosphate chain length (Fig. S4*B*). These data indicate the existence of sequence determinants that dictate the binding specificity of different dinucleoside polyphosphates. These sequence determinants might serve to specifically adapt the regulation of IMPDH to the metabolic requirements of each organism as anticipated above.

We next assayed the effects of Ap5G and Gp5G on the enzymatic activity of HsIMPDH1 *in vitro* and observed no significant effect for both nucleotides alone (Fig. 4*B*). However, as observed for AgIMPDH, Ap5G was able to inhibit the enzyme in combination with a subsaturating concentration of GDP; Gp5G, in contrast, showed no effect at all (Fig. 4*B*). Thereby, these data further corroborate the results obtained with the fungal protein, showing that Ap5G hypersensitizes the IMPDH enzyme to the GTP/GDP-mediated allosteric inhibition.

Altogether, the data reported here show that submicromolar amounts of dinucleoside polyphosphates modulate the conformational switch and the catalytic activity of IMPDHs *in vitro*. These concentrations are in the same range as the reported intracellular concentrations (26), which indicates that dinucleoside polyphosphates might have an important role in the physiological regulation of IMPDH. These results significantly contribute to the understanding of the regulation of IMPDH and yield relevant information for potential new pharmacological approaches to target IMPDH that definitively deserve further investigation.

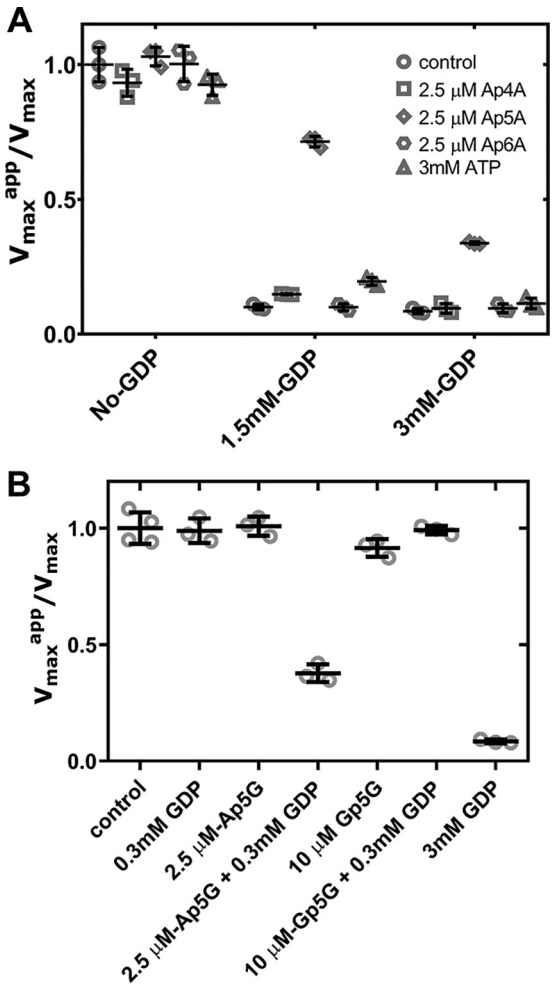


Figure 4. Effects of dinucleoside polyphosphates on the catalytic activity of HsIMPDH1 *in vitro*. Scatter plots show the normalized V_{max} values (V_{max}^{app} in the presence of nucleotide divided by the V_{max} in the absence of nucleotide) of several adenine dinucleoside polyphosphates compared with ATP (*A*) as well as Ap5G and Gp5G alone and in combination with GDP at a subsaturating concentration of 0.3 mM (*B*). V_{max} values are derived from the Michaelis–Menten analysis of the experimental data. The *empty symbols* (*light gray*) are the values obtained from independent experiments, and the *error bars* (*black*) represent S.E.

Experimental procedures

Proteins and nucleotides

Expression and purification of AgIMPDH and HsIMPDH proteins were performed as described previously (20, 22). PaIMPDH was overexpressed in *E. coli* (BL21) cells fused to an N-terminal His_8 tag and purified following standard immobilized metal affinity chromatography (HisTrap FF Crude column) and size-exclusion chromatography (HiPrep 16/60 Sephacryl S-300 HR column). All proteins were stored frozen at −80 °C in buffer (20 mM Tris-HCl, 500 mM KCl, 1 mM DTT, pH 8.0). Mononucleotides and dinucleoside polyphosphates were purchased from Sigma-Aldrich and Jena Bioscience.

Enzyme kinetics experiments

IMPDH activity was assayed at 28 (AgIMPDH) or 32 °C (HsIMPDH and PaIMPDH) using 384-well microtiter plates by

monitoring the reduction of NAD^+ to NADH and the subsequent increase in absorbance at 340 nm. IMPDH enzymes (15–55 μg/ml) in reaction buffer (100 mM Tris-HCl, 100 mM KCl, 2 mM DTT, 1 mM free $MgCl_2$, pH 8.0) were assayed using 0.5 mM NAD^+ and 0.039–5 mM IMP as substrates in the presence of different mononucleotide and dinucleoside polyphosphate concentrations. Experimental data were fitted by nonlinear regression to Michaelis–Menten and dose-response (four parameters, variable slope) equations to estimate the K_m or $K_{1/2}$ and V_{max} values using the software GraphPad Prism.

Crystallization and structure determination

Crystals of the ternary complex AgIMPDH–Ap5G–GDP were grown at 22 °C using the vapor-diffusion method by mixing a protein solution at 10 mg/ml in 10 mM Tris-HCl, 50 mM KCl, 1 mM DTT, 0.5 mM Ap5G, 3 mM GDP, 5 mM total $MgCl_2$, pH 8.0, with an equal volume of mother liquor consisting of 20% PEG-6000, 0.1 M sodium acetate, pH 5.0, 0.2 M sodium chloride. Protein crystals were cryoprotected by immersion in NVH oil before being flash cooled in liquid nitrogen. Diffraction data were collected at 100 K using monochromatic X-rays of ≈1-Å wavelength at the XALOC beamline (27) in the ALBA Synchrotron (Spain).

Diffraction intensities were indexed and integrated with the autoPROC toolbox (28), which makes use of STARANISO software (29) to deal with data anisotropy. Indeed, the experimental data showed strong anisotropy with ellipsoidal resolution limits defined by STARANISO at 2.10 (*a*), 2.10 (*b*), and 3.13 (*c*) Å using as threshold $I/\sigma I \geq 1.2$. The anisotropically truncated data were phased by molecular replacement using the program Phaser (30) and the structure of the complex AgIMPDH–ATP–GDP (PDB code 5TC3) as template. The initial structure obtained by Phaser was iteratively refined by alternating manual modeling with Coot (31) and automated refinement with the PHENIX crystallographic software suite (32) using rigid-body, gradient-driven positional, restrained individual isotropic B-factor and TLS (33). The R and R_{free} factors of the final model are 0.27 and 0.29, respectively, which seem relatively high given the maximum resolution of the data. However, it must be taken into account that the data are markedly anisotropic and the R factors in anisotropic refinement tend to be high, mostly due to the inclusion of numerous poorly measured reflections in anisotropic data sets.

Small angle X-ray scattering

SAXS measurements were performed at the B21 beamline in the Diamond Light Source. Buffer (20 mM Tris-HCl, pH 8.0, 150 mM KCl, 3 mM DTT, 2 mM free $MgCl_2$) and proteins at a concentration of 2.5 mg/ml were measured by flowing the solutions through a quartz capillary at 10 °C to minimize radiation damage. The beam energy was set to 12.4 keV, and the distance from the sample to the detector (Eiger 4M) was fixed at 4.04 m, which allows measurement of a scattering vector (q) range from 0.0032 to 0.38 $Å^{-1}$. Data reduction and analysis were performed by standard methodologies using the PRIMUS program (34) within the ATSAS software package (35).

Author contributions—D. F.-J., R. P., and R. M. B. formal analysis; D. F.-J. and R. M. B. investigation; D. F.-J. and R. M. B. methodology; R. P., J. L. R., and R. M. B. writing-original draft; J. L. R. and R. M. B. conceptualization; J. L. R. and R. M. B. validation; J. L. R. and R. M. B. project administration; J. L. R. and R. M. B. writing-review and editing; R. M. B. funding acquisition; R. M. B. visualization.

Acknowledgments—We thank María Dolores Sánchez, Silvia Domínguez, and Marta Santos for excellent technical help. Protein crystallography experiments were performed at the XALOC beamline at ALBA Synchrotron with the collaboration of the ALBA staff. We also acknowledge Diamond Light Source for time on Beamline B21, where the SAXS experiments were performed, under Proposal Infrastructure for NMR, EM and X-rays for Translational Research (iNEXT) number 8311.

References

1. Finamore, F. J., and Warner, A. H. (1963) The occurrence of P1,P4-diguanosine 5′-tetraphosphate in brine shrimp eggs. *J. Biol. Chem.* **238,** 344–348 Medline
2. Zamecnik, P. C., Stephenson, M. L., Janeway, C. M., and Randerath, K. (1966) Enzymatic synthesis of diadenosine tetraphosphate and diadenosine triphosphate with a purified lysyl-sRNA synthetase. *Biochem. Biophys. Res. Commun.* **24,** 91–97 CrossRef Medline
3. Rapaport, E., and Zamecnik, P. C. (1976) Presence of diadenosine 5′,5‴-P1,P4-tetraphosphate (Ap4A) in mammalian cells in levels varying widely with proliferative activity of the tissue: a possible positive "pleiotypic activator". *Proc. Natl. Acad. Sci. U.S.A.* **73,** 3984–3988 CrossRef Medline
4. Sillero, M. A., De Diego, A., Osorio, H., and Sillero, A. (2002) Dinucleoside polyphosphates stimulate the primer independent synthesis of poly(A) catalyzed by yeast poly(A) polymerase. *Eur. J. Biochem.* **269,** 5323–5329 CrossRef Medline
5. Nishimura, A., Moriya, S., Ukai, H., Nagai, K., Wachi, M., and Yamada, Y. (1997) Diadenosine 5′,5‴-P1,P4-tetraphosphate (Ap4A) controls the timing of cell division in *Escherichia coli*. *Genes Cells* **2,** 401–413 CrossRef Medline
6. Gómez-Villafuertes, R., Pintor, J., Gualix, J., and Miras-Portugal, M. T. (2004) GABA modulates presynaptic signalling mediated by dinucleotides on rat synaptic terminals. *J. Pharmacol. Exp. Ther.* **308,** 1148–1157 CrossRef Medline
7. Vartanian, A. A., Suzuki, H., and Poletaev, A. I. (2003) The involvement of diadenosine 5′,5‴-P1,P4-tetraphosphate in cell cycle arrest and regulation of apoptosis. *Biochem. Pharmacol.* **65,** 227–235 CrossRef Medline
8. Giraldez, L., Díaz-Hernandez, M., Gomez-Villafuertes, R., Pintor, J., Castro, E., and Miras-Portugal, M. T. (2001) Adenosine triphosphate and diadenosine pentaphosphate induce $[Ca^{2+}]_i$ increase in rat basal ganglia aminergic terminals. *J. Neurosci. Res.* **64,** 174–182 CrossRef Medline
9. Conant, A. R., Theologou, T., Dihmis, W. C., and Simpson, A. W. (2008) Diadenosine polyphosphates are selective vasoconstrictors in human coronary artery bypass grafts. *Vascul. Pharmacol.* **48,** 157–164 CrossRef Medline
10. Lüthje, J., Baringer, J., and Ogilvie, A. (1985) Effects of diadenosine triphosphate (Ap3A) and diadenosine tetraphosphate (Ap4A) on platelet aggregation in unfractionated human blood. *Blut* **51,** 405–413 CrossRef Medline
11. Lienhard, G. E., and Secemski, I. I. (1973) P1,P5-Di(adenosine-5′)pentaphosphate, a potent multisubstrate inhibitor of adenylate kinase. *J. Biol. Chem.* **248,** 1121–1123 Medline
12. Jankowski, V., van der Giet, M., Mischak, H., Morgan, M., Zidek, W., and Jankowski, J. (2009) Dinucleoside polyphosphates: strong endogenous agonists of the purinergic system. *Br. J. Pharmacol.* **157,** 1142–1153 CrossRef Medline
13. Johnstone, D. B., and Farr, S. B. (1991) AppppA binds to several proteins in *Escherichia coli*, including the heat shock and oxidative stress proteins

ASBMB

DnaK, GroEL, E89, C45 and C40. *EMBO J.* **10,** 3897–3904 CrossRef Medline
14. Marques, A. F., Teixeira, N. A., Gambaretto, C., Sillero, A., and Sillero, M. A. (1998) IMP-GMP 5′-nucleotidase from rat brain: activation by polyphosphates. *J. Neurochem.* **71,** 1241–1250 Medline
15. Anashkin, V. A., Salminen, A., Tuominen, H. K., Orlov, V. N., Lahti, R., and Baykov, A. A. (2015) Cystathionine β-synthase (CBS) domain-containing pyrophosphatase as a target for diadenosine polyphosphates in bacteria. *J. Biol. Chem.* **290,** 27594–27603 CrossRef Medline
16. Despotović, D., Brandis, A., Savidor, A., Levin, Y., Fumagalli, L., and Tawfik, D. S. (2017) Diadenosine tetraphosphate (Ap4A)—an *E. coli* alarmone or a damage metabolite? *FEBS J.* **284,** 2194–2215 CrossRef Medline
17. Guo, W., Azhar, M. A., Xu, Y., Wright, M., Kamal, A., and Miller, A. D. (2011) Isolation and identification of diadenosine 5′,5‴-P1,P4-tetraphosphate binding proteins using magnetic bio-panning. *Bioorg. Med. Chem. Lett.* **21,** 7175–7179 CrossRef Medline
18. Ereño-Orbea, J., Oyenarte, I., and Martínez-Cruz, L. A. (2013) CBS domains: ligand binding sites and conformational variability. *Arch. Biochem. Biophys.* **540,** 70–81 CrossRef Medline
19. Scott, J. W., Hawley, S. A., Green, K. A., Anis, M., Stewart, G., Scullion, G. A., Norman, D. G., and Hardie, D. G. (2004) CBS domains form energy-sensing modules whose binding of adenosine ligands is disrupted by disease mutations. *J. Clin. Investig.* **113,** 274–284 CrossRef Medline
20. Fernández-Justel, D., Nuñez, R., Martín-Benito, J., Jimeno, D., González-López, A., Soriano, E. M., Revuelta, J. L., and Buey, R. M. (2019) A nucleotide-dependent conformational switch controls the polymerization of human IMP dehydrogenases to modulate their catalytic activity. *J. Mol. Biol.* **431,** 956–969 CrossRef Medline
21. Buey, R. M., Fernández-Justel, D., Marcos-Alcalde, Í., Winter, G., Gómez-Puertas, P., de Pereda, J. M., and Luis Revuelta, J. (2017) A nucleotide-controlled conformational switch modulates the activity of eukaryotic IMP dehydrogenases. *Sci. Rep.* **7,** 2648 CrossRef Medline
22. Buey, R. M., Ledesma-Amaro, R., Velázquez-Campoy, A., Balsera, M., Chagoyen, M., de Pereda, J. M., and Revuelta, J. L. (2015) Guanine nucleotide binding to the Bateman domain mediates the allosteric inhibition of eukaryotic IMP dehydrogenases. *Nat. Commun.* **6,** 8923 CrossRef Medline
23. Duong-Ly, K. C., Kuo, Y. M., Johnson, M. C., Cote, J. M., Kollman, J. M., Soboloff, J., Rall, G. F., Andrews, A. J., and Peterson, J. R. (2018) T cell activation triggers reversible inosine-5′-monophosphate dehydrogenase assembly. *J. Cell Sci.* **131,** jcs223289 CrossRef Medline
24. Traut, T. W. (1994) Physiological concentrations of purines and pyrimidines. *Mol. Cell. Biochem.* **140,** 1–22 CrossRef Medline
25. Anthony, S. A., Burrell, A. L., Johnson, M. C., Duong-Ly, K. C., Kuo, Y. M., Simonet, J. C., Michener, P., Andrews, A., Kollman, J. M., and Peterson, J. R. (2017) Reconstituted IMPDH polymers accommodate both catalytically active and inactive conformations. *Mol. Biol. Cell* **28,** 2600–2608 CrossRef Medline
26. Garrison, P. N., and Barnes, L. D. (1992) Determination of dinucleoside polyphosphates, in *Ap4A and Other Dinucleoside Polyphosphates* (McLennan, A. G., ed) pp. 29–61, CRC Press Inc., Boca Raton, FL
27. Juanhuix, J., Gil-Ortiz, F., Cuní, G., Colldelram, C., Nicolás, J., Lidón, J., Boter, E., Ruget, C., Ferrer, S., and Benach, J. (2014) Developments in optics and performance at BL13-XALOC, the macromolecular crystallography beamline at the ALBA synchrotron. *J. Synchrotron Radiat.* **21,** 679–689 CrossRef Medline
28. Vonrhein, C., Flensburg, C., Keller, P., Sharff, A., Smart, O., Paciorek, W., Womack, T., and Bricogne, G. (2011) Data processing and analysis with the autoPROC toolbox. *Acta Crystallogr. D Biol. Crystallogr.* **67,** 293–302 CrossRef Medline
29. Tickle, I. J., Flensburg, C., Keller, P., Paciorek, W., Sharff, A., Vonrhein, C., and Bricogne, G. (2018) *STARANISO*, Global Phasing Ltd., Cambridge, UK
30. McCoy, A. J., Grosse-Kunstleve, R. W., Adams, P. D., Winn, M. D., Storoni, L. C., and Read, R. J. (2007) Phaser crystallographic software. *J. Appl. Crystallogr.* **40,** 658–674 CrossRef Medline
31. Emsley, P., Lohkamp, B., Scott, W. G., and Cowtan, K. (2010) Features and development of Coot. *Acta Crystallogr. D Biol. Crystallogr.* **66,** 486–501 CrossRef Medline
32. Adams, P. D., Afonine, P. V., Bunkóczi, G., Chen, V. B., Davis, I. W., Echols, N., Headd, J. J., Hung, L. W., Kapral, G. J., Grosse-Kunstleve, R. W., McCoy, A. J., Moriarty, N. W., Oeffner, R., Read, R. J., Richardson, D. C., *et al.* (2010) PHENIX: a comprehensive Python-based system for macromolecular structure solution. *Acta Crystallogr. D Biol. Crystallogr.* **66,** 213–221 CrossRef Medline
33. Winn, M. D., Isupov, M. N., and Murshudov, G. N. (2001) Use of TLS parameters to model anisotropic displacements in macromolecular refinement. *Acta Crystallogr. D Biol. Crystallogr.* **57,** 122–133 CrossRef Medline
34. Konarev, P. V., Volkov, V. V., Sokolova, A. V., Koch, M. H. J., and D.I., S. (2003) PRIMUS—a Windows-PC based system for small-angle scattering data analysis. *J. Appl. Crystallogr.* **36,** 1277–1282 CrossRef
35. Franke, D., Petoukhov, M. V., Konarev, P. V., Panjkovich, A., Tuukkanen, A., Mertens, H. D. T., Kikhney, A. G., Hajizadeh, N. R., Franklin, J. M., Jeffries, C. M., and Svergun, D. I. (2017) ATSAS 2.8: a comprehensive data analysis suite for small-angle scattering from macromolecular solutions. *J. Appl. Crystallogr.* **50,** 1212–1225 CrossRef Medline

SUPPORTING INFORMATION

The Bateman domain of IMP dehydrogenase is a binding target for dinucleoside polyphosphates

Running title: Binding of dinucleoside polyphosphates to IMPDH

David Fernández-Justel[1], Rafael Peláez[2], José Luis Revuelta[1*] and Rubén M Buey[1*]

[1]Metabolic Engineering Group, Dpto. Microbiología y Genética. Universidad de Salamanca. Campus Miguel de Unamuno, 37007, Salamanca, Spain

[2]Laboratorio de Química Orgánica y Farmacéutica, Dpto. Ciencias Farmacéuticas. Universidad de Salamanca Campus Miguel de Unamuno 37007, Salamanca, Spain

*To whom correspondence should be addressed: JLR (revuelta@usal.es) or RMB (ruben.martinez@usal.es)

SUPPLEMENTAL TABLES

Supplemental Table 1. Structural parameters derived from the SAXS data shown in the Figure 3B of the main text.

	TETRAMERS		**EXTENDED OCTAMERS**			**COMPACTED OCTAMERS**			
	1	**2**	**3**	**4**	**5**	**6**	**7**	**8**	**9**
	control	**0.3mM GDP**	**3mM ATP**	**0.1mM Ap6A**	**0.1mM Ap6A / 3mM GDP**	**3mM GDP**	**0.1mM Ap5G / 0.3mM GDP**	**0.1mM Ap4A / 3mM GDP**	**3mM ATP / 3mM GDP**
Guinier analysis									
Rg (Å)	45.6 ± 0.3	45.5 ± 0.3	52.7 ± 0.3	51.9 ± 0.2	53.0 ± 0.6	49.9 ± 0.2	49.7 ± 0.2	49.9 ± 0.3	50.0 ± 0.2
qRg max	1.3	1.3	1.2	1.3	1.3	1.3	1.2	1.3	1.2
P(r) analysis									
Rg (Å)	45.8 ± 0.4	45.7 ± 0.4	52.6 ± 0.8	51.7 ± 0.7	51.7 ± 0.3	50.0 ± 0.8	49.3 ± 0.8	49.9 ± 0.8	50.1 ± 0.8
d_{max} *(Å)*	157	155	148	148	158	150	146	151	155
Particle volumen (Å^3)	431000	426000	833000	874000	901000	899000	879000	894000	909000
GNOM quality estimate	0.85	0.83	0.76	0.75	0.86	0.73	0.72	0.73	0.73

SUPPLEMENTAL FIGURE CAPTIONS

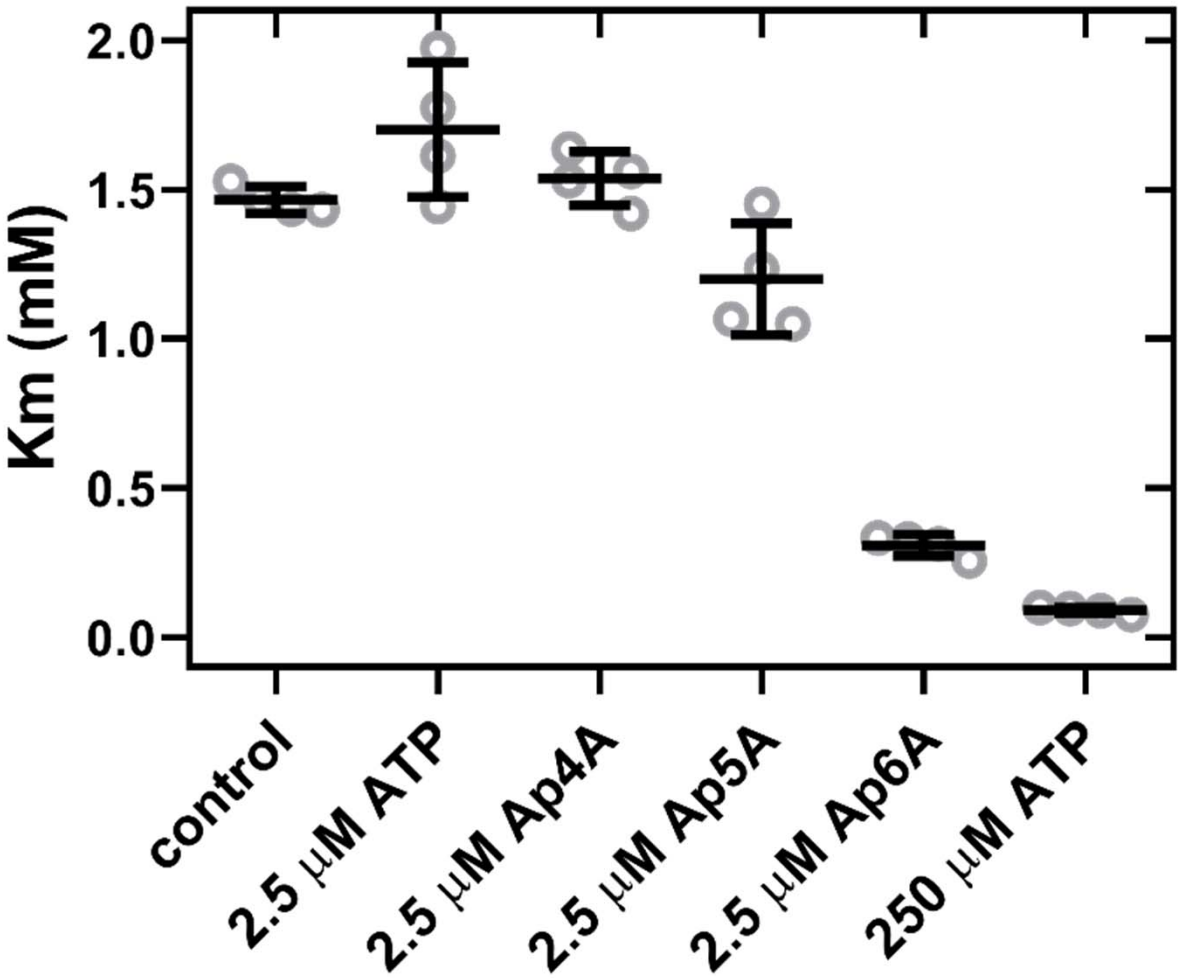
Supplemental Figure 1. *Dinucleoside polyphosphate activation of the bacterial PaIMPDH enzyme.* Scatter plot showing the K_M values (and the standard errors derived from 4 independent measurements) obtained from the Michaelis-Menten analysis of the experimental data. Reactive concentrations were set to 15 µg/mL enzyme, 0.5 mM NAD^+ and 0.039-5 mM IMP. The reaction buffer was 100 mM TrisHCl, pH 8.0, 100 mM KCl, 1 mM free $MgCl_2$, 2 mM DTT and the reactions were performed at 32ºC on 384-well plates by monitoring the increase in absorbance at 340 nm, due to NADH formation.

Supplemental Figure 2. *Structure of the ternary complex AgIMPDH-Ap5G-GDP.* **A.** Cartoon representation of the structure of AgIMPDH octamers formed in the presence of Ap5G (orange sticks) and GDP (red sticks). The catalytic domain is shown in light grey, while the Bateman regulatory domain is colored in blue. **B.** Structural alignment of monomers from AgIMPDH-ATP-GDP (PDB code 5TC3; orange cartoons), AgIMPDH-GDP (PDB code 4Z87; blue cartoons) and AgIMPDH-Ap5G-GDP (6RPU from this work; green cartoons).

Supplemental Figure 3. *Dinucleoside polyphosphates occupy a positively charged groove in the Bateman domain of IMPDHs.* **A.** Close-up stereoview of Ap5G (sticks) bound to the two canonical sites of the Bateman domain of AgIMPDH (green cartoon). The blue mesh represents the final SA-omit F_o-F_c electron density, contoured at 1.4σ level. **B.** Surface electrostatic potential representation showing the highly charged positive groove where the polyphosphate chain of Ap5G (shown in sticks) is buried.

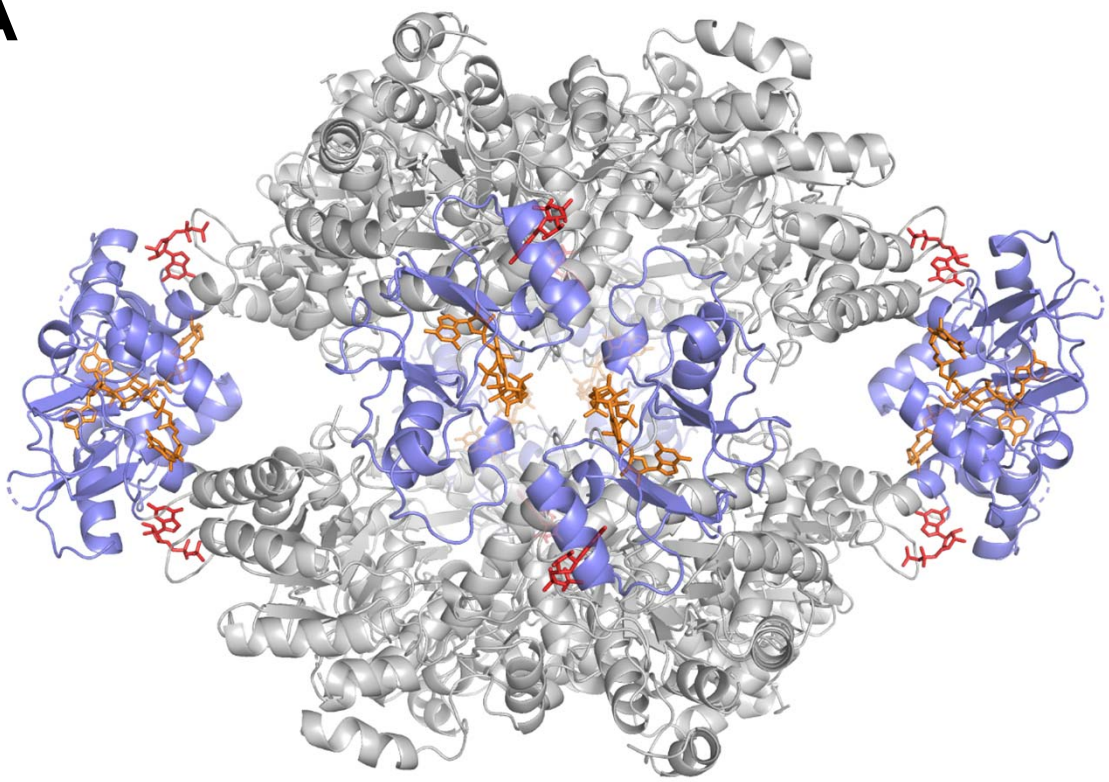
Supplemental Figure 4. *Differences in nucleotide binding to the Bateman domain of IMPDH.* **A.** Close-up views of the nucleotides (shown in sticks) bound to the two canonical sites of AgIMPDH (represented in semi-transparent blue cartoons). Blue: AgIMPDH-Ap5G (PDB code 6RPU from this work). Green: AgIMPDH-GDP (PDB code 4Z87). **B.** Red: HsIMPDH2-GDP (PDB code 6I0M). Green: AgIMPDH-GDP (PDB code 4Z87). The canonical binding sites (1 or 2) are indicated after the corresponding nucleotides, i.e. GDP1 means GDP bound to the canonical site 1.

SUPPLEMENTAL FIGURE 1

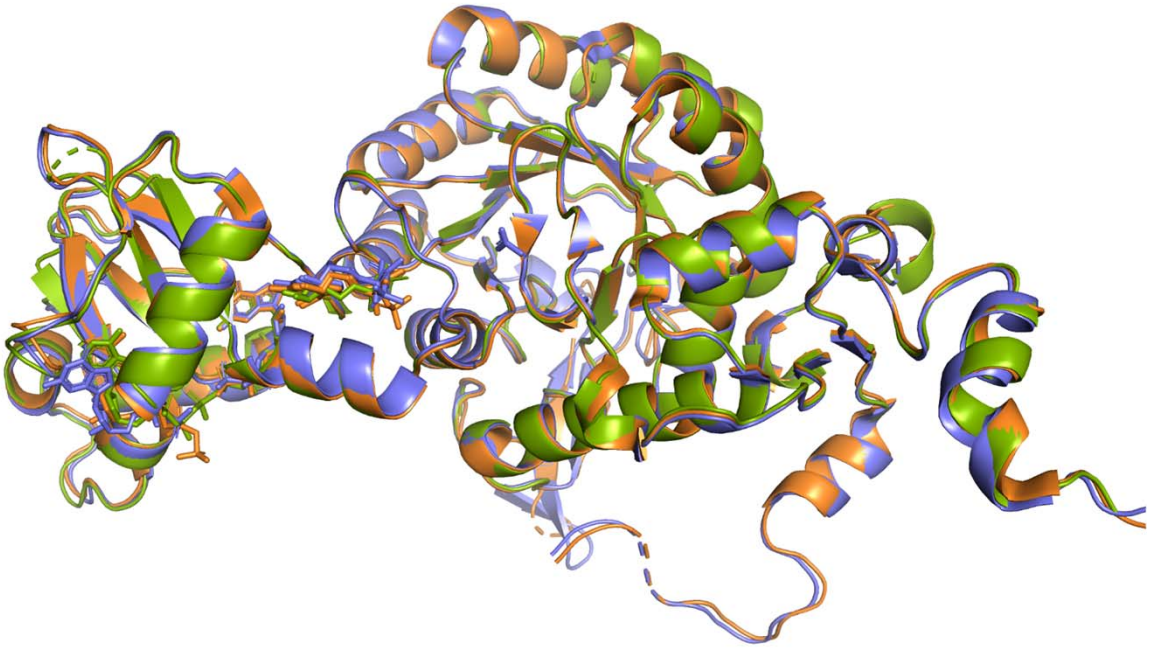


SUPPLEMENTAL FIGURE 2

A

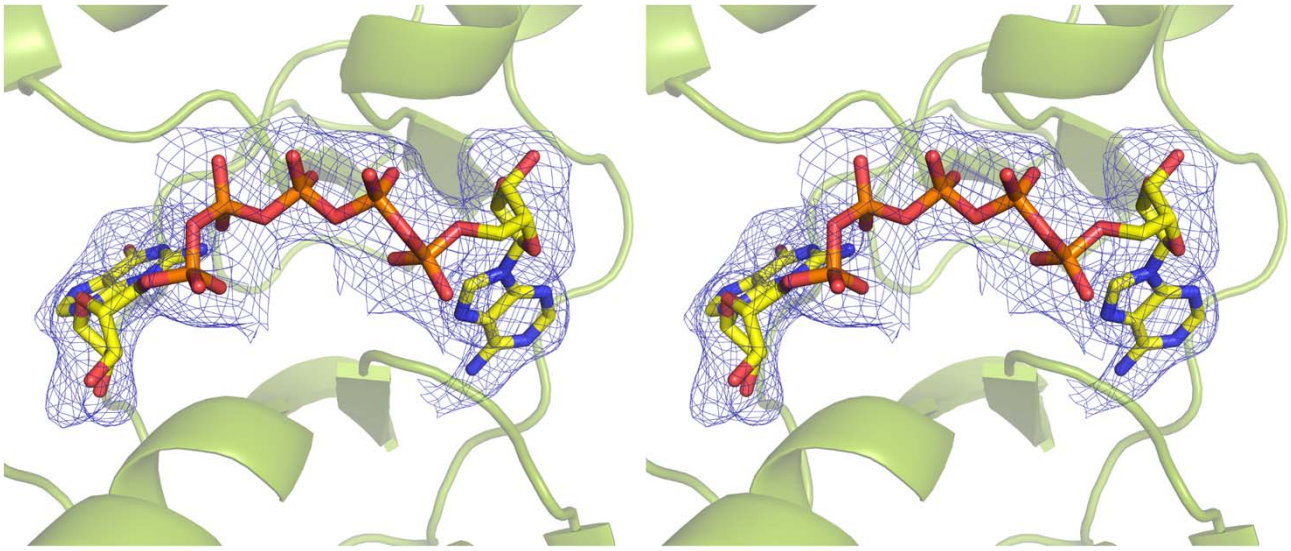


B

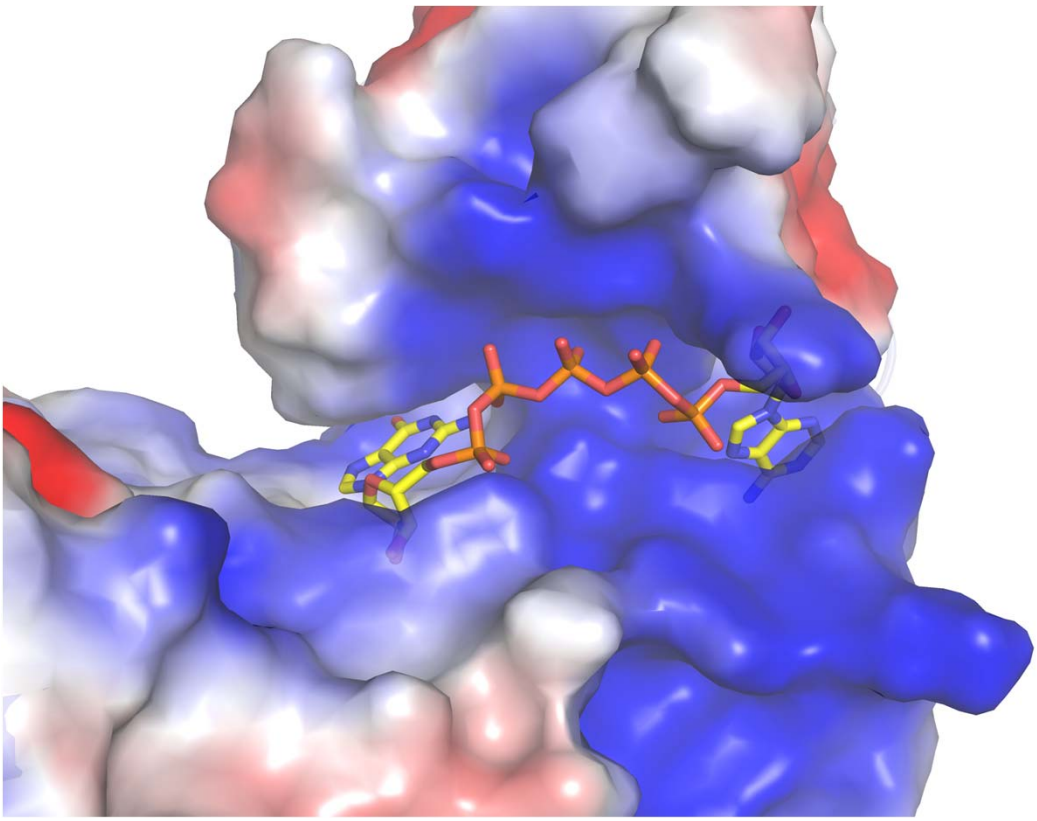


SUPPLEMENTAL FIGURE 3

A

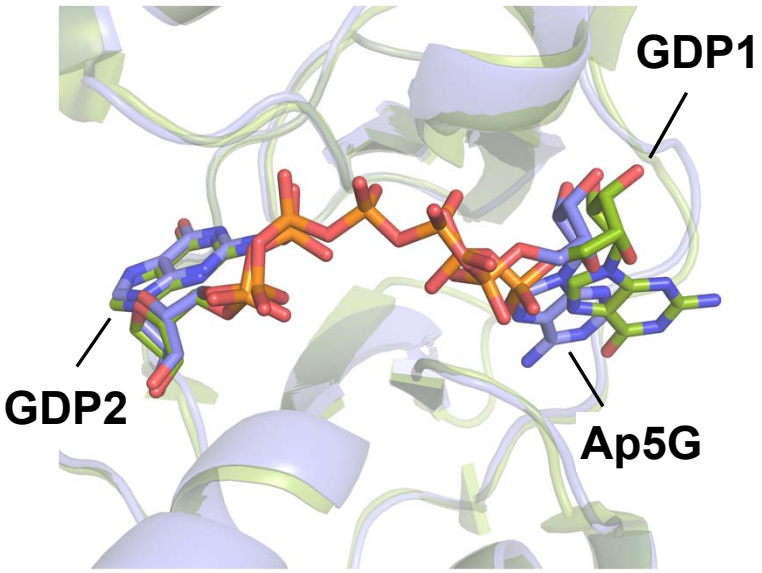


B

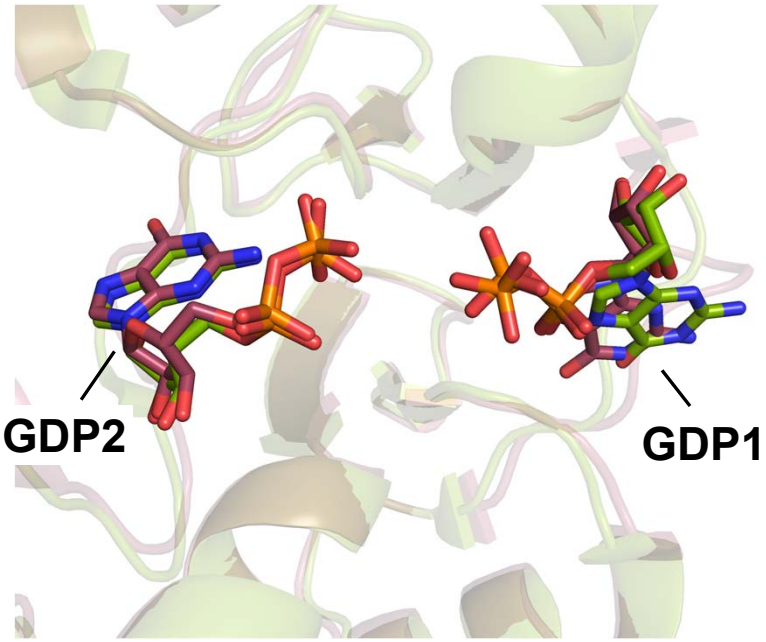


SUPPLEMENTAL FIGURE 4

A



B



Artículo 3

Título:

Diversidad de mecanismos para controlar la homeostasis del GTP en bacterias mediante la unión mutuamente excluyente de nucleótidos de adenina y guanina a la IMP deshidrogenasa.

Resumen:

La IMP deshidrogenasa es una enzima esencial que cataliza el paso limitante en la ruta de biosíntesis de nucleótidos de guanina. En células eucariotas, la unión de GTP al dominio regulador controla alostéricamente la actividad de la IMPDH por un mecanismo que está a su vez modulado por modificaciones post-traduccionales y polimerización enzimática. Sin embargo, en células bacterianas los mecanismos de regulación de la IMPDH permanecen sin clarificar. En este trabajo se propuso evaluar si el mecanismo alostérico de regulación está presente en IMPDHs bacterianas y caracterizar el modo de unión de los nucleótidos de purina que lo gobiernan; para lo que se hizo uso de análisis bioquímicos, estructurales y evolutivos.

Aquí, demostramos que, en la mayoría de grupos bacterianos, el (p)ppGpp compite con el ATP para modular alostéricamente la actividad de la IMPDH mediante la unión a un bolsillo en el dominio regulador desconocido hasta la fecha, conservado y de alta afinidad. Este bolsillo de unión se perdió durante la evolución de las Proteobacterias, haciendo a sus IMPDHs insensibles a estas alarmonas. En su lugar, la mayoría de las IMPDHs de Proteobacterias evolucionaron para ser directamente moduladas por el equilibrio entre ATP y GTP, que compiten por el mismo sitio alostérico de unión. En conjunto, demostramos que la actividad de las IMPDHs bacterianas está modulada alostéricamente por un *interruptor conformacional* controlado por nucleótidos y universalmente conservado que ha evolucionado divergentemente para adaptarse a las particularidades específicas de cada organismo. Estos resultados reconcilian los datos publicados sobre el diálogo entre la señalización por (p)ppGpp y la ruta de biosíntesis de nucleótidos de guanina y refuerzan el papel esencial de la regulación alostérica de la IMPDH en la homeostasis del GTP en bacterias.

Check for updates

Received: 11 February 2022 | Revised: 21 March 2022 | Accepted: 6 April 2022

DOI: 10.1002/pro.4314

FULL-LENGTH PAPER

THE PROTEIN SOCIETY WILEY

Diversity of mechanisms to control bacterial GTP homeostasis by the mutually exclusive binding of adenine and guanine nucleotides to IMP dehydrogenase

David Fernández-Justel[1] | Íñigo Marcos-Alcalde[2,3] | Federico Abascal[4] | Nerea Vidaña[1] | Paulino Gómez-Puertas[2] | Alberto Jiménez[1] | José L. Revuelta[1] | Rubén M. Buey[1]

[1]Metabolic Engineering Group, Department of Microbiology and Genetics, Universidad de Salamanca, Salamanca, Spain

[2]Molecular Modeling Group, Centro de Biología Molecular Severo Ochoa, CBMSO (CSIC-UAM), Madrid, Spain

[3]Biosciences Research Institute, School of Experimental Sciences, Universidad Francisco de Vitoria, Madrid, Spain

[4]Wellcome Sanger Institute, Hinxton, UK

Correspondence
Rubén M. Buey, Lab233, Edificio Departamental, Campus Miguel de Unamuno, s/n. 37007 Salamanca, Spain.
Email: ruben.martinez@usal.es

Funding information
Instituto de Salud Carlos III, Grant/Award Number: DTS20-00024; Ministerio de Ciencia e Innovación, Grant/Award Numbers: BIO2017-88435-R, PID2019-109671GB-I00, PID2020-118200RB-I00, RTC-2017-6494-1, RTI2018-094434-B-I00

Review editor: John Kuriyan

Abstract

IMP dehydrogenase(IMPDH) is an essential enzyme that catalyzes the rate-limiting step in the guanine nucleotide pathway. In eukaryotic cells, GTP binding to the regulatory domain allosterically controls the activity of IMPDH by a mechanism that is fine-tuned by post-translational modifications and enzyme polymerization. Nonetheless, the mechanisms of regulation of IMPDH in bacterial cells remain unclear. Using biochemical, structural, and evolutionary analyses, we demonstrate that, in most bacterial phyla, (p)ppGpp compete with ATP to allosterically modulate IMPDH activity by binding to a, previously unrecognized, conserved high affinity pocket within the regulatory domain. This pocket was lost during the evolution of Proteobacteria, making their IMPDHs insensitive to these alarmones. Instead, most proteobacterial IMPDHs evolved to be directly modulated by the balance between ATP and GTP that compete for the same allosteric binding site. Altogether, we demonstrate that the activity of bacterial IMPDHs is allosterically modulated by a universally conserved nucleotide-controlled conformational switch that has divergently evolved to adapt to the specific particularities of each organism. These results reconcile the reported data on the crosstalk between (p)ppGpp signaling and the guanine nucleotide biosynthetic pathway and reinforce the essential role of IMPDH allosteric regulation on bacterial GTP homeostasis.

KEYWORDS

(p)ppGpp, allosteric regulation, bacterial GTP homeostasis, IMP dehydrogenase, protein structure and function, purine nucleotide biosynthesis

1 | INTRODUCTION

Purine nucleotides are essential molecules that cells synthetize in two different ways. In the de novo pathway, the purine ring system is stepwise assembled from 5-phospho-α-D-ribose 1-diphosphate, while the *salvage* pathway recycles preformed nucleobases, nucleosides, and nucleotides.

This is an open access article under the terms of the Creative Commons Attribution License, which permits use, distribution and reproduction in any medium, provided the original work is properly cited.
© 2022 The Authors. *Protein Science* published by Wiley Periodicals LLC on behalf of The Protein Society.

IMP dehydrogenase (IMPDH) catalyzes the first step in the guanine nucleotide de novo biosynthetic pathway, at the bifurcation of the guanine and adenine routes, which share the precursor IMP (Figure 1a). This constitutes a rate-limiting step essential for balancing the metabolic flux through these parallel synthesis pathways. Therefore, IMPDH plays important roles in homeostasis maintenance and the inhibition of its catalytic activity has antiproliferative effects. Indeed, several drugs that target IMPDH are widely used at present for antiviral and immunosuppressive chemotherapy.[1–4] As an important pharmacological target, IMPDH has been object of various structural and functional studies that include the identification of a large variety of inhibitors.[5] Nonetheless, the physiological regulation of IMPDH remain unclear and it has only been since the past few years that we are starting to envisage the diversity and complexity of its regulatory mechanisms.[6–15]

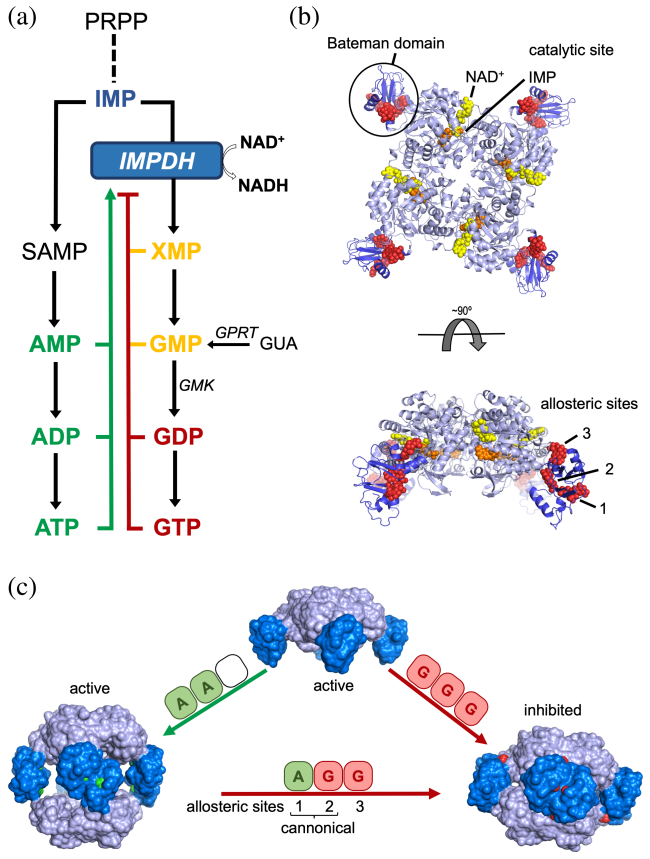


FIGURE 1 Structure, function, and regulation of eukaryotic IMPDHs. (a) Schematic and simplified scheme of the de novo purine nucleotide biosynthetic pathways. Competitive inhibitors are colored in yellow, while allosteric activators and inhibitors are colored in green and red, respectively. (b) Ribbon representation of an IMPDH tetramer, showing the catalytic domain (light blue) with the substrates NAD (yellow spheres) and IMP (orange spheres) and the regulatory Bateman domain (dark blue) with three GDP molecules (red spheres) bound. (c) Nucleotide binding to the allosteric sites in the Bateman domain promotes tetramer dimerization into octamers with different conformations and catalytic activities. IMPDH is represented as protein surface with the catalytic and regulatory domains light and dark blue colors, respectively. Adenine and guanine nucleotides bound to the Bateman regulatory domain are shown as spheres colored in green and red, respectively. IMPDH, IMP dehydrogenase

The basic units of IMPDH are tetramers that dimerize to form octamers upon nucleotide binding. An IMPDH monomer consists of a catalytic TIM barrel (Figure 1b; light blue) and a regulatory Bateman domain (Figure 1b; dark blue), which is not required for catalytic activity but is essential for allosteric regulation. GMP[16] and XMP[17] have been reported as competitive inhibitors of IMPDH in vitro (Figure 1a) although it remains unclear if this has relevance in vivo since these molecules are not strong inhibitors even at concentrations that are 10-fold greater than physiological.[7,18]

Eukaryotic IMPDHs contains three allosteric sites (Figure 1b) that operate coordinately to modulate the catalytic activity. Sites 1 and 2 are canonical cystathionine beta synthase motifs, conserved among Bateman domains,[19] that bind either adenine (ATP/ADP/AMP) or guanine (GTP/GDP) nucleotides. The third allosteric noncanonical site, exclusive of eukaryotic IMPDHs, can only bind the guanine nucleotides GTP or GDP.[6] The binding of adenine nucleotides to the canonical Sites 1 and 2 induces extended active octamers, while binding of guanine nucleotides to the allosteric Sites 2 and 3 induces compact octamers (Figure 1c). Octamer compaction forces the active sites of opposing tetramers to interact, forming an interdigitated pseudo beta-barrel that disfavors substrate binding and inhibits catalytic activity. The disruption of any of the three allosteric sites generate constitutively activated mutants[7] and several missense mutations mapping into these sites have been associated to severe retinopathies[20,21] and dystonia.[22]

The mechanism of IMPDH allosteric regulation is fine tuned in eukaryotic cells through post-translational modifications, such as phosphorylation,[23,24] as well as protein polymerization into mesoscale polymers denoted as *rod and rings* or *cytoophidia*.[25–28] Phosphorylation and polymerization desensitize IMPDH to GTP/GDP-mediated inhibition and are triggered when the cell needs a boost of GTP, for example, in conditions of high-rate growth or in response to light during the visual cycle in retinal photoreceptors.[8,13,14,23,25]

In bacteria, the IMPDH enzyme is encoded by the essential gene *guaB* (we will use IMPDH to refer indistinctly to bacterial and eukaryotic enzymes). In contrast to the eukaryotic enzymes, bacterial IMPDHs only contains two canonical allosteric binding sites in their Bateman domains. Bacterial IMPDHs have been

previously reported to be insensitive to guanine nucleotide allosteric inhibition.[7,10] In turn, the catalytic activity of some bacterial IMPDHs is modulated by the binding of ATP to the Bateman domain.[10] According to this observation, Munier–Lehmann's group proposed a classification for bacterial IMPDHs. *Class I* IMPDHs form inhibited compact octamers in vitro that switch to extended active octamers upon ATP binding, while *Class II* IMPDHs are active tetramers that shift to extended (also active) octamers in the presence of ATP.[12]

Increasing experimental evidence point to a relevant role of Bateman domains of IMPDHs in GTP homeostasis. In *Escherichia coli*, the regulatory domain is essential to maintain the intracellular ATP/GTP balance within a narrow physiological range.[18,29] In *Bacillus subtilis*, mutations within the Bateman domain of IMPDH suppress the characteristic phenotype of (p)ppGpp deficiency, suggesting a functional connection between IMPDH allosteric regulation and alarmone signaling.[30–32] Nonetheless, to our knowledge, no physiological mechanism of allosteric inhibition of bacterial IMPDHs has been reported.

In this study, we unveil the diversity of molecular mechanisms of allosteric regulation of bacterial IMPDHs and describe their structural and biochemical basis. These data explain the differences found on the regulation of the guanine nucleotide biosynthesis among bacterial phyla and allow us to propose their plausible evolutionary trajectory. Most possibly, the bacterial IMPDH ancestor was allosterically modulated by the mutually exclusive binding of ATP and (p)ppGpp to the Bateman domain of IMPDH. (p)ppGpp occupy a previously unrecognized site that partially overlaps with the canonical Site 2, where ATP also binds. During the evolution of the proteobacterial lineage, this site was lost and, in turn, the Bateman domain of the IMPDH from most Proteobacteria evolved to be directly modulated by the balance between ATP and GTP, which compete for the canonical Site 2.

In this way, high ATP/GTP—or ATP/(p)ppGpp—ratios favor an extended, catalytically active, conformation. In contrast, when these ratios decrease, guanine nucleotide binding to the regulatory domain induces a compact conformation that significantly reduce the catalytic activity. Thereby, the adenine/guanine nucleotide balance controls a conformational switch that closely resembles that reported for the eukaryotic enzymes, demonstrating the universality of this mechanism. Moreover, in line with eukaryotic enzymes, our data suggest that bacterial IMPDHs also fine-tune the conformational switch by post-translational modifications, such as lysine acetylation. Altogether, these observations represent an excellent example of how evolution has generated different versions of the same mechanism of regulation to adapt to the specific metabolic requirements of each organism. Furthermore, given the therapeutic value of IMPDH, the results presented in this manuscript might have important implications for drug design and boost novel therapeutic approaches.

2 | RESULTS

2.1 | In the presence of ATP, GTP, and GDP significantly inhibit the IMPDH of *E. coli* and *Pseudomonas aeruginosa*

We and others have reported that guanine nucleotides by themselves are not able to significantly inhibit the activity of bacterial IMPDHs in vitro, presumably because they lack the third noncanonical site, which is exclusive of eukaryotic enzymes.[7,10] Nonetheless, we revisited this issue bearing in mind that intracellular levels of ATP are usually significantly higher than GTP.[33] Thereby, we tested the effects of guanine nucleotides on the activity of preformed ATP-induced octamers in vitro.

Corroborating previous reports[7,10] that GTP/GDP alone did not have a significant effect on the catalytic activity of the four bacterial IMPDHs assayed in vitro (Figures 2 and SS1). In contrast, when 0.25 mM ATP is present in the solution, GTP/GDP could readily inhibit the enzymes from the γ-Proteobacteria *E. coli* and *P. aeruginosa* (EcIMPDH and PaIMPDH, respectively), with $K_{i,app}$ values in the mid-micromolar range (Figure 2). On the other side, GTP/GDP could only very weakly inhibit the enzymes from the Firmicute *B. subtilis* and the Actinobacteria *Streptomyces coelicolor* (BsIMPDH and StcIMPDH, respectively), with $K_{i,app}$ values in the millimolar range (Figures 2 and SS1).

2.2 | Crystallographic structures of *P. aeruginosa* bound to ATP and GDP

To gain further insights into the molecular mechanisms of inhibition of GTP/GDP in proteobacterial IMPDHs and to map their binding sites, we aimed at obtaining the high-resolution crystallographic 3D structures of enzyme–nucleotide complexes. After multiple cocrystallization trials, we were able to obtain the structure of PaIMPDH bound to both ATP and GDP at 1.65 Å resolution (Table SS1). The two monomers in the asymmetric unit (AU) contained well-defined electron density in the Bateman domain that could be unequivocally attributed to ATP and GDP bound to the canonical Sites 1 and 2, respectively, as well as a magnesium atom coordinated by their

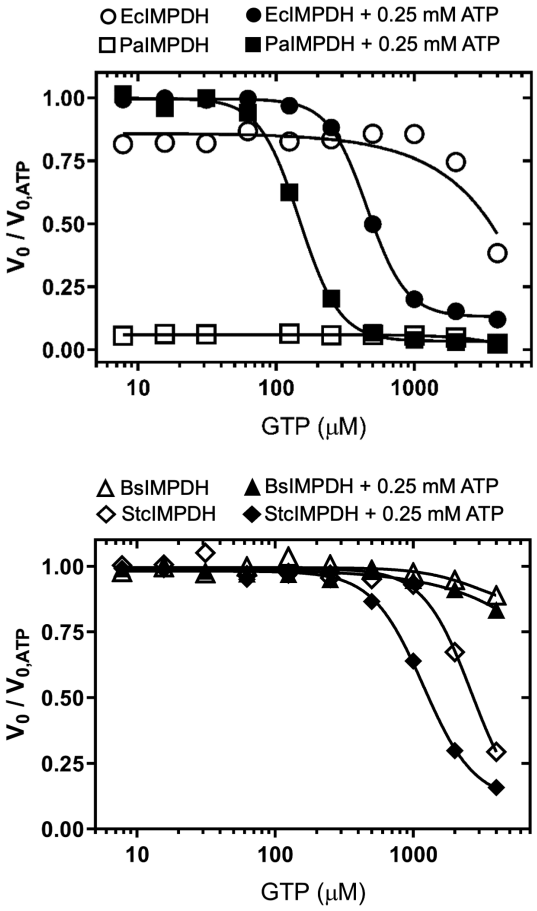


FIGURE 2 Effects of guanine nucleotides on the catalytic activity of IMPDH in vitro. Graphs showing the normalized initial velocity values (V_0 values in the absence of GTP divided by the respective values in the presence of GTP). The V_0 values used for the normalization of the data are EcIMPDH 16.6 ± 1.4, PaIMPDH 26.0 ± 0.7, BsIMPDH 14.2 ± 0.7, and StcIMPDH 14.0 ± 0.3 nM s^{-1} (mean ± std. error). Estimated IC_{50} values for are 455.3 ± 6.3 μM and 147.4 ± 3.9 μM (mean ± std. error) for EcIMPDH and PaIMPDH, respectively. Similar results were obtained for GDP inhibition (Figure S1). BsIMPDH, *Bacillus subtilis* IMPDH; EcIMPDH, *Escherichia coli* IMPDH; IMPDH, IMP dehydrogenase; PaIMPDH, *Pseudomonas aeruginosa* IMPDH; StcIMPDH, *Streptomyces coelicolor* IMPDH

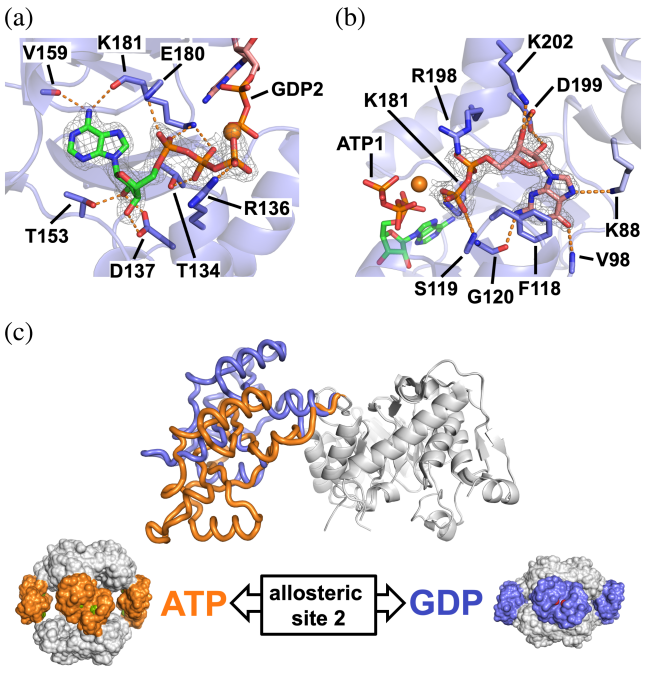


FIGURE 3 Structure of PaIMPDH bound to ATP and GDP. Detailed views of ATP (a) and GDP (b) bound in the Bateman domain to the first and second nucleotide canonical sites, respectively. IMPDH protein is represented in semitransparent blue cartoons with the side chain of key interacting residues shown in sticks. The $2mF_o–DF_c$ electron density map, contoured at the 1.6σ level, is shown as a grey mesh. Key protein–nucleotide atomic interactions are represented as orange dashed lines and the coordinated Magnesium atom is shown as an orange sphere. (c) Upper panel: structural superposition of the catalytic domains (white ribbons) of a monomer of PaIMPDH showing the different conformations adopted by the Bateman domain upon ATP (orange ribbons; PDB ID 4DQW)[10] or ATP/GDP (blue ribbons) binding. Lower panel: the conformational switch described in the upper panel, translated to the octameric structures. PaIMPDH octamers are represented as protein surfaces with the same color code as in the upper panel. IMPDH, IMP dehydrogenase; PaIMPDH, *Pseudomonas aeruginosa* IMPDH

β- and γ-phosphates (Figure 3a, b). The binding modes of ATP and GDP in the canonical sites are identical to those observed in the structures of eukaryotic IMPDHs,[6,13,14,34] where the nucleotide's phosphate groups position close together at the interface of two opposing Bateman domains (Figure S2b).

The recognition of the adenine ring of ATP bound to the canonical Site 1 (ATP1) was mainly due to hydrogen bonds from the backbone carbonyl atoms of residues V159 and K181 and N6 nitrogen atom of the adenine. The O2 and O3 hydroxyl groups of the ribose moiety hydrogen bonded to the side chain of the absolutely conserved aspartic acid D137, as well as residue T153. ATP1 phosphate groups interacted with the basic side chains of residues R136 and K181. Additionally, ATP1 γ-phosphate coordinated a Magnesium atom, together with the β-phosphate of GDP bound to the canonical Site 2 (GDP2) and the carboxylic acid in the side chain of residue E180 (Figure 3a). In the canonical Site 2, GDP2 guanine ring was sandwiched between the hydrophobic side chains of residues F118 and V94, with the hydroxyls of the ribose moiety tightly coordinated to the carboxylic acid of the absolutely conserved residue D199.[35] The negative charge of GDP2 phosphate groups was counteracted by the basic side chains of residues K181 and R198, as well as a Magnesium atom, as described above

(Figure 3b). Mutations in any of the conserved Aspartic residues that define the canonical Sites 1 and 2 in EcIMPDH (D138N and D200N, which correspond to D137and D199 in PaIMPDH), abrogate GTP/GDP-dependent allosteric inhibition (Figure S3a). These data further demonstrate the specificity of the interaction of these nucleotides in the Site 2 and the necessity of ATP bound to Site 1 for the inhibition.

Monomers in the AU are related by non-crystallographic symmetry axes that allow to reconstruct IMPDH octamers within the crystal lattice. These octamers are assembled as dimers of tetramers that pile up tail-to-tail, forcing the finger domains of opposing tetramers to interact and placing their catalytic sites close together (Figure S2b) to inhibit the catalytic activity. The comparison of the crystallographic structures of PaIMPDH-ATP1/GDP2 (this work) and PaIMPDH-ATP1/ATP2 (PDB code 4DQW)[10] allows the identification of a conformational switch, which is controlled by the competition between adenine and guanine nucleotides for the allosteric Site 2 in the Bateman domain (Figure 3c). Small angle X-ray scattering (SAXS) experiments further corroborate that the conformations observed in the crystal structures reliably represent those occurring in solution (Figure S4a). Remarkably, this conformational switch is essentially identical to the previously reported for eukaryotic IMPDHs.[6–8,13,14,34] Thereby, these data indicate that the purine nucleotide-controlled conformational switch that modulates the activity of IMPDH is universally conserved form bacteria to eukaryotes.

Remarkably, no electron density surrounding the area corresponding to the eukaryotic noncanonical Site 3 is observed in the inhibited PaIMPDH structure, suggesting that, in contrast to eukaryotic IMPDHs, the occupancy of the canonical Site 2 by GTP/GDP (when ATP is bound at the canonical Site 1) is necessary and sufficient to induce compact octamers and, subsequently, inhibit the activity of PaIMPDH and EcIMPDH. To corroborate this hypothesis, we performed computational targeted molecular dynamics (TMD) simulations of monomers of PaIMPDH bound to different nucleotides. These simulations induce conformational changes by applying an external force to minimize the root mean square deviation between initial and final (target) structures, thus driving the molecule to the target conformation during the simulation. As shown in Figure S5a,b, when both canonical sites are occupied by ATP, PaIMPDH can easily oscillate between the active (extended) and inhibited (compacted) conformations, since the applied external force (and the subsequent accumulated work) needed to drive these changes (both extension and compaction) is very low. On the other hand, when GDP occupies Site 2, an increasing supply of energy is needed to activate (extend) the inhibited conformation but essentially no work is needed for the opposite change (Figure S5a,b). These results indicate that GDP binding to Site 2 strongly stabilizes PaIMPDH into the inhibited compacted conformation.

2.3 | ATP/GTP balance allosterically modulates the activity of PaIMPDH and EcIMPDH

The results shown above clearly indicate that the binding of adenine and guanine nucleotides in the second canonical site is mutually exclusive and, thereby, the balance between the concentration of these nucleotides will presumably determine the activity of the enzyme. We tested this hypothesis by assaying the effects of different concentrations of ATP and GTP in vitro on proteobacterial IMPDHs at IMP and NAD^+ concentrations within the expected physiological levels.[18,33,36] Figure 4 clearly shows how ATP and GTP compete to modulate the activity of IMPDH. Remarkably, EcIMPDH (panel a) and PaIMPDH (panel b) showed significant differences in nucleotide affinities, in accordance with the different IC_{50} values estimated from Figure 2.

At constant 3 mM ATP, which is in the expected range of intracellular levels in *E. coli* cells exponentially growing in minimal media,[18] 1.3 and 2.3 mM GTP concentrations are needed to duplicate and raise 10-fold the Km values of EcIMPDH, respectively (Figure S6). These GTP concentrations are easily reached in exponentially growing *E. coli* cells, and can be even higher upon addition of purine nucleobases and nucleosides to the culture media.[18] Similarly, 0.8 and 1.3 mM GTP is required to duplicate and raise 10-fold the K_m values of PaIMPDH (Figure S6). Altogether, these data indicate that the intracellular ATP/GTP ratio modulates proteobacterial IMPDH activity.

2.4 | (p)ppGpp potently inhibit the catalytic activity of *B. subtilis* but has no effect on *E. coli* IMPDH

As described in Section 1, it seems evident that bacterial IMPDHs must play a relevant role on (p)ppGpp signaling in vivo, despite the scarce information available and the reported differences among organisms.[30–32,37–40] Prompted by this, we assayed the effects of (p)ppGpp on the activity of IMPDH in vitro in the presence or absence of ATP. As shown in Figure 5, ppGpp by itself has no

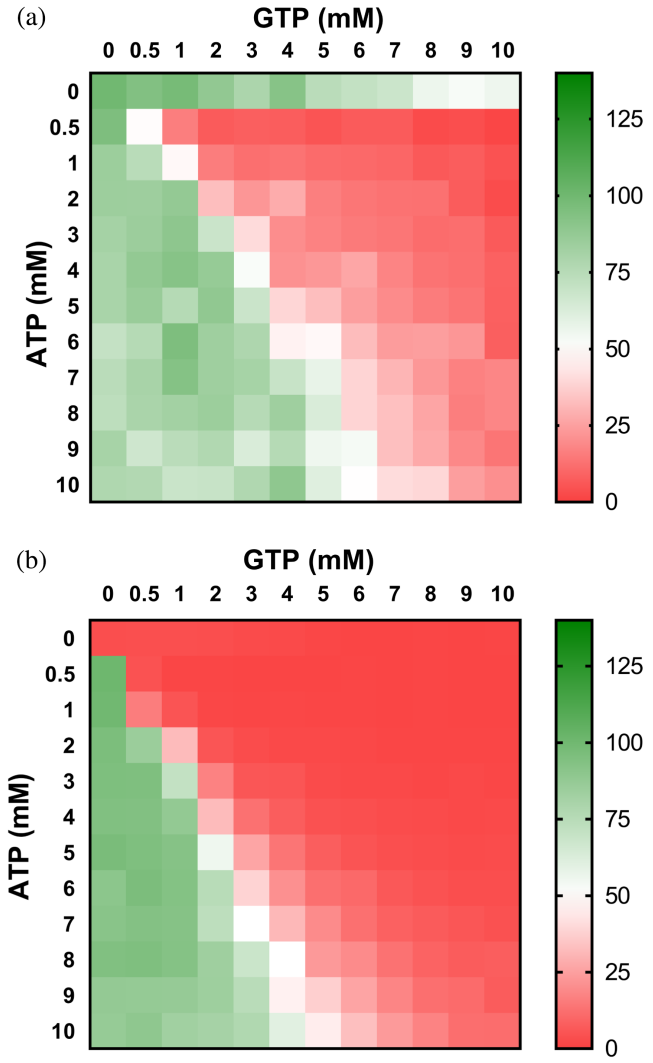


FIGURE 4 The ATP/GTP balance modulates the activity of proteobacterial IMPDHs. Heatmap representation of the enzymatic percent activity. V_0 values at different ATP versus GTP concentrations, normalized to the V_0 values in the absence of nucleotide for EcIMPDH (a) and at 1 mM ATP for PaIMPDH (b). The V_0 values used for normalization are EcIMPDH 15.9 and PaIMPDH 16.4 nM s^{-1} (note that PaIMPDH is inactive in vitro in the absence of ATP[10]). IMPDH, IMP dehydrogenase; PaIMPDH, *Pseudomonas aeruginosa* IMPDH

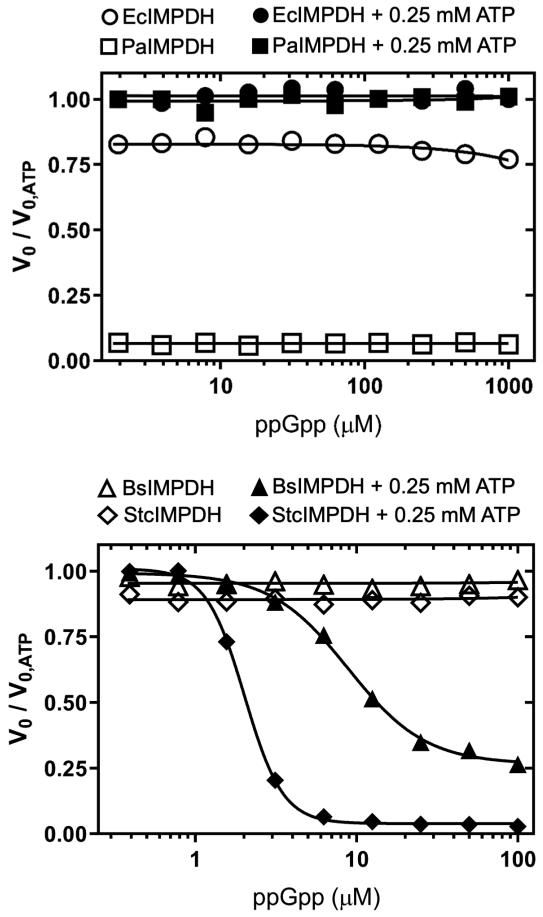


FIGURE 5 Effects of ppGpp on the catalytic activity of IMPDH in vitro. Graphs showing the normalized initial velocity values (V_0 values in the absence of ppGpp divided by the respective values in the presence of ppGpp. The V_0 values used for the normalization of the data are EcIMPDH 18.5 ± 1.0, PaIMPDH 26.7 ± 0.9, BsIMPDH 12.9 ± 0.8, and StcIMPDH 12.6 ± 0.4 nM s^{-1} (mean ± std. error). Estimated IC_{50} values are 8.9 ± 0.4 μM and 2.0 ± 0.03 μM (mean ± std. error) for BsIMPDH and StcIMPDH, respectively. Similar results were obtained for pppGpp inhibition (Figure S1). BsIMPDH, *Bacillus subtilis* IMPDH; EcIMPDH, *Escherichia coli* IMPDH; IMPDH, IMP dehydrogenase; PaIMPDH, *Pseudomonas aeruginosa* IMPDH; StcIMPDH, *Streptomyces coelicolor* IMPDH

significant effect on the catalytic activity in vitro of any of the enzymes assayed. In contrast, when combined with ATP, ppGpp can potently inhibit (in the low micromolar range) BsIMPDH and StcIMPDH (Figure 5). Similar results were obtained for pppGpp (Figure SS1). These data clearly indicate that in the presence of ATP, (p)ppGpp can inhibit these enzymes even at basal concentrations.[41] In contrast, (p)ppGpp had no detectable effect in vitro on the activity of EcIMPDH or PaIMPDH, even at millimolar concentrations and independently on the presence or absence of ATP (Figures 5 and SS1).

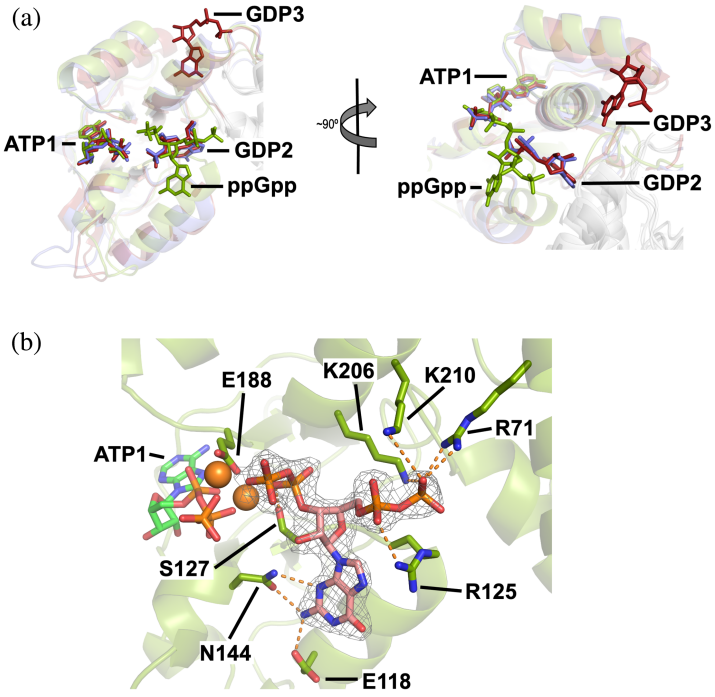
2.5 | Crystallographic structure of *S. coelicolor* IMPDH complexed to ATP and ppGpp

We then set cocrystallization experiments to obtain high-resolution structures of (p)ppGpp-IMPDH complexes and were able to solve the structure of the IMPDH from *S. coelicolor* bound to ATP and ppGpp at 2.0 Å resolution (Table SS1). The AU contained 16 IMPDH monomers that are related by symmetry axes and allow the reconstruction of IMPDH octamers within the crystal lattice. These octamers are formed by dimers of tetramers assembled with a conformation that resembles, with only

minor deviations, those adopted in the presence of ATP and GDP by the proteobacterial PaIMPDH enzyme (Figure S7). SAXS experiments further corroborate that the conformation observed in the crystal structure matches that found in solution in the presence of ATP and ppGpp (Figure S4b). Moreover, in the presence of ATP alone, StcIMPDH adopts a conformation similar to PaIMPDH-ATP (PDB ID 4DQW), highlighting the universality of the purine nucleotide-controlled conformational switch.

All monomers in the AU showed well-defined electron density in the Bateman domain that could be unequivocally attributed to ATP, ppGpp, and two magnesium atoms. ATP was found in the first canonical site (ATP1) with a binding mode identical to that observed in other IMPDH structures (5TC3, 4DQW, 5MCP, 6U8N, and 7RES).[6,10,14,34] Surprisingly, ppGpp was bound to a previously unrecognized pocket within the Bateman domain adopting an elongated T shape conformation.[42] The (p)ppGpp binding site is different from either the second canonical (GDP2) or the third eukaryotic noncanonical site, although its δ- and ε-phosphates partially occupy the canonical Site 2 (Figure 6a).

The ppGpp binding pocket in StcIMPDH is mostly formed by the polar side chains of residues E118, R125, and N144, that form hydrogen bonds with different atoms of the guanine ring. The α- and β-phosphates tightly interact with the basic sidechain of residues, R71, R125, K206, and K210, whereas δ- and ε-phosphates, which point toward the γ-phosphate of ATP1, coordinate two Magnesium atoms, together with the carboxylic acid of residue E188 (Figure 6b). BsIMPDH mutant enzymes with the most relevant (p)ppGpp interacting residues substituted by their equivalents in EcIMPDH showed significantly reduced inhibition with respect to the wild-type enzyme in vitro (Figure S3b). These data demonstrates that the newly discovered (p)ppGpp pocket of StcIMPDH is not artifactual but functional and conserved between *S. coelicolor* and *B. subtilis*. Furthermore, our mutational analysis also revealed that the absolutely conserved Aspartic residues



(c)

		(p)ppGpp site				Canonical site 2		
		71	118	125	144	188	206	210
A. tumefaciens	α-Proteobacteria	Q	Q	S	N	E	K	K
N. meningitidis	β-Proteobacteria	Q	L	K	N	E	K	K
E. coli	γ-Proteobacteria	Q	K	G	G	E	K	K
S. coelicolor	Actinobacteria	R	D	R	N	E	K	K
B. subtilis	Firmicutes	R	E	R	N	E	K	K
T. thermophilus	Thermus	R	E	R	N	E	K	K
A. gossypii	Ascomycota	L	R	G	S	G	T	K

FIGURE 6 Structure of StcIMPDH bound to ATP and ppGpp. (a) Structural superimposition of the Bateman domains of PaIMPDH-ATP/GDP (blue), StcIMPDH-ATP-ppGpp (green), and AgIMPDH-ATP/GDP (red; PDB ID 5TC3).[6] (b) Detailed view of the ppGpp binding site in the Bateman domain. IMPDH protein is represented in semitransparent green cartoons with the side chain of key interacting residues shown in sticks. The $2mF_o–DF_c$ electron density map, contoured at the 1.6σ level, is shown as a grey mesh. Key protein–nucleotide atomic interactions are represented as orange dashed lines and the coordinated Magnesium atoms are shown as orange spheres. (c) The taxonomic distribution of the (p)ppGpp binding site within the Bateman domain is shown. The phylogenetic tree on the left shows the evolutionary relationships among the groups of bacteria (color-coded according to a) and is extracted from a more detailed analysis shown in Figures S9 and S10. IMPDH, IMP dehydrogenase; PaIMPDH, *Pseudomonas aeruginosa* IMPDH; StcIMPDH, *Streptomyces coelicolor* IMPDH

that define the two canonical nucleotide binding sites in Bateman domains are also required for (p)ppGpp mediated inhibition (Figure S3b).

The analysis of a bacterial IMPDH multiple sequence alignment revealed that the (p)ppGpp binding site is conserved among most bacterial phyla but is consistently absent in α-β-γ-Proteobacteria and some δ-Proteobacteria genera (Figures 6c and S8). This observation perfectly explains why EcIMPDH and PaIMPDH cannot be inhibited by (p)ppGpp (Figures 5 and S1). The resulting phylogenetic tree (best model LG + G + I[43]) suggests that the allosteric regulation of IMPDH by (p)ppGpp is the ancestral state in bacteria and that its loss occurred during the evolution of Proteobacteria (Figure S9). However, the low bootstrap values of this tree prevented drawing solid conclusions. To obtain further support for this hypothesis, we also reconstructed a species tree for the set of bacteria under study, using multiple conserved proteins data obtained from a reference phylogeny database.[44] The resulting phylogenetic tree (best model LG +- G + F) perfectly agrees with the well stablished tree of life[45] and resembles the IMPDH tree (Figure S10). Altogether, these data strongly support the hypothesis that the bacterial ancestral IMPDH was regulated by (p)ppGpp and this regulation was lost during the evolution of Proteobacteria.

No electron density was found in the canonical Site 2 or the noncanonical Site 3. Nonetheless, the results described above indicate that, in the presence of ATP bound to the canonical Site 1, the occupancy of the (p)ppGpp pocket is necessary and sufficient to induce the inhibited conformation. We then performed computational TMD simulations to corroborate this hypothesis. When the two canonical sites were occupied by ATP, StcIMPDH readily oscillates between the active (extended) and inhibited (compacted) conformations. In contrast, the occupancy of the (p)ppGpp pocket, in the presence of ATP1, implies a large amount of accumulated work to activate (extend) the inhibited conformation (Figure S5c and d). These results indicate that the occupancy of the (p)ppGpp binding pocket in StcIMPDH strongly stabilizes the inhibited compact conformation, similar to the binding of GTP/GDP to PaIMPDH (Figure S5a and b).

Altogether, these results further demonstrate that the allosteric control of the catalytic activity of IMPDH is mediated by a universal purine nucleotide-controlled conformational switch. They also illustrate how evolution has diverged to adapt this regulatory mechanism to the specific particularities of each organism through the invention of different nucleotide-binding pockets within the Bateman domain.

2.6 | The ratio ATP/(p)ppGpp allosterically controls the activity of IMPDH

The results reported above indicate that occupancy of either the canonical Site 2 by ATP or the (p)ppGpp binding pocket is mutually exclusive. We then tested the activity of IMPDH in vitro in the presence of different amounts of ATP and ppGpp, at IMP and NAD^+ concentrations within the expected intracellular range.[18,33,36] Figure 7 shows that, within the assayed ATP

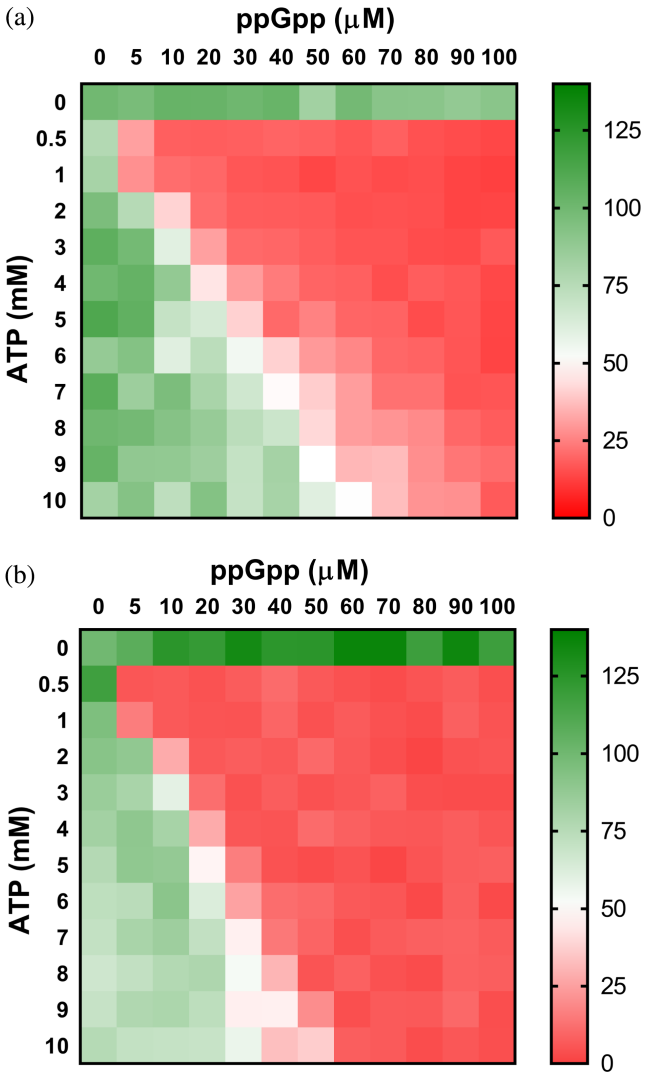


FIGURE 7 *ppGpp modulates the activity of IMPDH in Actinobacteria and Firmicutes*. Heatmap representation of the enzymatic percent activity (V_0 values normalized to the V_0 values in the absence of nucleotide) of BsIMPDH (a) and StcIMPDH (b) at different ATP versus ppGpp concentrations. The V_0 values used for normalization are BsIMPDH 32.9 and StcIMPDH 7.6 nM s^{-1}. BsIMPDH, *Bacillus subtilis* IMPDH; IMPDH, IMP dehydrogenase; StcIMPDH, *Streptomyces coelicolor* IMPDH

concentration range, ppGpp can strongly inhibit the enzyme activity even at basal concentrations, in the mid micromolar range.[41]

3 | DISCUSSION

Purine nucleotides are essential metabolites, involved in multiple metabolic pathways and cellular functions that need a fine-tuned balance between adenine and guanine derivatives. Maintenance of GTP levels across species is critical to fitness, and GTP dysregulation has relevance to malignancy, genetic disease and genomic instability.[46–48] In some gram-positive bacteria, including *B. subtilis*, the intracellular levels of GTP must be maintained within a narrow range and excess GTP is severely detrimental for cell growth and survival.[30,31,38] On the other hand, high GTP levels do not lead to a loss of viability in Proteobacteria, such as *E. coli*, although they inhibit cell growth.[49,50] In any case, despite the notable differences in tolerance to excess purine nucleotide levels among bacteria, the tight control of the purine nucleotide biosynthetic pathways must be a key facet of the cell homeostasis and the global metabolic response to environmental and nutritional changes. It is evident, for instance, that bacteria need to tightly modulate the purine biosynthetic pathways in response to the availability of these nucleotides in the culture media or downregulate them in conditions of nutritional stress, as part of the stringent response.[49] Thereby, it is essential to elucidate the mechanisms, most probably redundant, that regulate purine nucleotide biosynthesis and keep the ATP/GTP ratio within a narrow physiological range within the cell.

In eukaryotic cells, IMPDH allosteric regulation, mediated by the binding of adenine and guanine nucleotides to the regulatory Bateman domain, plays an essential role in the maintenance of the balance between adenine and guanine nucleotide pools and GTP homeostasis. The physiological relevance of this mechanism of regulation is stressed by the fact that missense mutations that map in the allosteric binding sites of human IMPDHs are associated to severe retinopathies and dystonia.[20,22]

In bacterial cells, however, no physiological mechanism of allosteric inhibition of IMPDH has been reported. In this study, we demonstrate that (p)ppGpp is a potent allosteric inhibitor of the IMPDHs from most bacterial phyla, except Proteobacterias, whose IMPDHs are allosterically controlled by the intracellular ratio of ATP/GTP. We found that a, previously ignored, key point to unveil bacterial IMPDH allosteric inhibition in vitro is the requirement of simultaneous binding of adenine and guanine nucleotides to the allosteric sites. Different from the eukaryotic enzymes, bacterial IMPDHs need ATP bound to the canonical Site 1 to be inhibited by guanine nucleotides that bind to either the canonical Site 2 (GTP/GDP) or a contiguous pocket ((p)ppGpp). This is most possibly the primary reason why guanine nucleotides have been previously unnoticed as allosteric inhibitors of bacterial IMPDHs in vitro.[7,10,30,32] Indeed, from the analysis of the high-resolution structures of eukaryotic and prokaryotic enzymes, it is hard to define the structural determinants responsible for the different nucleotide specificities of the canonical allosteric sites in the Bateman domain of IMPDHs.

Given that the intracellular concentrations of ATP are millimolar[18,33,36] and the ATP affinities for bacterial IMPDHs are in the micromolar range,[6,10,51] it is expected that purine nucleotide-induced octamers are the most abundant species in the cytoplasm. A recent report indicates that this might also be the case for eukaryotic IMPDHs, as crystals of recombinant *Trypanosoma brucei* IMPDH grown in the cytoplasm of intact insect cells show octamers that contain ATP bound to the canonical Site 1 of the Bateman domain.[15] With ATP bound to the canonical Site 1, the activity of bacterial IMPDHs is then modulated by the mutually exclusive binding of adenine nucleotides to the canonical Site 2 and guanine nucleotides to either this site or the newly discovered (p)ppGpp binding site, which partially overlaps with the former. The occupancy of these sites determines the conformation of the enzyme: high ATP/GTP or ATP/(p)ppGpp ratios favor the extended conformation of catalytically active octamers. In contrast, when these ratios drop, octamer compaction occurs to inhibit the enzymatic activity.

We have recently reported that phosphorylation of residues in the nucleotide-binding sites of the Bateman domain modulates the allosteric regulation of the retinal isoforms of human IMPDH.[23] By analogy, it might then be plausible that post-translational modifications control the allosteric regulation of bacterial IMPDHs. According to public databases (PLMD[52] and dbPSP[53]), lysine acetylation is a recurrent modification within the Bateman domain of bacterial IMPDH. Within this domain, acetylation of residue K203 in *E. coli*, and the equivalent K206 in *B. subtilis*, called our attention because is evolutionarily conserved (Figure S8) and directly involved in the binding of GTP (Figure 3) and ppGpp (Figure 6). As an initial approach, we tested the effects of acetylation in vitro by using the K-to-Q point mutation that has been previously described to simulate the acetylation-dependent neutralization of the positive lysine charge.[54] Figure S11 shows how K203Q and K206Q substitutions significantly compromise allosteric inhibition in *E. coli*

and *B. subtilis* enzymes, respectively. Although not conclusive, these results definitively encourage to perform new experiments to decipher if the allosteric regulation of bacterial IMPDHs is fine-tuned by post-translational modifications.

We propose the Bateman domain of IMPDH as a new crosstalk point between the adenine and guanine nucleotide pathways downstream IMP. This regulatory point, together with the crosswise utilization of GTP and ATP as cosubstrates of Adenylosuccinate and GMP synthases, respectively, might help to adjust the balance of purine nucleotides according to the cell metabolic demands. Our in vitro data on the allosteric inhibition of IMPDH is in good agreement with previously published in vivo data, since the deletion of the Bateman domain of IMPDH in *E. coli*, results in altered purine nucleotide concentrations and the inability to maintain the ATP/GTP balance within a fairly narrow physiological range.[18,29] Nonetheless, although our data points to a key role of the allosteric modulation of IMPDH by the intracellular ratios of ATP/GTP, we cannot discard additional mechanisms that contribute to maintain the purine nucleotide balance and GTP homeostasis. These mechanisms might imply the putative moonlighting functions of IMPDH,[29,55–57] as well as different enzymes.

The alarmones (p)ppGpp bind to a conserved -previously unrecognized- high affinity (p)ppGpp binding pocket within the Bateman domain that partially overlaps with the canonical Site 2. Multiple sequence alignments of bacterial IMPDH and phylogenetic analysis show that this site is present in most bacterial phyla, except for some classes of Proteobacteria, including γ and the closely related α- and ß-proteobacteria, as well as some δ-Proteobacteria genera. In contrast, ε-Proteobacteria retained the (p)ppGpp binding site (Figures S8–S10) and the corresponding allosteric inhibition, as we have experimentally demonstrated for *Helicobacter pylori* IMPDH (HpIMPDH; Figure S12). The IMPDH phylogenetic tree, together with the species tree, allows us to propose that the bacterial IMPDH ancestor contained the (p)ppGpp binding site, and this was lost during the evolution of the proteobacterial lineage.

Remarkably, a similar evolutionary history has been reported for the enzymes guanylate kinase (Gmk, downstream from IMPDH in the guanine nucleotide de novo pathway[58]) and hypoxanthine phosphoribosyltransferase (HprT, GPRT in Figure 1, in the *salvage* pathway[59]). (p)ppGpp inhibit bacterial IMPDHs with IC_{50} in the low microM range, similar to the IC_{50} values reported for Gmk and HprT,[58,59] which represent basal levels of these alarmones.[41] Therefore, our results confirm the vital housekeeping function of (p)ppGpp on GTP homeostasis. They tightly control the guanine nucleotide de novo and *salvage* pathways in response to both extrinsic stress and intrinsic cell status, buffering GTP against fluctuations and preserving metabolic stability.

The loss of (p)ppGpp inhibition of the enzymes IMPDH, Gmk, and HprT during the evolution of the proteobacterial lineage was paralleled with the acquisition of (p)ppGpp regulation by the RNA polymerase (RNAP). This is demonstrated by the presence of the MAR motif at the N-terminal region of the ω-subunit of RNAP in α, β, δ, and γ, but neither in ε-proteobacteria nor in most other bacterial phyla[60] (Figure S10). Moreover, it is plausible to propose that the loss of the tight control exerted by basal levels of (p)ppGpp over IMPDH, Gmk, and HprT enzymes is possibly correlated with the low GTP toxicity in Proteobacteria.[50] In any case, these observations represent fascinating examples on how evolution has found different (p)ppGpp targets and rewired regulatory networks to achieve the same regulatory ends.

Altogether, the results presented here indicate an essential role of IMPDH allosteric regulation on bacterial GTP homeostasis and further expand our knowledge about the crosstalk between (p)ppGpp signaling and the guanine nucleotide biosynthetic pathway. We demonstrate that the activity of bacterial IMPDHs is allosterically controlled by an evolutionarily conserved nucleotide-controlled conformational switch that has been divergently adapted to the specific particularities of each organism. Moreover, we have identified significant differences in the mechanisms of regulation between eukaryotic and prokaryotic IMPDH enzymes, opening the door to the development of approaches to antibiotic discovery.

4 | METHODS

4.1 | Cloning, site-directed mutagenesis, and protein purification

Open reading frames of the different enzymes were amplified by PCR using genomic DNA as template and inserted into an ad hoc modified pET15b bacterial expression vector with the thrombin cleavage site substituted by the tobacco echt virus protease recognition sequence. Site-directed mutagenesis was performed using the QuikChange II method (Agilent Technologies). All plasmids were corroborated by DNA sequencing.

IMPDH enzymes were overexpressed overnight in *E. coli* BL21 (DE3) strain in terrific broth[61] at 18°C and purified by immobilized metal affinity chromatography according to standard protocols. The 8-histidine tail present at the N-terminal of the overexpressed proteins was cleaved by overnight digestion at room temperature with

tobacco etch virus protease. The cleaved proteins were then injected into a HiPrep Sephacryl S-300 16/60 HR size-exclusion chromatography column (Cytiva) equilibrated in buffer 20 mM Tris–HCl, 5% glycerol, 500 mM KCl, 1 mM DTT, pH 8.0. Fractions containing IMPDH proteins were pooled, concentrated at 4°C using a 10 kDa cutoff Amicon Ultra centrifugal filter (Millipore), aliquoted and stored at −80°C. All the enzymes showed at least 98% purity by SDS-PAGE densitometric analysis and did not significantly lose activity after one cycle of freezing/thawing. Protein and nucleotide concentrations were determined spectrophotometrically.

4.2 | Enzyme kinetics assays

IMPDH activity was assayed using 384-well microtiter plates by monitoring the appearance of NADH by fluorescence (λ_{exc} = 340 nm and λ_{em} = 460 nm, using a 10 nm slit window for both excitation and emission).

The buffer used for the guanine nucleotide titration curves shown in Figures 2 and 5 were 100 mM Tris–HCl pH 8.0, 100 mM KCl, 2 mM $MgCl_2$ (free), 2 mM DTT, 0.5 mM NAD^+, 0.5 mM IMP, 0- or 0.25-mM ATP, and 50 nM enzyme, measured at 28°C (BsIMPDH and StcIMPDH) or 32°C. The total amount of $MgCl_2$ was adjusted for each nucleotide concentration to keep 1 mM free Mg^{2+} constant concentration, as previously described.[6] The experimental data were fitted to the Michaelis–Menten and allosteric sigmoidal equations using GraphPad Prism (GraphPad Software).

The buffer used for the heat map plot shown in Figure 4 and 7 in the main text and Supplemental Figure 11 was 100 mM Tris-HCl, pH 8.0, 100 mM KCl, 1 mM $MgCl_2$, 2 mM DTT, 1 mM NAD^+, 0.2 mM IMP. Nucleotides: ATP-Mg^{2+}, GTP-Mg^{2+}, and ppGpp-Mg^{2+} were added at the indicated concentrations, and 20 nM of EcIMPDH, EcIMPDH-K203Q, PaIMPDH, and StcIMPDH and 40 nM of BsIMPDH and BsIMPDH-K206Q enzymes were used. Measurements we performed at 32°C for EcIMPDH and PaIMPDH and 28°C for BsIMPDH and StcIMPDH.

4.3 | Protein crystallization and structure solution

Crystals of PaIMPDH-ATP-GDP were grown at 22°C in sitting drops using the vapor diffusion method by mixing a protein solution at 10 mg ml^{-1} in 5 mM Tris–HCl, 100 mM KCl, 0.5 mM ATP, 5 mM GDP, 3.52 mM total $MgCl_2$ (1 mM free Mg^{2+} estimated as described in Reference 6), pH 8.0, with an equal volume of mother liquor corresponding to the condition D11 of the commercial screening Morpheus[62]: 0.02 M sodium formate; 0.02 M ammonium acetate; 0.02 M sodium citrate tribasic dihydrate; 0.02 M potassium sodium tartrate tetrahydrate; 0.02 M sodium oxamate, 12.5% v/v MPD; 12.5% PEG 1000; 12.5% w/v PEG 3350 in 0.1 M of the buffer system Tris (base), bicine, pH 8.5.

Crystals of StcIMPDH-ATP-ppGpp were obtained as before by mixing 10 mg ml^{-1} of StcIMPDH in buffer in 5 mM Tris–HCl, 100 mM KCl, 1.5 mM ATP, 0.5 mM ppGpp, 3 mM total $MgCl_2$, pH 8.0 with equal volume of mother liquor corresponding to the condition H9 of the commercial screening Morpheus-II[63]: 0.01 M spermine tetrahydrochloride, 0.01 M spermidine trihydrochloride, 0.01 M 1,4-diaminobutane dihydrochloride, 0.01 M DL-ornithine monohydrochloride, 15% w/v PEG 3000, 20% v/v 1,2,4-butanetriol, 1% w/v NDSB 256, and 0.1 M of the buffer system Gly-Gly, AMPD, pH 8.5.

Protein crystals were flashed-cooled in liquid nitrogen and data were collected at 100 K, using monochromatic X-rays of 1.00 Å wavelength, at the Diamond and ALBA synchrotrons. Diffraction intensities were indexed, integrated and anisotropically truncated by using the software autoPROC.[64,65] The structures were solved by molecular replacement with the program PHASER[66] from the CCP4 software suite,[67] using as template the structure of *P. aeruginosa* IMPDH (PDB ID 4AVF).[68] The structural models were iteratively improved by alternating automated refinement, using the PHENIX crystallographic software package[69] with manual modeling, using the program COOT.[70] Simulated annealing (torsion coordinates), gradient-driven positional, restrained individual isotropic B-factor and TLS refinement[71] were used for refinement. The figures showing three-dimensional protein structures were generated using PyMOL.[72]

4.4 | Small angle X-ray scattering

SAXS measurements were performed at the B21 beamline in the Diamond synchrotron, using buffer: 20 mM Tris–HCl, 300 mM KCl, 3 mM DTT, 5% glycerol, pH 8.0 and a protein concentration of 2.5 mg ml^{-1} (PaIMPDH) and 3 mg ml^{-1} (StcIMPDH). Nucleotide concentrations were 2 mM ATP, 0.25 mM ATP + 1.5 mM GDP, or 1 mM ATP + 0.1 mM ppGpp. The total amount of $MgCl_2$ was adjusted for each nucleotide concentration to keep 1 mM free Mg^{2+} constant concentration, as previously described.[6] During the measurements, the beamline was used in the default configuration: a beam energy of 13 keV, a sample-to-detector distance of 3.7 m.[73] The samples were flowing through an in-vacuum cell, kept at 10°C, to minimize radiation damage.

All nondamaged protein frames were averaged and buffer scattering was subtracted using the ATSAS software suite.[74] The theoretical scattering curves in Figure S4a were calculated from the PaIMPDH-ATP (PDB ID 4DQW),[10] PaIMPDH-ATP-GDP and PaIMPDH-APO (PDB ID 6GJV)[51] crystal structures using the program CRYSOL.[75] The theoretical scattering curves in Figure S4b were calculated from the PaIMPDH-ATP (PDB ID 4DQW),[10] StcIMPDH-ATP-ppGpp (this work) and an isolated tetramer of PaIMPDH-ATP (for StcIMPDH-APO).

4.5 | Molecular dynamics simulations

Previous to the TMD procedures, crystal structures were subjected to 100 ns of unrestrained molecular dynamics (MD) simulations in presence of the different ligands using the AMBER18 MD package (http://ambermd.org; University of California-San Francisco), essentially as previously described.[6,76] The structures were solvated with a periodic octahedral pre-equilibrated solvent box using the LeaP module of AMBER, with 12 Å as the shortest distance between any atom in the protein subdomain and the periodic box boundaries. MD simulation was performed using the PMEMD program of AMBER18 and the ff14SB force field (http://ambermd.org), applying the SHAKE algorithm, a time step of 2 fs and a nonbonded cutoff of 12 Å. Systems were initially relaxed over 10,000 steps of energy minimization, using 1000 steps of steepest descent minimization followed by 9,000 steps of conjugate-gradient minimization. Simulations were then started with a 20 ps heating phase, raising the temperature from 0 to 300 K in 10 temperature change steps, after each of which velocities were reassigned. During minimization and heating, the Cα trace dihedrals were restrained with a force constant of 500 kcal mol^{-1} rad^{-2} and gradually released in an equilibration phase in which the force constant was progressively reduced to 0 over 200 ps. After the equilibration phase, 100 ns of unrestricted MD simulation were obtained for the structures

To compare the work and force required to adopt the active (extended) conformation from the inhibited (compacted) conformation, and vice versa, of both PaIMPDH and StcIMPDH monomers in the presence of the different ligands, the calculation of the accumulated work (kcal mol^{-1}) and force (kcal mol^{-1} $Å^{-1}$) was performed for each case using TMD. In all cases, a spring constant of 5 kcal mol^{-1} $Å^{-2}$ was used and the whole trajectory was divided into 1,000 discrete steps of 0.1 ns per step and a final root main square deviation (rmsd) of 2.0 Å. For each calculation step, rmsd values were recorded to later reconstruct the forces and works generated along with each trajectory. MD and TMD trajectories were analyzed using VMD software.[77]

4.6 | Multiple sequence alignment and phylogenetic analysis

IMPDH protein sequences were obtained by recursive BLAST[78] searches at NCBI and aligned with Mafft v7.305b.[79] Alignments were inspected with Jalview[80] and cleaned for unreliably aligned regions using Trimal v1.4.rev5,[81] removing sites containing gaps in more than 50% of the sequences (−gt 0.5). Phylogenetic trees were reconstructed with Phyml 3.0.[82] Best fit models of evolution were identified with SMS,[83] and 100 bootstrap replicates were requested. Phylogenetic trees were edited with FigTree (http://tree.bio.ed.ac.uk/software/figtree).

ACKNOWLEDGEMENTS

This work was funded by the Spanish Ministerio de Ciencia e Innovación-FEDER-Fondo Social Europeo (grants PID2019-109671GB-I00 to Rubén M. Buey; BIO2017-88435-R and PID2020-118200RB-I00 to José L. Revuelta and Alberto Jiménez; RTC-2017-6494-1 and RTI2018-094434-B-I00 to Paulino Gómez-Puertas) and Instituto de Salud Carlos III (grant DTS20-00024 to Paulino Gómez-Puertas). David Fernández-Justel was supported by a pre-doctoral contract from the Junta de Castilla y León. We thank María Dolores Sánchez, Silvia Domínguez and Marta Santos for excellent technical support, Dr Ramón Santamaría and Dr Margarita Díaz for kindly sharing the genomic DNA of *Streptomyces coelicolor*, and Dr Michele Felletti for his critical comments and helpful suggestions. Protein crystallography experiments were performed at the XALOC and i04 beamlines at ALBA and Diamond synchrotrons, respectively, with the collaboration of the ALBA and DLS staff. We also acknowledge the help and excellent support from the staff of the B21 beamline at DLS, where the SAXS experiments were performed. The computational support of the "Centro de Computación Científica CCC-UAM" is also gratefully recognized. The atomic coordinates and the structure factors described in this work have been deposited in the Research Collaboratory for Structural Bioinformatics Protein Data Bank under the PDB IDs: 7PJI and 7PMZ.

AUTHOR CONTRIBUTIONS

David Fernández-Justel: Investigation (equal). **Íñigo Marcos-Alcalde:** Investigation (equal). **Federico Abascal:** Investigation (equal). **Nerea Vidaña:** Investigation (equal). **Paulino Gómez-Puertas:** Investigation

(equal). **Alberto Jiménez:** Investigation (equal). **José L. Revuelta:** Conceptualization (equal); funding acquisition (supporting); project administration (equal). **Rubén M. Buey:** Conceptualization (lead); funding acquisition (lead); investigation (lead); project administration (equal); writing – original draft (lead); writing – review and editing (lead).

ORCID

Rubén M. Buey https://orcid.org/0000-0003-1263-0221

REFERENCES

1. Fotie J. Inosine 5'-monophosphate dehydrogenase (IMPDH) as a potential target for the development of a new generation of antiprotozoan agents. Mini Rev Med Chem. 2018;18(8):656–671. https://doi.org/10.2174/1389557516666160620065558.
2. Juvale K, Shaik A, Kirubakaran S. Inhibitors of inosine 5′-monophosphate dehydrogenase as emerging new generation antimicrobial agents. Med Chem Commun. 2019;10(8):1290–1301.
3. Braun-Sand SB, Peetz M. Inosine monophosphate dehydrogenase as a target for antiviral, anticancer, antimicrobial and immunosuppressive therapeutics. Future Med Chem. 2010;2(1):81–92. https://doi.org/10.4155/FMC.09.147.
4. Naffouje R, Grover P, Yu H, et al. Anti-tumor potential of IMP dehydrogenase inhibitors: A century-long story. Cancers (Basel). 2019;11(9). 1346–1375. https://doi.org/10.3390/cancers11091346.
5. Cuny GD, Suebsuwong C, Ray SS. Inosine-5′-monophosphate dehydrogenase (IMPDH) inhibitors: A patent and scientific literature review (2002-2016). Expert Opin Ther Pat. 2017;27(6):677–690. https://doi.org/10.1080/13543776.2017.1280463.
6. Buey RM, Fernandez-Justel D, Marcos-Alcalde I, et al. A nucleotide-controlled conformational switch modulates the activity of eukaryotic IMP dehydrogenases. Sci Rep. 2017;7(1):2648. https://doi.org/10.1038/s41598-017-02805-x.
7. Buey RM, Ledesma-Amaro R, Velazquez-Campoy A, et al. Guanine nucleotide binding to the Bateman domain mediates the allosteric inhibition of eukaryotic IMP dehydrogenases. Nat Commun. 2015;6:8923. https://doi.org/10.1038/ncomms9923.
8. Fernandez-Justel D, Nunez R, Martin-Benito J, et al. A nucleotide-dependent conformational switch controls the polymerization of human IMP dehydrogenases to modulate their catalytic activity. J Mol Biol. 2019;431:956–969. https://doi.org/10.1016/j.jmb.2019.01.020.
9. Fernandez-Justel D, Pelaez R, Revuelta JL, Buey RM. The Bateman domain of IMP dehydrogenase is a binding target for dinucleoside polyphosphates. J Biol Chem. 2019;294(40):14768–14775. https://doi.org/10.1074/JBC.AC119.010055.
10. Labesse G, Alexandre T, Vaupré L, et al. MgATP regulates allostery and fiber formation in IMPDHs. Structure. 2013;21(6):975–985. https://doi.org/10.1016/j.str.2013.03.011.
11. Labesse G, Alexandre T, Gelin M, Haouz A, Munier-Lehmann H. Crystallographic studies of two variants of Pseudomonas aeruginosa IMPDH with impaired allosteric regulation. Acta Crystallogr Sect D Biol Crystallogr. 2015;71:1890–1899. https://doi.org/10.1107/S1399004715013115.
12. Alexandre T, Rayna B, Munier-Lehmann H. Two classes of bacterial IMPDHs according to their quaternary structures and catalytic properties. PLoS One. 2015;10(2):e0116578. https://doi.org/10.1371/journal.pone.0116578.
13. Anthony SA, Burrell AL, Johnson MC, et al. Reconstituted IMPDH polymers accommodate both catalytically active and inactive conformations. Mol Biol Cell. 2017;28:2600–2608. https://doi.org/10.1091/mbc.E17-04-0263.
14. Johnson MC, Kollman JM. Cryo-EM structures demonstrate human IMPDH2 filament assembly tunes allosteric regulation. Elife. 2020;9:e53243. https://doi.org/10.7554/ELIFE.53243.
15. Nass K, Redecke L, Perbandt M, et al. In cellulo crystallization of Trypanosoma brucei IMP dehydrogenase enables the identification of genuine co-factors. Nat Commun. 2020;11(1):620. https://doi.org/10.1038/S41467-020-14484-W.
16. Gilbert HJ, Lowe CR, Drabble WT. Inosine 5′-monophosphate dehydrogenase of *Escherichia coli*. Purification by affinity chromatography, subunit structure and inhibition by guanosine 5′-monophosphate. Biochem J. 1979;183(3):481–494. https://doi.org/10.1042/BJ1830481.
17. Buey RM, Ledesma-Amaro R, Balsera M, de Pereda JM, Revuelta JL. Increased riboflavin production by manipulation of inosine 5′-monophosphate dehydrogenase in Ashbya gossypii. Appl Microbiol Biotechnol. 2015;99(22):9577–9589. https://doi.org/10.1007/s00253-015-6710-2.
18. Pimkin M, Markham GD. The CBS subdomain of inosine 5′-monophosphate dehydrogenase regulates purine nucleotide turnover. Mol Microbiol. 2008;68(2):342–359. https://doi.org/10.1111/J.1365-2958.2008.06153.X.
19. Bateman A. The structure of a domain common to archaebacteria and the homocystinuria disease protein. Trends Biochem Sci. 1997;22(1):12–13. https://doi.org/10.1016/S0968-0004(96)30046-7.
20. McGrew DA, Hedstrom L. Towards a pathological mechanism for IMPDH1-linked retinitis pigmentosa. Adv Exp Med Biol. 2012;723:539–545. https://doi.org/10.1007/978-1-4614-0631-0_68.
21. Aherne A, Kennan A, Kenna PF, et al. On the molecular pathology of neurodegeneration in IMPDH1-based retinitis pigmentosa. Hum Mol Genet. 2004;13(6):641–650. https://doi.org/10.1093/HMG/DDH061.
22. Zech M, Jech R, Boesch S, et al. Monogenic variants in dystonia: An exome-wide sequencing study. Lancet Neurol. 2020;19(11):908–918. https://doi.org/10.1016/S1474-4422(20)30312-4.
23. Plana-Bonamaiso A, Lopez-Begines S, Fernondez-Justel D, et al. Post-translational regulation of retinal IMPDH1 in vivo to adjust GTP synthesis to illumination conditions. Elife. 2020;9:e56418. https://doi.org/10.7554/ELIFE.56418.
24. Duong-Ly KC, Kuo Y-M, Johnson MC, et al. T cell activation triggers reversible inosine-5′-monophosphate dehydrogenase assembly. J Cell Sci. 2018;131(17). 1–8. https://doi.org/10.1242/jcs.223289.
25. Chang CC, Lin WC, Pai LM, et al. Cytoophidium assembly reflects upregulation of IMPDH activity. J Cell Sci. 2015;128(19):3550–3555. https://doi.org/10.1242/jcs.175265.
26. Liu J. The cytoophidium and its kind: Filamentation and compartmentation of metabolic enzymes. Annu Rev Cell Dev Biol. 2016;32(1):349–372. https://doi.org/10.1146/annurev-cellbio-111315-124907.
27. Calise SJ, Purich DL, Nguyen T, et al. "Rod and ring" formation from imp dehydrogenase is regulated through the one-carbon metabolic pathway. J Cell Sci. 2016;129(15):3042–3052. https://doi.org/10.1242/jcs.183400.

28. Aughey GN, Liu JL. Metabolic regulation via enzyme filamentation. Crit Rev Biochem Mol Biol. 2016;51(4):282–293. https://doi.org/10.3109/10409238.2016.1172555.
29. Pimkin M, Pimkina J, Markham GD. A regulatory role of the Bateman domain of IMP dehydrogenase in adenylate nucleotide biosynthesis. J Biol Chem. 2009;284(12):7960–7969. https://doi.org/10.1074/JBC.M808541200.
30. Kriel A, Bittner AN, Kim SH, et al. Direct regulation of GTP homeostasis by (p)ppGpp: A critical component of viability and stress resistance. Mol Cell. 2012;48(2):231–241. https://doi.org/10.1016/J.MOLCEL.2012.08.009.
31. Bittner AN, Kriel A, Wang JD. Lowering GTP level increases survival of amino acid starvation but slows growth rate for Bacillus subtilis cells lacking (p)ppGpp. J Bacteriol. 2014;196(11):2067–2076. https://doi.org/10.1128/JB.01471-14.
32. Osaka N, Kanesaki Y, Watanabe M, et al. Novel (p)ppGpp 0 suppressor mutations reveal an unexpected link between methionine catabolism and GTP synthesis in Bacillus subtilis. Mol Microbiol. 2020;113(6):1155–1169. https://doi.org/10.1111/MMI.14484.
33. Traut TW. Physiological concentrations of purines and pyrimidines. Mol Cell Biochem. 1994;140(1):1–22.
34. Burrell AL, Nie C, Said M, et al. IMPDH1 retinal variants control filament architecture to tune allosteric regulation. Nat Struct Mol Biol. 2022;29(1):47–58. https://doi.org/10.1038/S41594-021-00706-2.
35. Ereno-Orbea J, Oyenarte I, Martinez-Cruz LA. CBS domains: Ligand binding sites and conformational variability. Arch Biochem Biophys. 2013;540(1–2):70–81. https://doi.org/10.1016/j.abb.2013.10.008.
36. Bennett BD, Kimball EH, Gao M, Osterhout R, Van Dien SJ, Rabinowitz JD. Absolute metabolite concentrations and implied enzyme active site occupancy in Escherichia coli. Nat Chem Biol. 2009;5(8):593–599. https://doi.org/10.1038/nchembio.186.
37. Kasai K, Nishizawa T, Takahashi K, Hosaka T, Aoki H, Ochi K. Physiological analysis of the stringent response elicited in an extreme thermophilic bacterium *Thermus thermophilus*. J Bacteriol. 2006;188(20):7111–7122. https://doi.org/10.1128/JB.00574-06.
38. Kriel A, Brinsmade S, Tse J, et al. GTP dysregulation in Bacillus subtilis cells lacking (p)ppGpp results in phenotypic amino acid auxotrophy and failure to adapt to nutrient downshift and regulate biosynthesis genes. J Bacteriol. 2014;196(1):189–201. https://doi.org/10.1128/JB.00918-13.
39. Ochi K. Metabolic initiation of differentiation and secondary metabolism by Streptomyces griseus: Significance of the stringent response (ppGpp) and GTP content in relation to a factor. J Bacteriol. 1987;169(8):3608–3616. https://doi.org/10.1128/JB.169.8.3608-3616.1987.
40. Pao C, Dyes B, Dyess B. Effect of unusual guanosine nucleotides on the activities of some *Escherichia coli* cellular enzymes. Biochim Biophys Acta. 1981;677(3–4):358–362. https://doi.org/10.1016/0304-4165(81)90247-6.
41. Steinchen W, Zegarra V, Bange G. (p)ppGpp: Magic modulators of bacterial physiology and metabolism. Front Microbiol. 2020;2020:2072. https://doi.org/10.3389/FMICB.2020.02072.
42. Anderson BW, Fung DK, Wang JD. Regulatory themes and variations by the stress-signaling nucleotide alarmones (p)ppGpp in bacteria. Annu Rev Genet. 2021;55(1). 115–133. https://doi.org/10.1146/ANNUREV-GENET-021821-025827.
43. Le SQ, Gascuel O. An improved general amino acid replacement matrix. Mol Biol Evol. 2008;25(7):1307–1320. https://doi.org/10.1093/MOLBEV/MSN067.
44. Zhu Q, Mai U, Pfeiffer W, et al. Phylogenomics of 10,575 genomes reveals evolutionary proximity between domains bacteria and archaea. Nat Commun. 2019;10(1):5477. https://doi.org/10.1038/S41467-019-13443-4.
45. Hug LA, Baker BJ, Anantharaman K, et al. A new view of the tree of life. Nat Microbiol. 2016;1(5):1–6. https://doi.org/10.1038/nmicrobiol.2016.48.
46. Mathews CK. Deoxyribonucleotide metabolism, mutagenesis and cancer. Nat Rev Cancer. 2015;15(9):528–539. https://doi.org/10.1038/nrc3981.
47. Pai C, Kearsey SE. A critical balance: dNTPs and the maintenance of genome stability. Genes. 2017;8(2):57. https://doi.org/10.3390/GENES8020057.
48. Rudd SG, Valerie NKC, Helleday T. Pathways controlling dNTP pools to maintain genome stability. DNA Repair (Amst). 2016;44:193–204. https://doi.org/10.1016/J.DNAREP.2016.05.032.
49. Irving SE, Choudhury NR, Corrigan RM. The stringent response and physiological roles of (pp)pGpp in bacteria. Nat Rev Microbiol. 2021;19(4):256–271. https://doi.org/10.1038/S41579-020-00470-Y.
50. Wang B, Grant RA, Laub MT. ppGpp coordinates nucleotide and amino-acid synthesis in *E. coli* during starvation. Mol Cell. 2020;80(1):29–42.e10. https://doi.org/10.1016/J.MOLCEL.2020.08.005.
51. Alexandre T, Lupan A, Helynck O, et al. First-in-class allosteric inhibitors of bacterial IMPDHs. Eur J Med Chem. 2019;1:124–132. https://doi.org/10.1016/j.ejmech.2019.01.064.
52. Xu H, Zhou J, Lin S, Deng W, Zhang Y, Xue Y. PLMD: An updated data resource of protein lysine modifications. J Genet Genomics. 2017;44(5):243–250. https://doi.org/10.1016/J.JGG.2017.03.007.
53. Shi Y, Zhang Y, Lin S, et al. dbPSP 2.0, an updated database of protein phosphorylation sites in prokaryotes. Sci data. 2020;7(1):164. https://doi.org/10.1038/S41597-020-0506-7.
54. Kamieniarz K, Schneider R. Tools to tackle protein acetylation. Chem Biol. 2009;16(10):1027–1029. https://doi.org/10.1016/J.CHEMBIOL.2009.10.002.
55. Kozhevnikova EN, Van Der Knaap JA, Pindyurin AV, et al. Molecular cell metabolic enzyme IMPDH is also a transcription factor regulated by cellular state. Mol Cell. 2012;47:133–139. https://doi.org/10.1016/j.molcel.2012.04.030.
56. McLean JE, Hamaguchi N, Belenky P, Mortimer SE, Stanton M, Hedstrom L. Inosine 5′-monophosphate dehydrogenase binds nucleic acids in vitro and in vivo. Biochem J. 2004;379(Pt 2):243–251. https://doi.org/10.1042/BJ20031585.
57. Mortimer SE, Xu D, McGrew D, et al. IMP dehydrogenase type 1 associates with polyribosomes translating rhodopsin mRNA. J Biol Chem. 2008;283(52):36354–36360. https://doi.org/10.1074/JBC.M806143200.
58. Liu K, Myers AR, Pisithkul T, et al. Molecular mechanism and evolution of guanylate kinase regulation by (p)ppGpp. Mol Cell. 2015;57(4):735–749. https://doi.org/10.1016/J.MOLCEL.2014.12.037.

59. Anderson BW, Liu K, Wolak C, et al. Evolution of (P)ppGpp-HPRT regulation through diversification of an allosteric oligomeric interaction. Elife. 2019;8:e47534. https://doi.org/10.7554/ELIFE.47534.
60. Hauryliuk V, Atkinson GC, Murakami KS, Tenson T, Gerdes K. Recent functional insights into the role of (p)ppGpp in bacterial physiology. Nat Rev Microbiol. 2015;13(5):298–309. https://doi.org/10.1038/NRMICRO3448.
61. Lessard JC. Growth media for *E. coli*. Methods Enzymol. 2013;533:181–189. https://doi.org/10.1016/B978-0-12-420067-8.00011-8.
62. Gorrec F. The MORPHEUS protein crystallization screen. J Appl Crystallogr. 2009;42(6):1035–1042. https://doi.org/10.1107/S0021889809042022.
63. Gorrec F. The MORPHEUS II protein crystallization screen. Acta Crystallogr F Struct Biol Commun. 2015;71(7):831–837. https://doi.org/10.1107/S2053230X1500967X.
64. Tickle IJ, Flensburg C, Keller P, et al. STARANISO. Cambridge, UK: Global Phasing Ltd, 2018.
65. Vonrhein C, Flensburg C, Keller P, et al. Data processing and analysis with the autoPROC toolbox. Acta Crystallogr D Biol Crystallogr. 2011;67(Pt 4):293–302. https://doi.org/10.1107/S0907444911007773.
66. McCoy AJ, Grosse-Kunstleve RW, Adams PD, Winn MD, Storoni LC, Read RJ. Phaser crystallographic software. J Appl Cryst. 2007;40(Pt 4):658–674. https://doi.org/10.1107/S0021889807021206.
67. Potterton E, Briggs P, Turkenburg M, Dodson E. A graphical user interface to the CCP4 program suite. Acta Crystallogr D Biol Crystallogr. 2003;59(Pt 7):1131–1137.
68. Moynie L, Schnell R, McMahon SA, et al. The AEROPATH project targeting Pseudomonas aeruginosa: crystallographic studies for assessment of potential targets in early-stage drug discovery. Acta Crystallogr Sect F Struct Biol Cryst Commun. 2012;69(1):25–34. https://doi.org/10.1107/S1744309112044739.
69. Adams PD, Afonine PV, Bunkoczi G, et al. PHENIX: A comprehensive python-based system for macromolecular structure solution. Acta Crystallogr D Biol Crystallogr. 2010;66(Pt 2):213–221. https://doi.org/10.1107/S0907444909052925.
70. Emsley P, Lohkamp B, Scott WG, Cowtan K. Features and development of Coot. Acta Crystallogr D Biol Crystallogr. 2010;66(Pt 4):486–501. https://doi.org/10.1107/S0907444910007493.
71. Winn MD, Isupov MN, Murshudov GN. Use of TLS parameters to model anisotropic displacements in macromolecular refinement. Acta Crystallogr D Biol Crystallogr. 2001;57(Pt 1):122–133.
72. Schrödinger, LLC. The {PyMOL} Molecular Graphics System, Version 18; 2015.
73. Cowieson NP, Edwards-Gayle CJC, Inoue K, et al. Beamline B21: High-throughput small-angle X-ray scattering at diamond light. Sources. 2020;27(5):1438–1446. https://doi.org/10.1107/S1600577520009960.
74. Franke D, Petoukhov MV, Konarev PV, et al. ATSAS 2.8: A comprehensive data analysis suite for small-angle scattering from macromolecular solutions. J Appl Cryst. 2017;50(Pt 4):1212–1225. https://doi.org/10.1107/S1600576717007786.
75. Svergun D, Barberato C, Koch MHJ. CRYSOL—A program to evaluate X-ray solution scattering of biological macromolecules from atomic coordinates. J Appl Cryst. 1995;28(6):768–773. https://doi.org/10.1107/S0021889895007047.
76. Marcos-Alcalde Í, Mendieta-Moreno JI, Puisac B, et al. Two-step ATP-driven opening of cohesin head. Sci Rep. 2017;7(1):1–14. https://doi.org/10.1038/s41598-017-03118-9.
77. Humphrey W, Dalke A, Schulten K. VMD: Visual molecular dynamics. J Mol Graph. 1996;14(1):33–38. https://doi.org/10.1016/0263-7855(96)00018-5.
78. Altschul SF, Madden TL, Schaffer AA, et al. Gapped BLAST and PSI-BLAST: A new generation of protein database search programs. Nucleic Acids Res. 1997;25(17):3389–3402. https://doi.org/10.1093/nar/25.17.3389
79. Katoh K, Standley DM. MAFFT multiple sequence alignment software version 7: Improvements in performance and usability. Mol Biol Evol. 2013;30(4):772–780. https://doi.org/10.1093/MOLBEV/MST010.
80. Waterhouse AM, Procter JB, Martin DM, Clamp M, Barton GJ. Jalview version 2—A multiple sequence alignment editor and analysis workbench. Bioinformatics. 2009;25(9):1189–1191. https://doi.org/10.1093/bioinformatics/btp033.
81. Capella-Gutiérrez S, Silla-Martínez JM, Gabaldón T. trimAl: A tool for automated alignment trimming in large-scale phylogenetic analyses. Bioinformatics. 2009;25(15):1972–1973. https://doi.org/10.1093/BIOINFORMATICS/BTP348.
82. Guindon S, Dufayard J-F, Lefort V, Anisimova M, Hordijk W, Gascuel O. New algorithms and methods to estimate maximum-likelihood phylogenies: Assessing the performance of PhyML 3.0. Syst Biol. 2010;59(3):307–321. https://doi.org/10.1093/sysbio/syq010.
83. Lefort V, Longueville JE, Gascuel O. SMS: Smart model selection in PhyML. Mol Biol Evol. 2017;34(9):2422–2424. https://doi.org/10.1093/MOLBEV/MSX149.

SUPPORTING INFORMATION

Additional supporting information may be found in the online version of the article at the publisher's website.

How to cite this article: Fernández-Justel D, Marcos-Alcalde Íñigo, Abascal F, Vidaña N, Gómez-Puertas P, Jiménez A, et al. Diversity of mechanisms to control bacterial GTP homeostasis by the mutually exclusive binding of adenine and guanine nucleotides to IMP dehydrogenase. Protein Science. 2022;31(5):e4314. https://doi.org/10.1002/pro.4314

SUPPLEMENTAL INFORMATION

Diversity of mechanisms to control bacterial GTP homeostasis by the mutually exclusive binding of adenine and guanine nucleotides to IMP dehydrogenase

David Fernández-Justel[1], Íñigo Marcos-Alcalde[2,3], Federico Abascal[4], Nerea Vidaña[1], Paulino Gómez-Puertas[2], Alberto Jiménez[1], José L Revuelta[1] and Rubén M Buey[1*]

[1]Metabolic Engineering Group. Dept. Microbiology and Genetics. Universidad de Salamanca

[2] Molecular Modeling Group, Centro de Biología Molecular Severo Ochoa, CBMSO (CSIC-UAM), 28049 Madrid, Spain

[3] Biosciences Research Institute, School of Experimental Sciences, Universidad Francisco de Vitoria, 28223. Pozuelo de Alarcón, Madrid, Spain

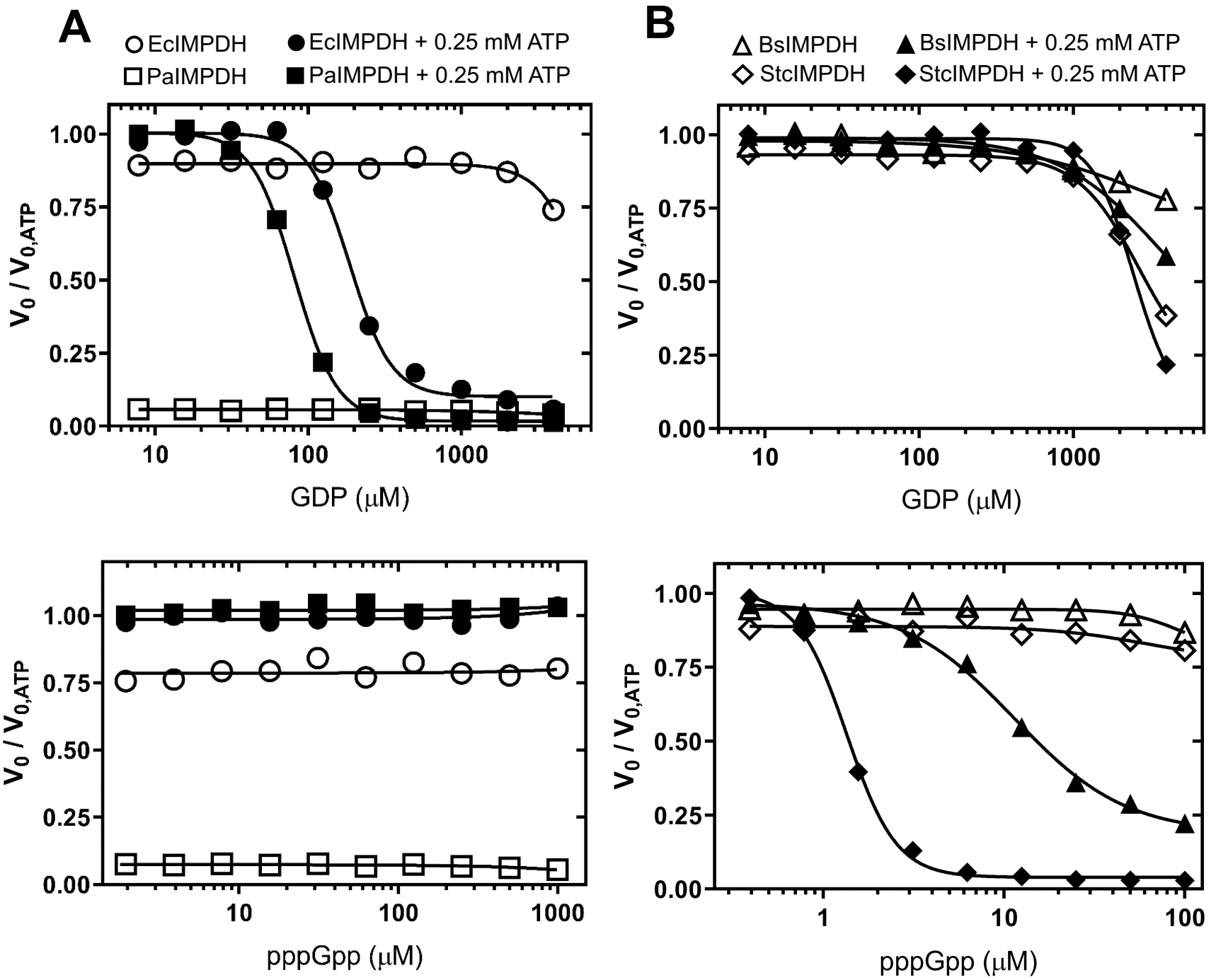
[4] Wellcome Sanger Institute. Hinxton, UK

[*]To whom correspondence should be addressed: ruben.martinez@usal.es

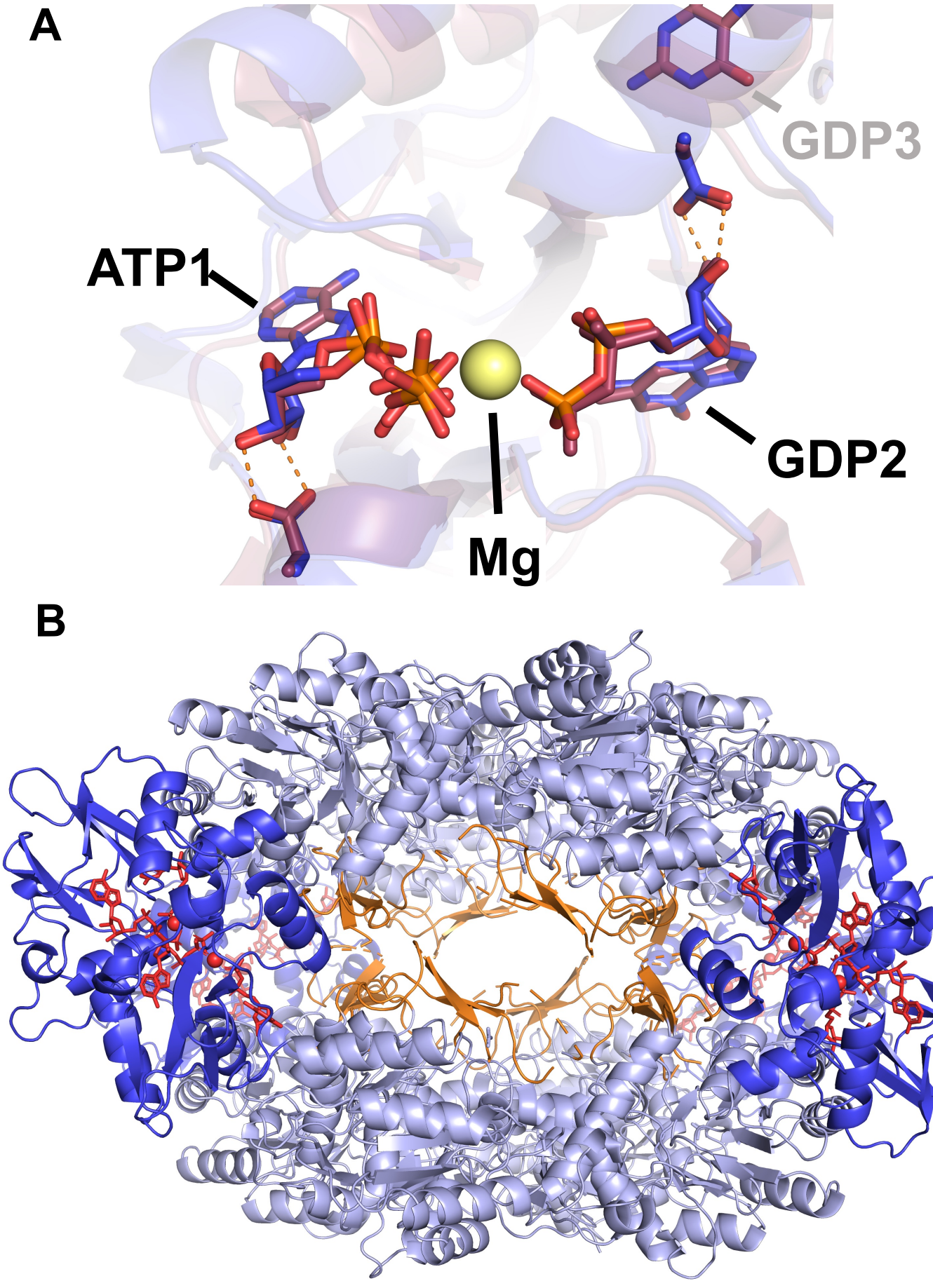
Supplemental Table 1. *X-ray crystallography and data collection and refinement statistics.*

	PalMPDH ATP-GDP	StcIMPDH ATP-ppGpp
PDB ID	**7PJI**	**7PMZ**
Wavelength (Å)	1.00	1.00
Resolution (Å)	1.65	2.03
Space group	I4	$P2_1$
Unit cell (Å / º)	120.95 120.95 145.49 90.00 90.00 90.00	119.29 300.90 123.09 90.00 90.29 90.00
Unique reflections	84861 (4228)	474239 (23712)
Multiplicity	14.0 (13.9)	4.6 (4.5)
Completeness spherical (%)	67.8 (17.8)	84.9 (27.1)
Completeness ellipsoidal (%)	95.7 (69.7)	94.2 (58.1)
Mean I/sigma(I)	16.8 (1.5)	9.4 (1.5)
Wilson B-factor	25.18	30.62
R-merge	0.09 (1.76)	0.10 (0.99)
R-meas	0.09 (1.83)	0.11 (1.13)
R-pim	0.03 (0.49)	0.055 (0.53)
CC1/2	0.999 (0.620)	0.998 (0.589)
Reflections used in refinement	84628 (880)	474175 (9428)
Reflections used for R-free	4286 (44)	23521 (454)
R-work	0.18 (0.32)	0.18 (0.26)
R-free	0.20 (0.33)	0.21 (0.30)
Non-H atoms:	7258	53302
macromolecules	6476	48630
ligands	182	1456
solvent	654	3569
Protein residues	892	6842
RMS(bonds)	0.007	0.009
RMS(angles)	1.06	1.19
Ramachandran favored (%)	98.06	97.83
Ramachandran allowed (%)	1.94	2.13
Ramachandran outliers (%)	0.00	1.0
Rotamer outliers (%)	0.16	0.93
Clashscore	4.32	4.08
Average B-factor:	35.28	39.31
macromolecules	34.61	39.22
ligands	35.88	38.80
solvent	42.25	40.66

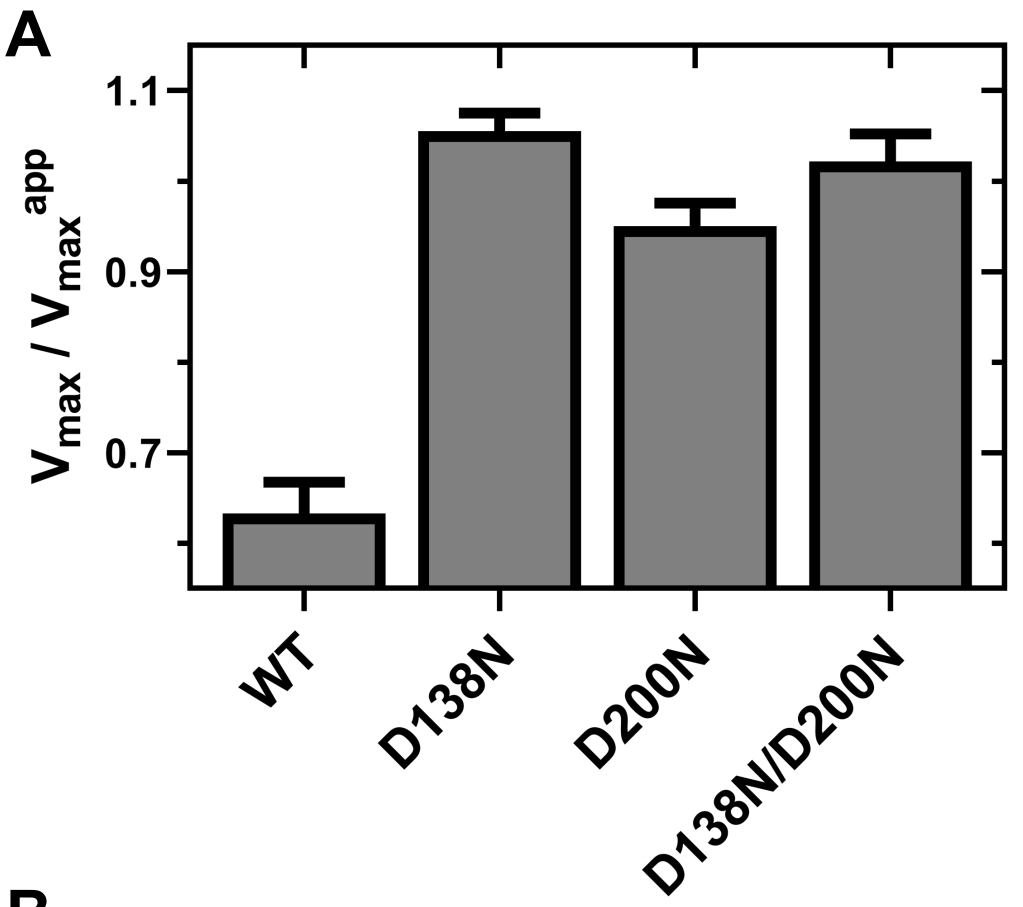
Statistics for the highest-resolution shell are shown in parentheses.



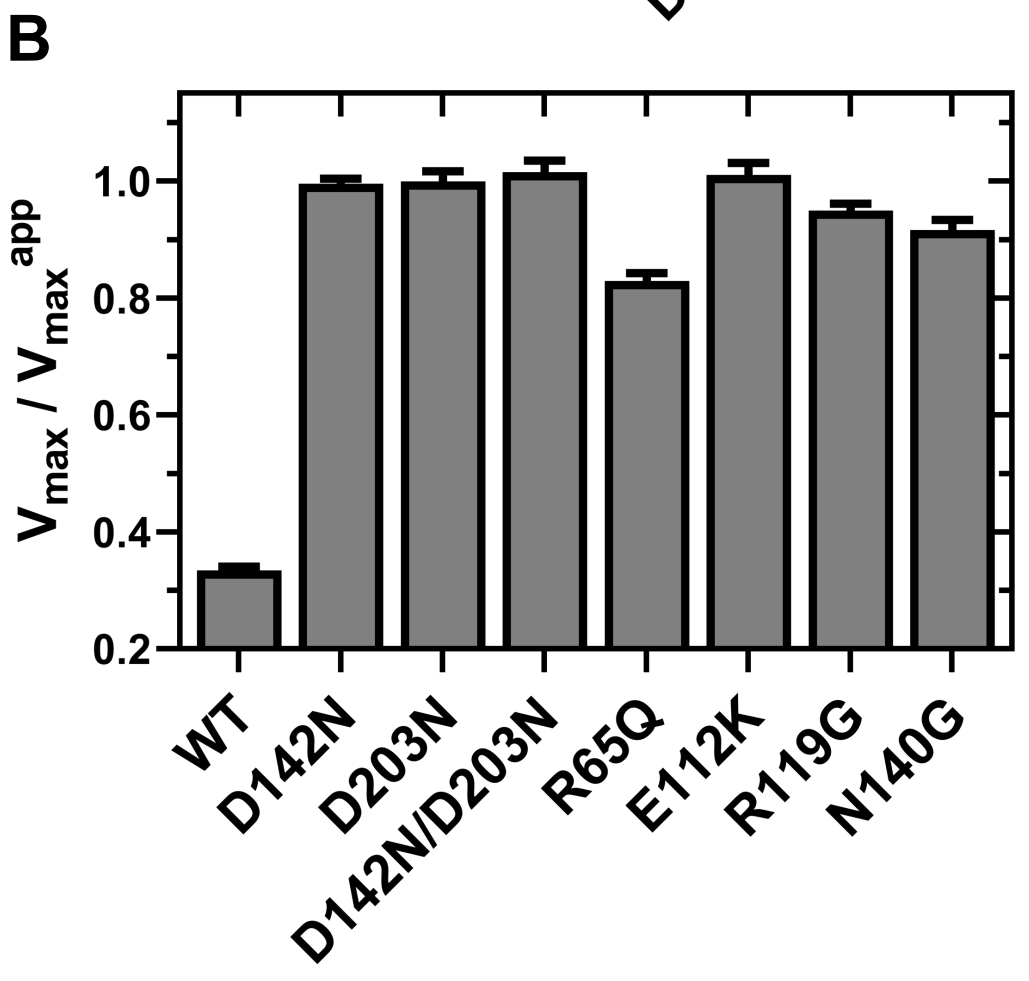
Supplemental Figure 1. *Effects of GDP (A) and pppGpp (B) on the catalytic activity of IMPDH in vitro*. Graphs showing the normalized initial velocity values (V_0 values in the absence of GDP or pppGpp divided by the respective values in the presence of GDP or ppGpp. The V_0 values used for the normalization of the data are: EclMPDH 18.5 ± 1.0, PalMPDH 26.7 ± 0.9, BslMPDH 12.9 ± 0.8, and StclMPDH 12.6 ± 0.4 nM/sec (mean ± std. error). Estimated IC_{50} values for GDP are 187.2 ± 8.8 μM μM and 81.3 ± 1.0 μM (mean ± std. error) for BslMPDH and StclMPDH, respectively. Estimated IC_{50} values for pppGpp are 11.4 ± 1.2 μM and 1.4 ± 0.03 μM (mean ± std. error) for BslMPDH and StclMPDH, respectively.



Supplemental Figure 2. *The compaction of octamers mediates the allosteric inhibition of PaIMPDH.* **A.** Structural superimposition of the structures of PaIMPDH-ATP/GDP (blue ribbons) and AgIMPDH-ATP/GDP/GDP (red ribbons; PDB ID 5TC3), showing the identical binding modes of the nucleotides on the canonical sites of the Bateman domain. **B.** Octameric structure of PaIMPDH-ATP/GDP reconstructed from the crystallographic lattice contacts, showing a compacted octamer where the finger domains (orange ribbons) of opposing tetramers are forced to interact. The catalytic and the regulatory Bateman domains are colored in light and dark blue, respectively. Bound nucleotides are shown in red sticks.

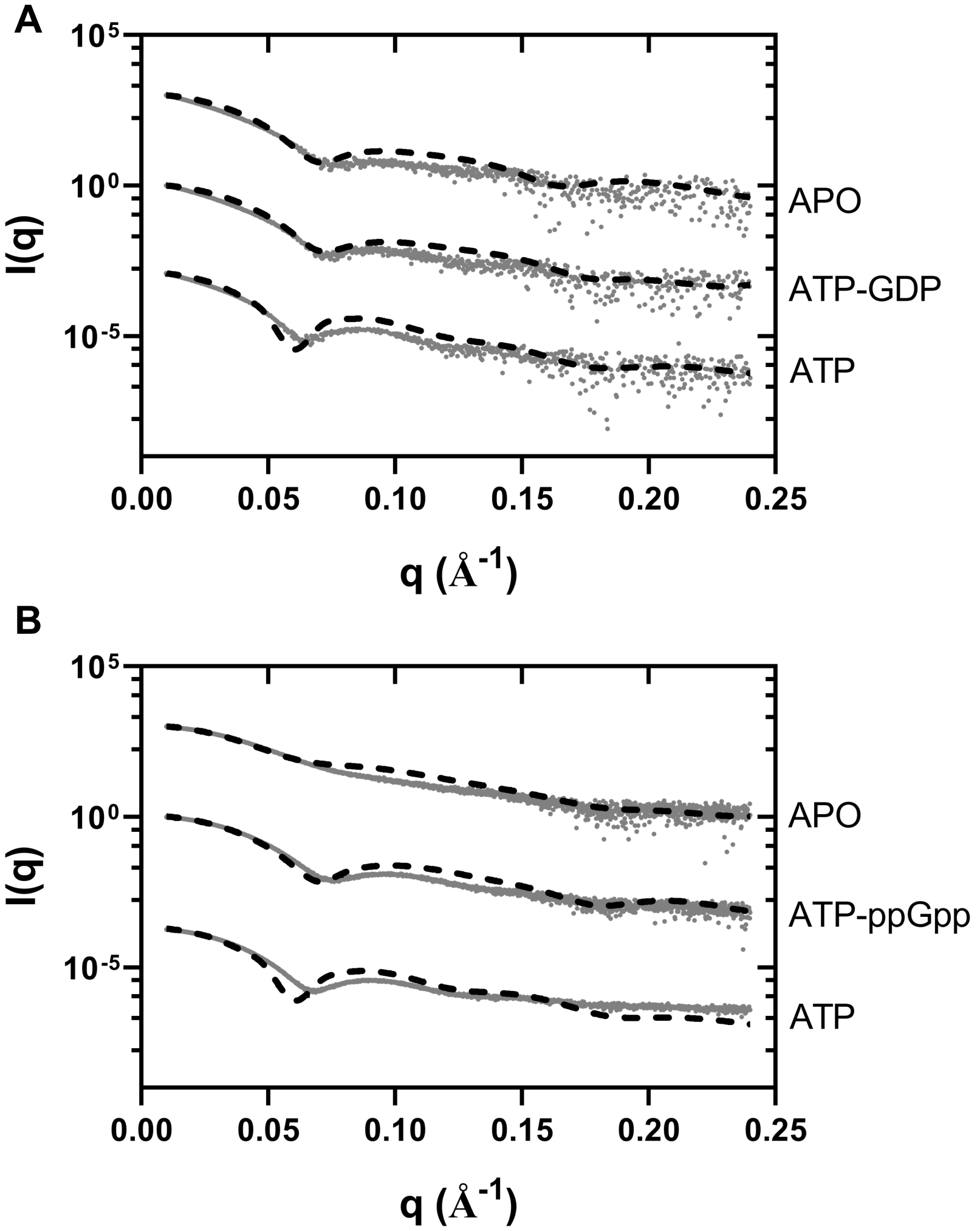


	Vmax (nM/sec)
WT	30.22 ± 0.93
D138N	22.82 ± 0.51
D200N	22.78 ± 0.51
D138N/D200N	14.79 ± 0.41

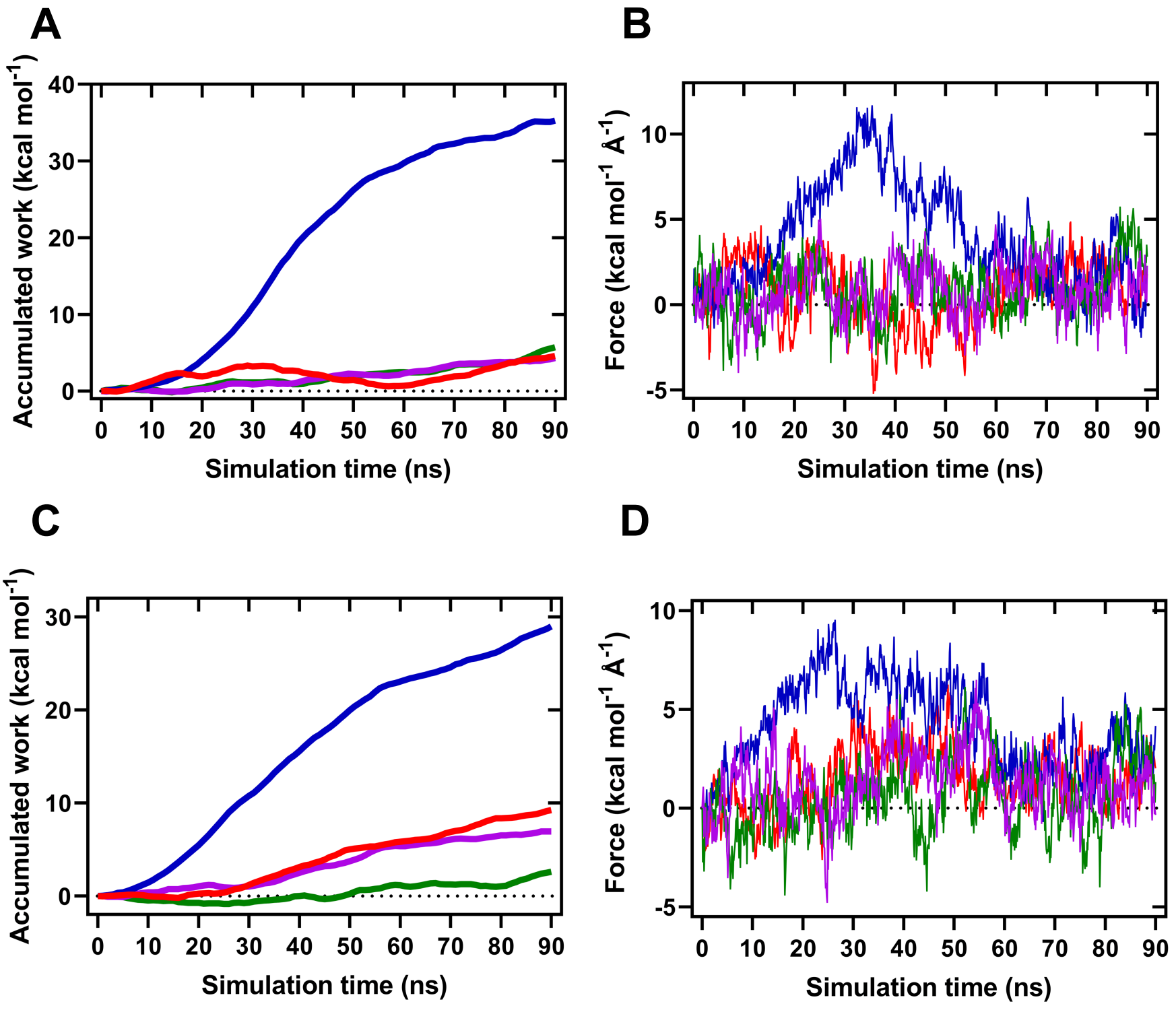


	Vmax (nM/sec)
WT	22.24 ± 0.37
D142N	18.05 ± 0.28
D203N	15.26 ± 0.31
D142N/D203N	16.37 ± 0.29
R65Q	17.24 ± 0.24
E112K	21.79 ± 0.42
R119G	20.19 ± 0.19
N140G	22.95 ± 0.24

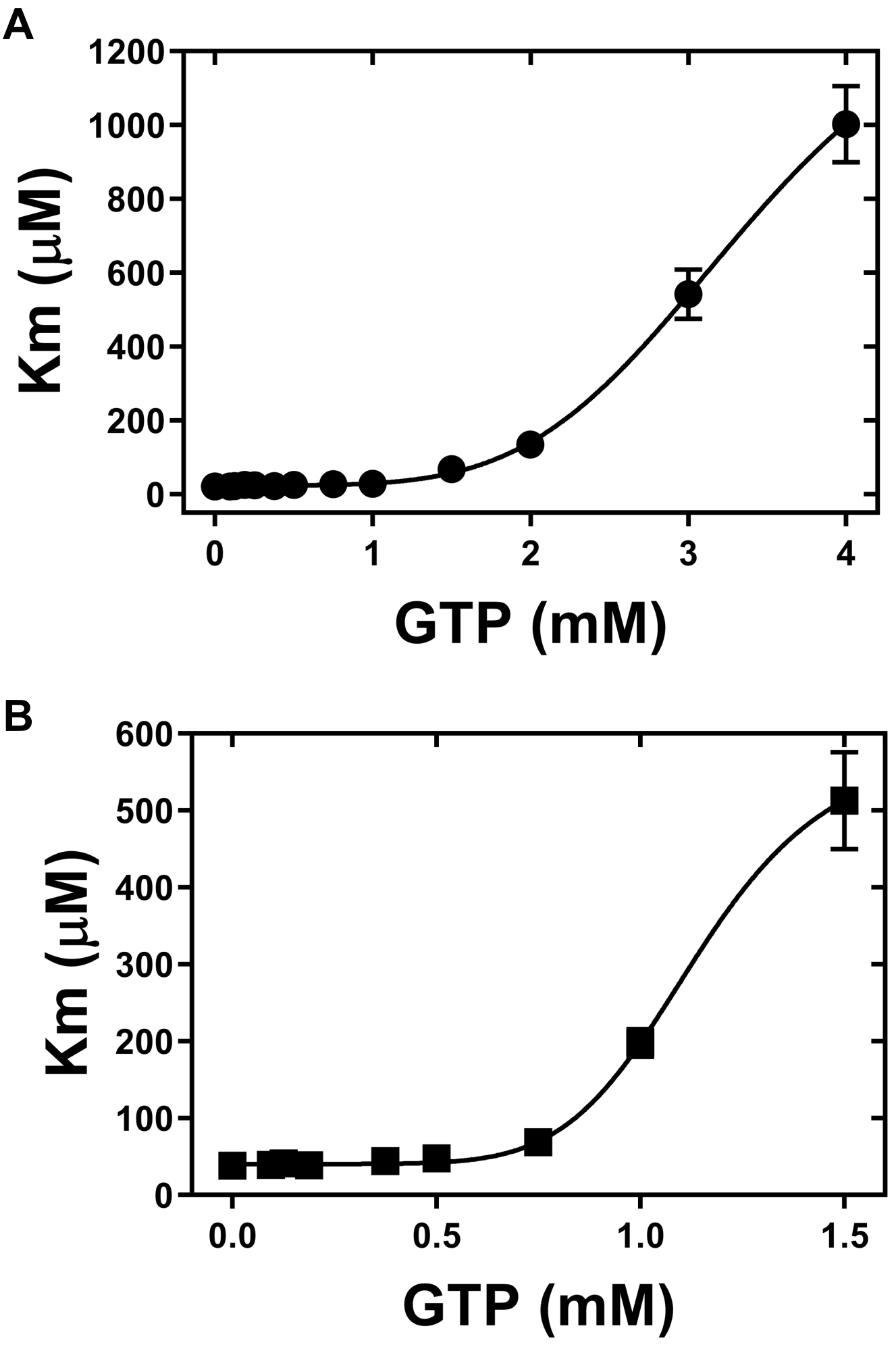
Supplemental Figure 3. *Mutational analysis of the allosteric binding sites*. Normalized V_{max} values (V_{max} in the presence of ATP / V_{max} in the presence of ATP and guanine nucleotides; mean and standard deviations) for the WT and different mutants of EcIMPDH (**A**) and BsIMPDH (**B**). Nucleotide concentrations for EcIMPDH were: 0.25 mM ATP and 1 mM GTP, measured at 32ºC, and for BsIMPDH: 1 mM ATP and 50 µM ppGpp, measured at 28ºC. The enzymatic reactions were performed in all cases using 50 nM enzyme in bufffer 100 mM TrisHCl, pH 8.0, 100 mM KCl, 1 mM DTT, 1 mM free $MgCl_2$, 0.5 mM NAD and IMP concentrations ranging from 4 µM to 5mM. The V_{max} values used for normalization are shown in the tables.



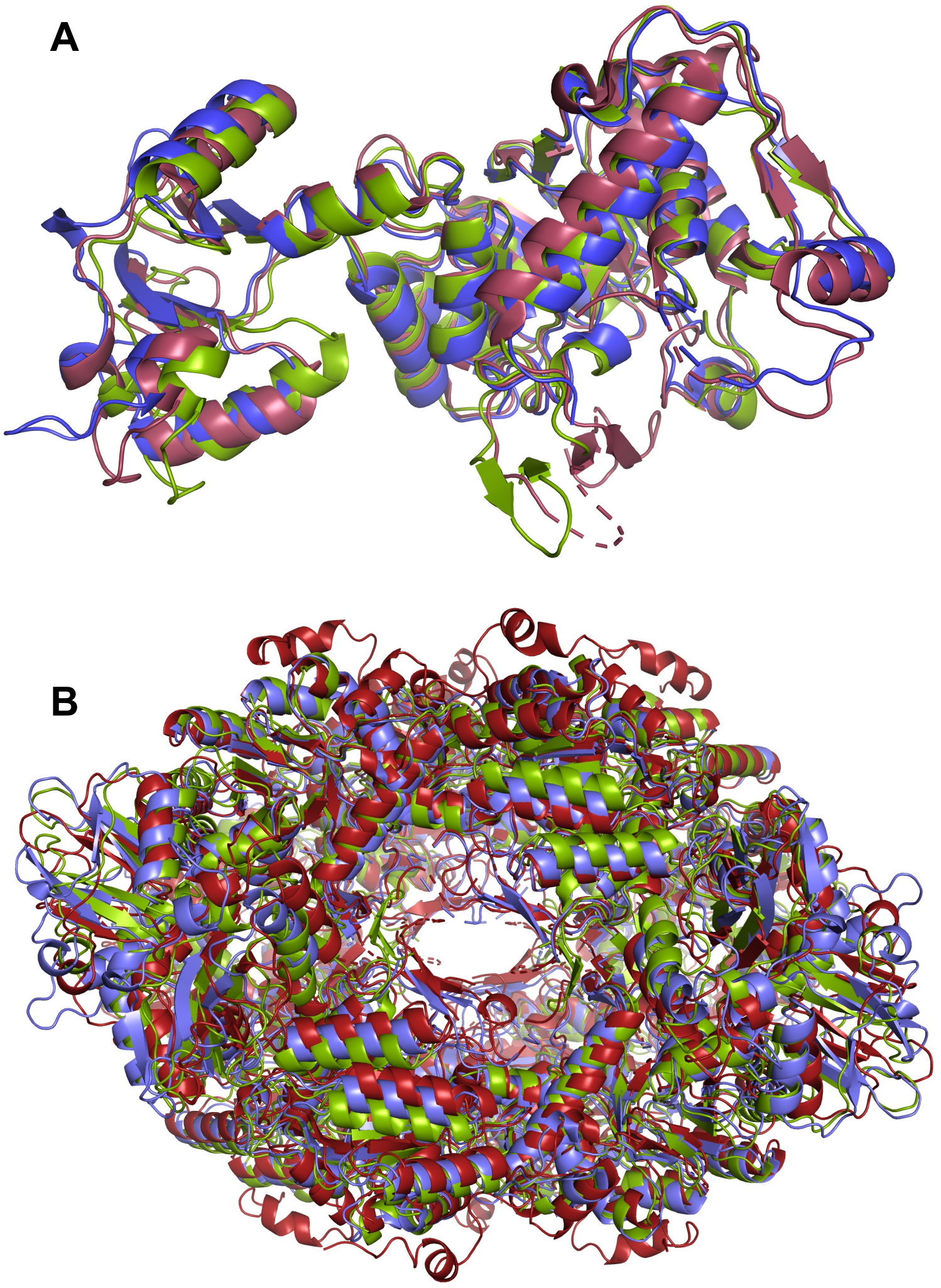
Supplemental Figure 4. *The conformational switch of IMPDH observed in solution by SAXS.* SAXS profiles of PaIMPDH (**A)** and StcIMPDH (**B**) in the presence of different nucleotides. To facilitate visualization, the curves have been conveniently displaced along the y axis. At the SAXS resolution, the profiles for ATP-GTP and ATP-pppGpp are indistinguishable from ATP-GDP and ATP-ppGpp, respectively.



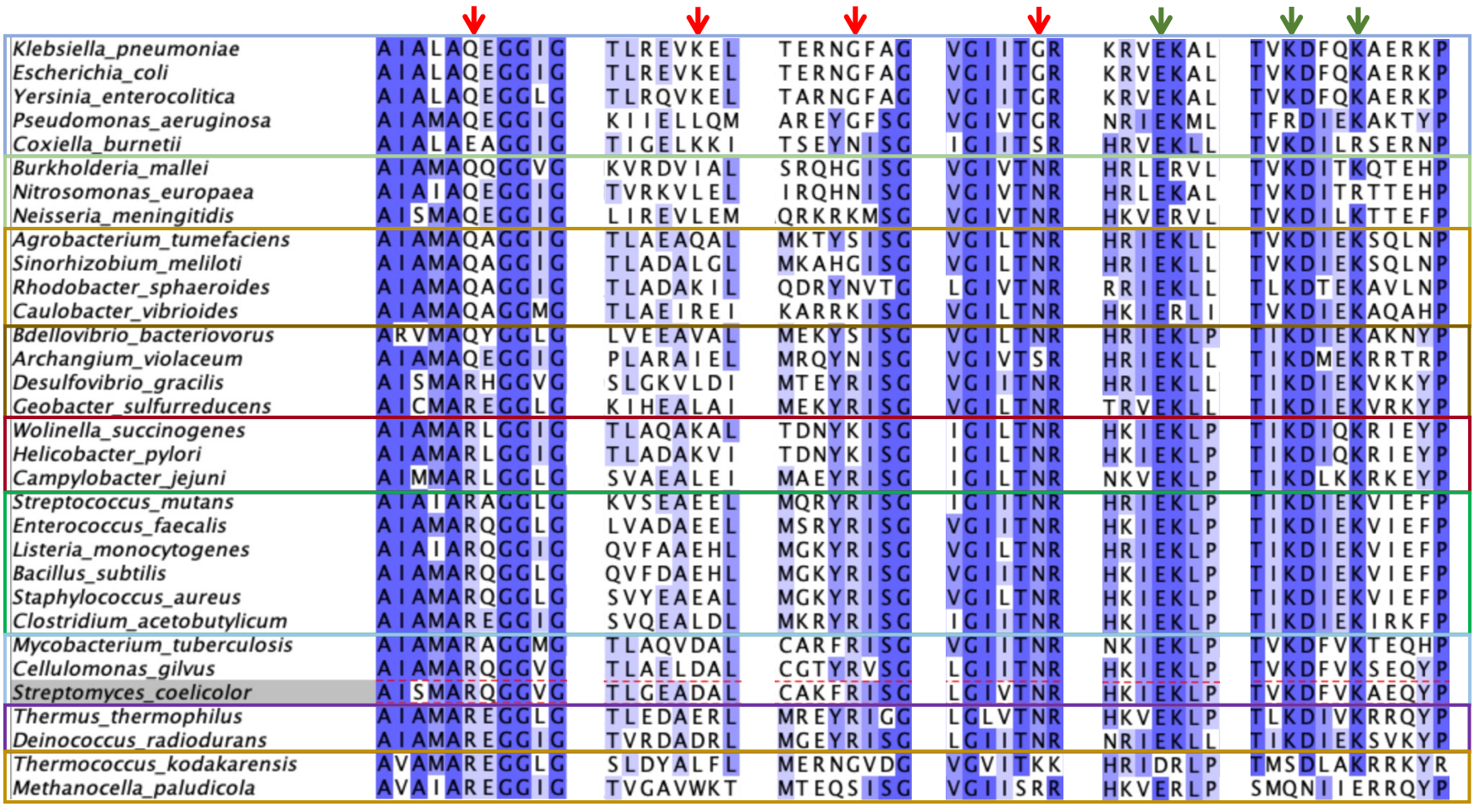
Supplemental Figure 5. *GTP/GDP and (p)ppGpp binding to the Bateman domain strongly stabilize the inhibited IMPDH conformation.* Accumulated work and forces exerted along the targeted molecular dynamics simulations of monomers of PaIMPDH (panels **A** and **B**) and StcIMPDH (panels **C** and **D**) induced to adopt a compact conformation, starting from the extended one, in the presence of ATP1/ATP2 (purple lines), ATP1/GDP2 or ATP1/ppGpp (green lines). Alternatively, IMPDH monomers were induced to adopt an extended conformation, starting from the compacted one, in the presence of ATP1/ATP2 (red lines), ATP1/GDP2 or ATP1/ppGpp (blue lines), monitoring also the ccumulated work and the forces applied during the process.



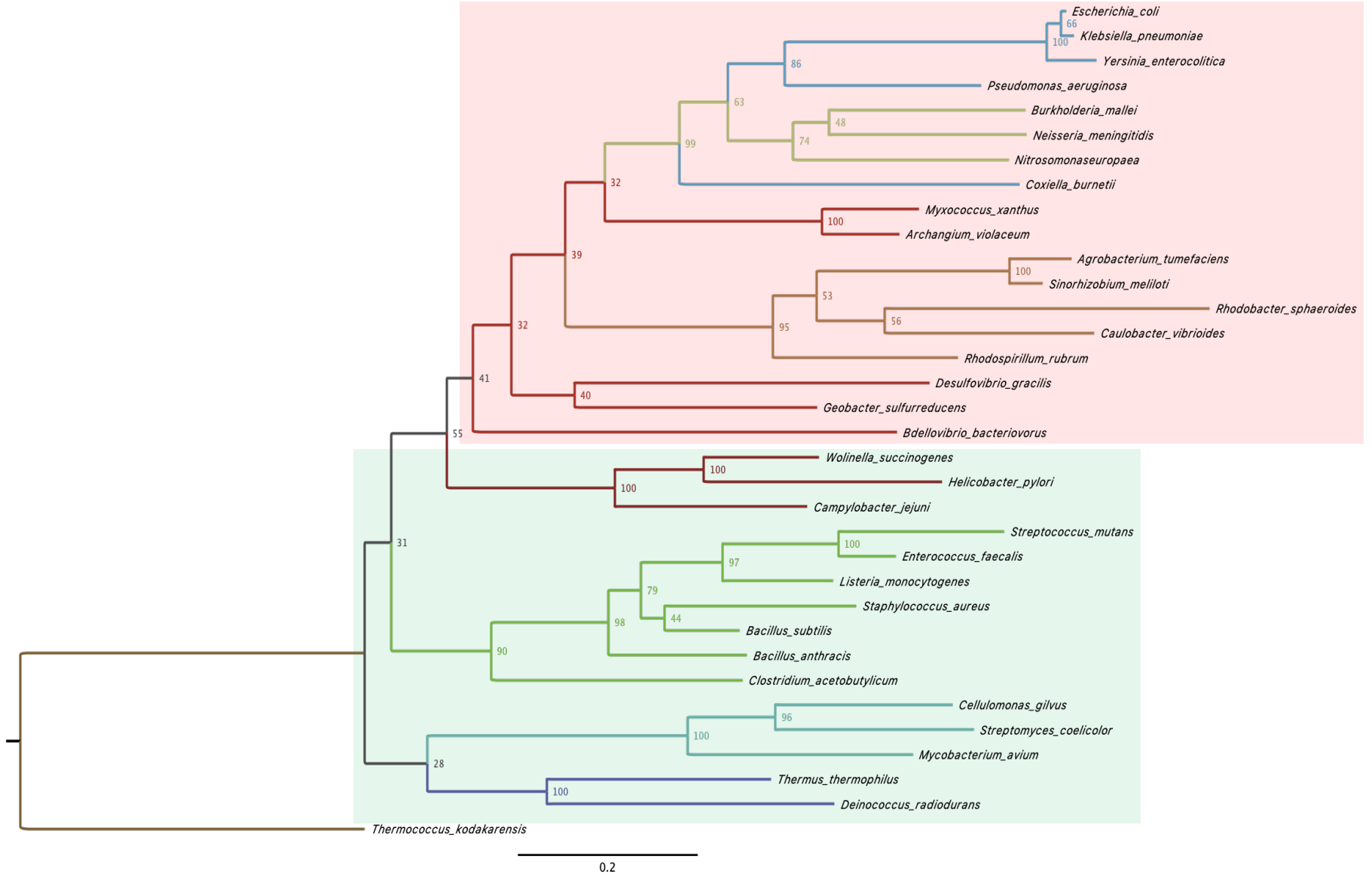
Supplemental Figure 6. *Allosteric inhibition of GTP at physiological ATP concentration.* GTP titration curves of EcIMPDH (**A)** and PaIMPDH (**B)** measured at 32ºC in buffer 100 mM Tris-HCl, pH 8.0, 100 mM KCl, 1 mM DTT, 1 mM free $MgCl_2$, 20 nM enzyme, 3 mM ATP, 0.5 mM NAD and IMP concentrations ranging from 4 μM to 5mM. The Km values in the absence of GTP were 23.45 ± 1.47 μM for EcIMPDH and 36.96 ± 1.62 μM for PaIMPDH.



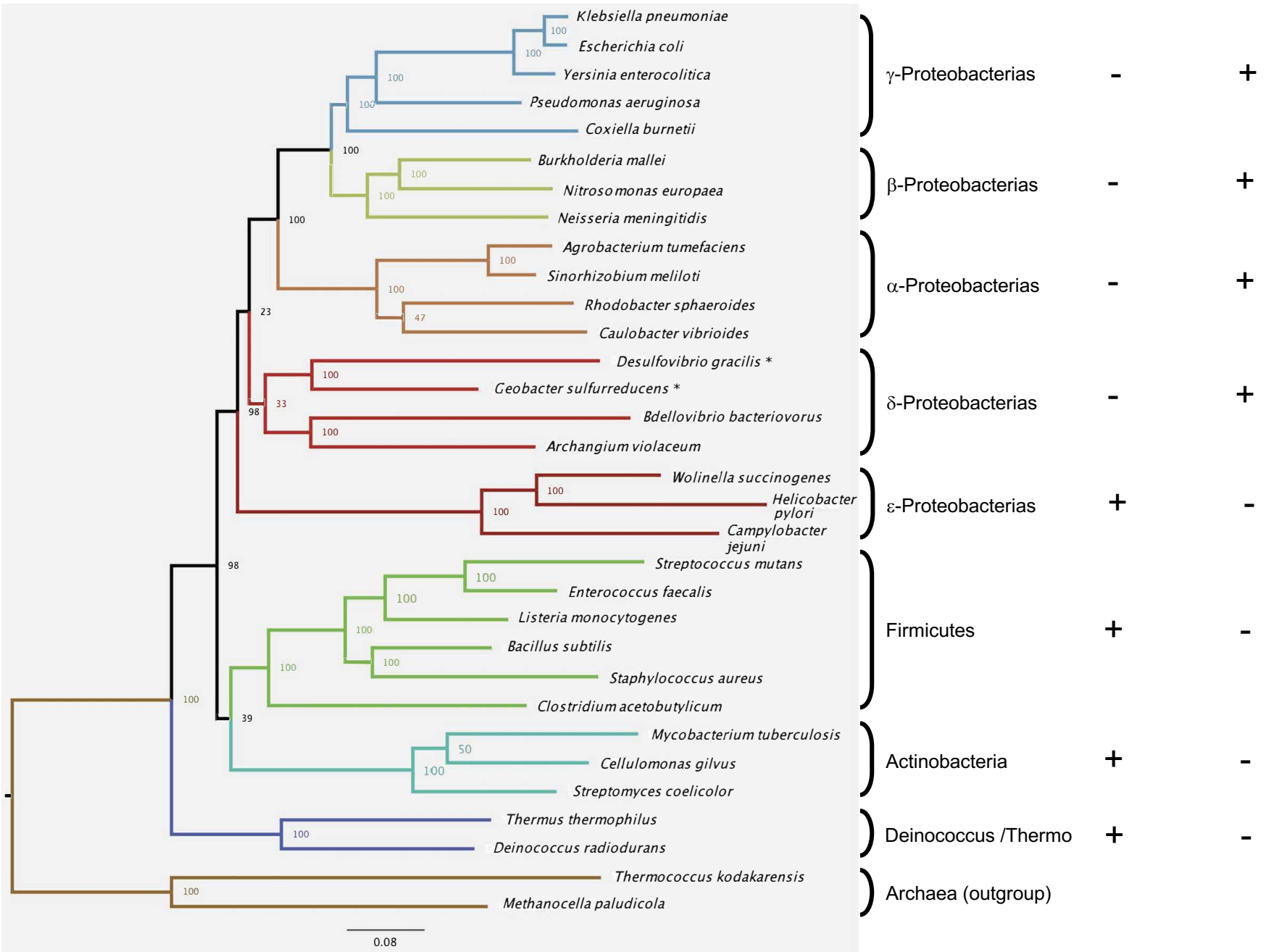
Supplemental Figure 7. *Eukaryotic and bacterial IMPDHs adopt similar compact conformation upon allosteric inhibition*. **A**. Structural comparison of the conformation adopted by IMPDH monomers, upon allosteric inhibition. Blue ribbons: PaIMPDH-ATP/GDP; Green ribbons: StcIMPDH-ATP/ppGpp; Red ribbons: AgIMPDH-ATP/GDP/GDP (PDB ID 5TC3). **B**. Structural superimposition of the octamers formed by the monomers in panel A.



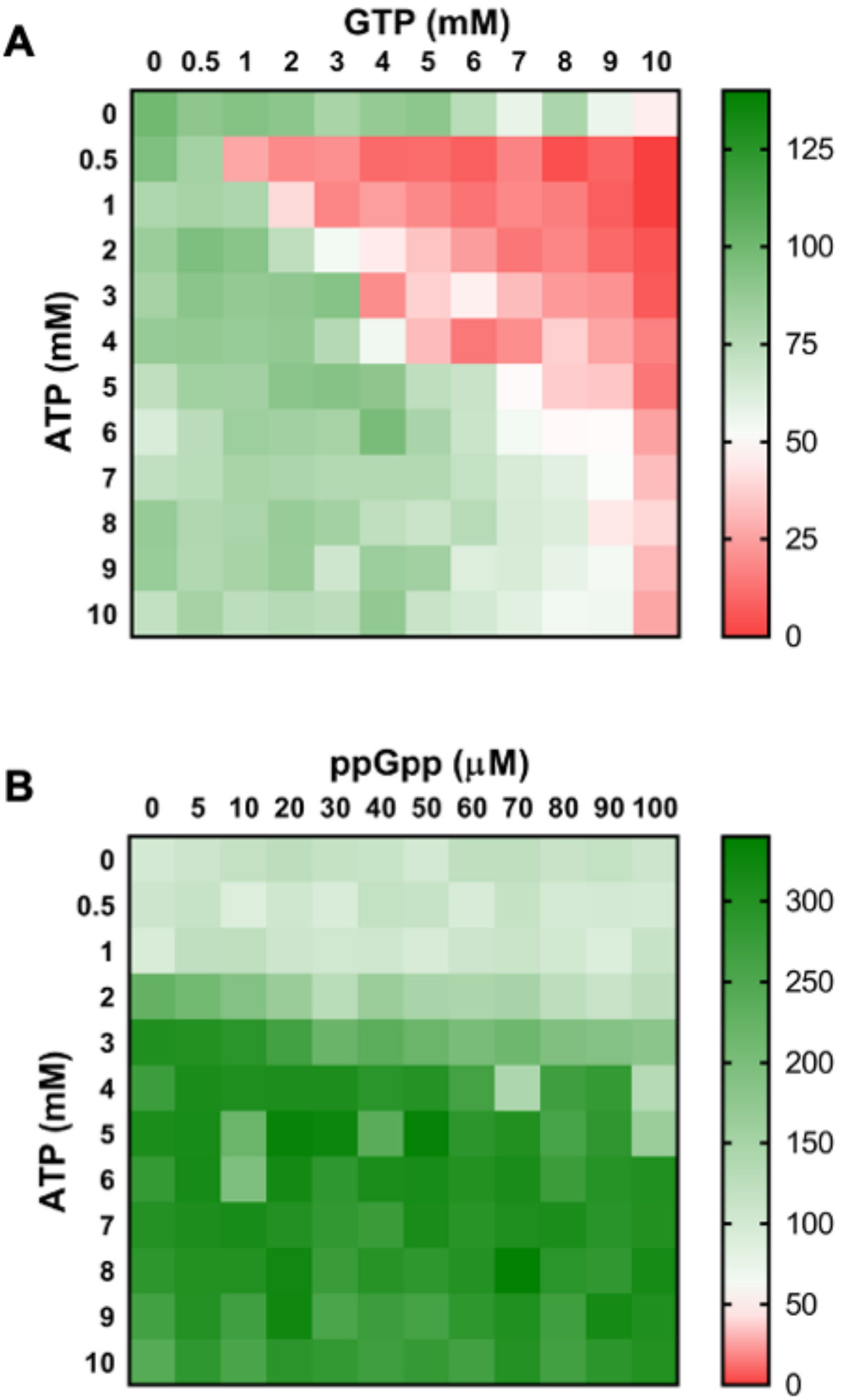
Supplemental Figure 8. *Sequence alignment of the Bateman domain of selected prokaryotic IMPDHs.* Fragment of a multiple sequence alignment of the Bateman domain of selected bacterial IMPDHs. The red arrows indicate key nucleotide-interacting residues, exclusive of the (p)ppGpp binding site, numbered from left to right according to the *S. coelicolor* IMPDH sequence (highlighted): Arg71, Asp118, Arg125 and Asn144. The green arrows indicate the key nucleotide interacting residues shared by the second canonical and the (p)ppGpp sites: Glu 188, Lys206 and Lys210.



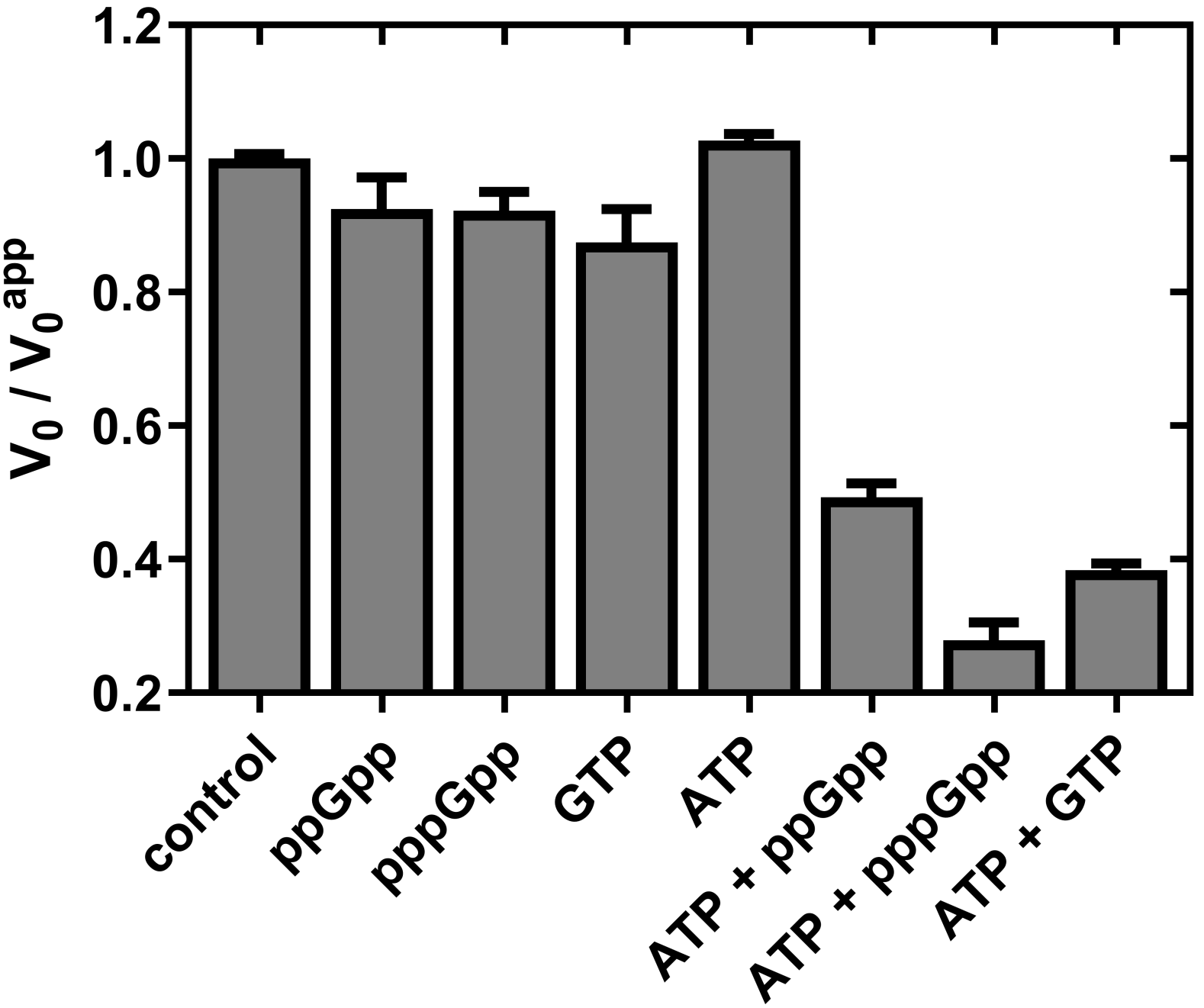
Supplemental Figure 9. *Evolutionary analysis of bacterial IMPDHs.* Rooted phylogenetic tree of bacterial IMPDHs (best model LG+G+I, (Le and Gascuel, 2008)). Branches are colored according to the taxonomical classification. Archaeal sequences serve as an outgroup. The length of the radius branches indicates the amount of change (substitutions/site) between a pair of nodes. The IMPDH enzymes that do and don´t contain the (p)ppGpp binding site are indicated in light green and red boxes, respectively.



Supplemental Figure 10. *Tree of life of selected organisms*. Rooted phylogenetic tree of life constructed by the neighbor-joining method, showing bootstrap values (best model LG+G+F, (Le and Gascuel, 2008)), and branches colored as in Supplemental figure 6. Presence or absence of the (p)ppGpp binding site in IMPDH and RNAP sensitivity to (p)ppGpp is indicated on the right, according to our results and to the presence of the MAR motif in the w-subunit (Hauryliuk et al. 2015. Nat Rev Microb 13, 298-309). α, β, γ and δ-Proteobacteria do not contain the (p)ppGpp binding site, in contrast to ε-Proteobacteria. Nonetheless, some δ-Proteobacteria IMPDHs (marked with an asterisk: *D. gracilis* and *G. sulfurreducens*) contain the (p)ppGpp binding site. Although the pattern observed in δ-Proteobacteria is unexpected, reassuringly, the species tree confidently groups all delta proteobacteria in a monophyletic clade. Thereby, it is possible that there has been a horizontal gene transfer into δ-Proteobacteria, but the low resolution in the phylogenetic tree of IMPDH, and the ambiguous positioning of δ-Proteobacteria within this tree, prevents drawing reliable conclusions. Alternatively, convergent evolution may be at play, with loss of (p)ppGpp sensitivity happening twice, once in the ancestor of α, β and γ-Proteobacteria and once within δ-Proteobacteria.



Supplemental Figure 11. *Lysine acetylation fine-tune bacterial IMPDH allosteric regulation in vitro.* Heatmap representation of the enzymatic percent activity. V_0 values normalized to the V_0 values in the absence of nucleotide of lysine acetylation mimetic mutants EcIMPDH-K203Q (**A**) and BsIMPDH-K206Q (**B**) at different ATP versus ppGpp or GTP concentrations. The V_o values used for normalization are 7.8 and 9.3 nM/sec for EcIMPDH-K203Q and BsIMPDH-K206Q, respectively.



Supplemental Figure 12. *Effects of guanine nucleotides on the catalytic activity of HpIMPDH in vitro*. Normalized initial velocity (V_0) values calculated as the V_0 in the absence of nucleotides divided by the corresponding values in the presence of the indicated ones. The experiment was performed at 32ºC in buffer 100 mM Tris-HCl, pH 8.0, 100 mM KCl, 1 mM DTT, 1 mM free $MgCl_2$, 50 nM enzyme, 0.5 mM NAD^+ and 0.5 mM IMP. Nucleotide concentrations were (from left to right): 0.5 mM (p)ppGpp, 4 mM GTP, 2 mM ATP, 0.25 mM ATP + 0.5 mM (p)ppGpp, 0.25 mM ATP + 4 mM GTP. The V_o value used for normalization was 6.83 ± 0.1 nM/sec.